

THERMAL CHARACTERIZATION OF ACETONE PEROXIDE MIXTURES WITH HIGH ENERGETIC MATERIALS AND RAMAN BASED DETECTION OF CONCEALED CHEMICAL THREATS

by

Michael L. Ramirez

A thesis submitted in partial fulfillment of the requirements for the degree of

Doctor in Philosophy
in
Applied Chemistry

UNIVERSITY OF PUERTO RICO
MAYAGÜEZ CAMPUS
2009

Approved by:

Nairmen Mina, PhD.
Member, Graduate Committee

Date

Julio Briano, PhD.
Member, Graduate Committee

Date

Miguel Castro, PhD
Member, Graduate Committee

Date

Arturo Hernandez, PhD
Member, Graduate Committee

Date

Samuel P. Hernández, PhD.
President, Graduate Committee

Date

Aldo Acevedo, PhD
Representative of Graduate Studies

Date

Francis Patron, PhD
Chairperson of the Department

Date

ABSTRACT

This study was aimed at making contributions toward the understanding and detection of homemade explosives (HME). The properties and interactions between components in a blend of energetic materials with acetone peroxide, powerful and unstable homemade explosives, were studied by thermal analysis, spectroscopic tools and by the use of computational methods. First, the thermal stability of triacetone triperoxide (AP), a HME, was evaluated by differential scanning calorimetry (DSC) and thermal gravimetric analysis (TGA). The enthalpy of sublimation and the activation energy for decomposition were obtained by kinetics analysis and modeling. The results were compared to other known energetic materials. The relationship between structure and thermal behavior was also studied. Then, AP was combined with other energetic materials. The spectroscopic signatures of these systems and the thermal decomposition curves of such blends were reported. Computational analysis was used to estimate interaction energies for possible conformations.

Also, as part of the contributed work, Raman spectroscopy was evaluated as a detection tool for concealed hazardous materials. Liquid explosives, chemical warfare agent stimulants and toxic industrial compounds were analyzed by fiber optic coupled and standoff detection Raman systems. The liquids were concealed within consumer products such as beverages and personal care products.

RESUMEN

Este trabajo estuvo dirigido a hacer una contribución hacia el conocimiento y detección de mezclas de materiales energéticos con peróxido de acetona, un explosivo casero muy conocido por su potencia e inestabilidad. Las propiedades e interacciones entre componentes de estas mezclas fueron estudiadas por herramientas espectroscópicas, análisis térmico y por métodos computacionales. Primero la estabilidad térmica de peróxido de acetona (AP) fue evaluada por calorimetría de rastreo diferencial (DSC) y análisis gravimétrico térmico (TGA). Se utilizó análisis cinético para estimar la energía de activación para la descomposición y la entalpía de sublimación. Los resultados fueron comparados con otros materiales energéticos más conocidos. También se estudió la relación entre energía y propiedades térmicas. Luego AP fue mezclado con otros materiales energéticos. La firma espectroscópica de estas mezclas y las curvas de su descomposición térmica fueron reportadas. Análisis computacional fue utilizado para estimar la energía de interacción de posibles conformaciones. Por último este trabajo evalúa el uso de la espectroscopia Raman como herramienta de detección de líquidos peligrosos escondidos. Explosivos líquidos y otros agentes químicos tóxicos analizados por Raman acoplado a fibra óptica y por un sistema Raman de detección a distancia. Los líquidos se encontraban escondidos en productos comunes de consumo como bebidas artículos de cuidado personal. .

**Copyright © by
Michael L. Ramírez
2009**

To Myrna Cedeño, Luis A. Ramírez, Jeannette Recio, Myrna M.

Ramírez and Xavier Rosario.

ACKNOWLEDGMENTS

Above all I thank God for the challenges and opportunities that are brought to me every day, for my great family and friends. I want to acknowledge many people and institutions which without them my travel to this point would have been different. First I want to mention my wife Jeannie Recio for her love, patience and sacrifice. These have been long and challenging years, time to move on. Also my trip to this point would not have been possible without my parents Luis A. Ramirez and Myrna Cedeño, my sister Myrna Marie and her husband Xavier. They have always supported every new endeavor. What's next?

I want to acknowledge my advisor Dr. Samuel P. Hernandez for the opportunity to work with him in an environment of trust, respect, motivation and professional development. During all this time he has become an advisor, a mentor and a collaborator for the future. I also want to thank my committee: Dr. Nairmen Mina, Dr. Arturo Hernandez, Dr. Miguel Castro and Dr. Julio Briano for their time, interest and comments.

Other people that have contributed to my professional development include Dr. Richard Lyon, Dr. Susan Hallowell and many other fine scientists and great human beings at the Federal Aviation Administration Fire Resistant Materials Lab and the DHS Transportation Security Lab at Atlantic City, New Jersey. I will be forever thankful for the great experience at the FAA.

I started in the program as part of my development plan at Hewlett Packard in Aguadilla. During my time there I met very special people that supported this step for the future of the company and my own professional development. Working at HP contributed greatly to my career. It was really a learning experience. I want to recognize specially to Lester Ortiz, Tito Ortega, Julio Cartagena, Peter Melendez, Reinyka Velez and the Lab crew. They have been a critical element of this process. Thanks you for your time and patience.

Finally I want to acknowledge the friends, professors and personnel of the Chemistry Department and the Center for Chemical Sensors Development and Chemical Imaging Center. In particular I have to mention Orlando Ruiz, Alexis Morales, Hilsamar Felix, Oliva Primera, Leonardo Pacheco and Omar Rivera. You are a great team. Working with you was an unforgettable experience. Thank you for your friendship and support

This research was supported in part by U.S. Department of Defense, University Research Initiative (URI)-MURI Program, the Department of Homeland Security ALERT Center of Excellence and NACME.

Table of Contents

ABSTRACT	II
ACKNOWLEDGMENTS	VI
TABLE OF CONTENTS	VIII
TABLE LIST	X
FIGURE LIST	XI
1 INTRODUCTION	2
1.1 MOTIVATION	2
1.2 LITERATURE REVIEW	7
1.2.1 <i>Thermal characterization of energetic materials</i>	7
1.2.2 <i>Characterization of triacetone peroxide (AP) and other peroxides</i>	10
1.2.3 <i>Use of computational analysis to study energetic systems</i>	11
1.2.4 <i>Raman based characterization of hazardous liquids</i>	12
1.3 SUMMARY OF FOLLOWING CHAPTERS	13
2 MATERIALS AND METHODS	15
2.1 MATERIALS	15
2.1.1 <i>AP mixtures</i>	15
2.1.2 <i>Hazardous liquids</i>	17
2.1.3 <i>Commercial products</i>	17
2.1.4 <i>Containers</i>	17
2.2 DIFFERENTIAL SCANNING CALORIMETRY (DSC)	18
2.3 THERMAL GRAVIMETRIC ANALYSIS (TGA)	20
2.4 VIBRATIONAL SPECTROSCOPY	21
2.5 COMPUTATIONAL METHODS	23
3 THERMAL CHARACTERIZATION OF ACETONE PEROXIDE	23
3.1 INTRODUCTION	23
3.2 RESULTS	24
3.2.1 <i>Differential Scanning Calorimetry</i>	24
3.2.2 <i>Thermal Gravimetric Analysis</i>	31
3.2.3 <i>Structure Property Relationships</i>	38
3.3 CONCLUSIONS	41
4 STUDY OF THE INTERACTION OF AP WITH ENERGETIC	42
MATERIALS USING THERMAL ANALYSIS, SPECTROSCOPY AND COMPUTATIONAL METHODS	42
4.1 INTRODUCTION	42
4.2 RESULTS	43

4.2.1	<i>The AP/ ammonium nitrate system</i>	43
4.2.2	<i>The AP – Nitroguanidine system</i>	45
4.2.3	<i>The AP – TNT system</i>	48
4.2.4	<i>The computational analysis</i>	55
4.3	CONCLUSIONS	59
5	IDENTIFICATION OF CHEMICAL THREATS IN COMMERCIAL PRODUCTS USING RAMAN SPECTROSCOPY	60
5.1	INTRODUCTION	60
5.2	RESULTS	61
5.2.1	<i>Detection of peroxide in liquors</i>	61
5.2.2	<i>Detection of toxic industrial compounds in personal care products</i>	68
5.2.3	<i>Detection of CWAs in soft beverages</i>	71
5.2.4	<i>Effect of the type of container</i>	73
5.2.5	<i>Detection in colored liquids</i>	79
5.3	CONCLUSIONS	82
6	FINAL COMMENTS AND PATH FORWARD	83
7	REREFENCES	84

TABLE LIST

Tables	Page
Table 1 Volatility and IDLH levels for hazardous chemicals that are liquid at room temperature.	6
Table 2 Properties of the energetic materials used for the study.	16
Table 3. Description of containers.	18
Table 4. DSC results for energetic materials studied.....	28
Table 5. Activation energies for energetic materials.	30
Table 6. Summary of sublimation results.	37
Table 7. Thermal properties and descriptors used for the study.	40
Table 8. Statistical correlation of thermal data and structural descriptors.	40
Table 9. Interaction energies of AP based systems.....	58
Table 10. Thickness of common containers evaluated with FOC Raman.	75
Table 11. LOD and LOQ for TEP in colored liquids.	81

FIGURE LIST

Figures	Page
Figure 1. Example of the type of consumer products evaluated with Raman Fiber Optic for concealed hazardous liquids detection.	18
Figure 2. DSC thermogram of 2.5 mg TNT ran at 5 °C/min in a high pressure pan. (A) Melting transition, (B) Exothermic decomposition transition, (C) Onset for decomposition, (D) Peak decomposition temperature, (E) Enthalpy of decomposition	25
Figure 3. Thermogram of 2.3 mg AP ran at 5°C/min in a high pressure pan.	27
Figure 4. Overlay the decomposition peak of AP at different heating rates.	28
Figure 5. Heating rate vs. peak transition temperature for energetic materials. This representation is used to estimate the activation energy for decomposition. (slope = -E/R)	29
Figure 6. TGA and DSC curves for TNT at 5°C/min. The overlay presents the thermal stability of TNT though heating. The mass loss after 150°C can be associated to vaporization.	32
Figure 7. TGA and DSC curves for AP at 5°C/min. The high mass loss before melting is associated to the high sublimation and not to decomposition.....	33
Figure 8. Comparison of the mass loss of AP at different temperatures.	34
Figure 9. Curves of the rate of mass loss vs. temperature for AP, RDX, TNT and 2,4-DNT. This plot is used to estimate the enthalpy of sublimation. (slope = -ΔH/R)	36
Figure 10. Determination of enthalpy of sublimation by dynamic analysis. An extrapolation to heating rate = 0 gives an enthalpy of sublimation of 78048 KJ/mol.	38
Figure 11. Raman spectra of mixture of AP + AN containing 35% AN. Samples were solidified from a melt. Parameters: 3 scans, 30 s with a 785 nm laser.	44
Figure 12. Comparison of the DSC thermograms of AP, AN and a mixture containing 35% AN. Parameters: 2-3 mg sealed in a high pressure pan, 5 °/min.	45
Figure 13. Raman Spectra of AP + 40% NQ. Sample was solidified from a melt. Parameters: 3 scans, 30 s with a 785 nm laser.	47
Figure 14. Comparison of the DSC thermogram of AP + 40% NQ with the individual components. Parameters: 2-3 mg sealed in a high pressure pan, heating rate 5°C/min.	47
Figure 15. Raman spectra of a mixture 50% TNT and AP. Samples were melted and co-solidified. Parameters: 3 scans, 30 s with a 785 nm laser.	49
Figure 16. Comparison of the DSC thermogram of 50% TNT and AP. Parameters: 2-3 mg sealed in a high pressure pan, heating rate: 5 °/min.	49

Figure 17. Melting transition of a 39% AP mix with TNT. Sample was first melted and solidified. Parameters: 2-3 mg sealed in a high pressure pan, heating rate: 5 °/min.....	51
Figure 18. Effect of AP on the melting temperature of TNT.	52
Figure 19. FTIR-ATR spectra of AP-TNT mixtures (600-850 cm ⁻¹).....	53
Figure 20. FTIR ATR spectra of AP TNT blends (850-1100 cm ⁻¹).....	54
Figure 21. FTIR ATR spectra of AP TNT blends (1100–1400 cm ⁻¹).....	54
Figure 22. FTIR-ATR spectra of AP-TNT mixtures (2800–3200 cm ⁻¹).....	55
Figure 23. PM3 interaction conformations of: (A) NQ- AP, (B) TNT-AP,(C) NH ₃ –AP, (D) NQ-AP, (E) AP-AP.....	57
Figure 24. Shift in the decomposition temperature of AP mixed with nitro compounds.	59
Figure 25. Raman spectrum of liquors in their original containers acquired with fiber optic probe. Parameters were: 785 nm laser, 200mW and 2 sec of integration time.....	62
Figure 26. Raman spectra of acetone, peroxide and acetone peroxide explosive within a clear glass bottle at 785 nm, 10 second and a laser power of 200 mW.	64
Figure 27. Spectroscopic signatures of rum vs. acetone and peroxide at 785 nm, 10 second and a laser power of 200 mW.	65
Figure 28. Raman spectra of a mixture of hydrogen peroxide and Dewar's whiskey, using a 785 nm laser 3 scans at 10 s with 200 mW laser power.	66
Figure 29. Prediction of the concentration of peroxide in whiskey. Preprocess: None, Rank: 4, RMSECV: 2.41, Region: 539-1080 cm ⁻¹	67
Figure 30. Prediction of presence of peroxide in whiskey using PLS. In this model, 1 = present and 0 =not present.....	68
Figure 31. Raman spectrum of a perfume and mouthwash acquired with fiber optic probe. Parameters were: 785 nm laser, 100 mW and 1 s of integration time.....	69
Figure 32. Raman spectra of toxic compounds within a perfume clear glass bottle at 532 nm, 1 s and a laser power of 12 mW.....	70
Figure 33. Raman spectra of mouthwash-peroxide and mouthwash acetone mixtures.	71
Figure 34. Raman based detection of DMMP (a): Within Snapple clear glass bottle (532 nm laser, 1 acquisition, 1 s, 10 mW)	72
Figure 35. Raman based detection of DMMP. (a) Kiwi flavores Snapple; (b) DMMP in a mixture with Snapple juice in a clear glass bottle. (488 laser source, 1 acquisition, 30 s, 63 mW).....	73
Figure 36. Raman spectra of acetone obtained from different bottles. Parameters: 532 nm laser, 1 scan, 20 s, 33 mW.....	74
Figure 37. Raman spectra of acetone obtained from different bottles. Parameters: 785 nm 30 s at 200 mW.	75

Figure 38. Area of the 800 cm^{-1} peak of acetone at different collection times inside different bottles at 532 nm and 18 mW (1 scan).....	77
Figure 39. Transmission spectra of different bottles materials. Solid vertical lines indicate excitation lines in Raman experiments. Dashed lines indicate range for detected scattered radiation in the $200\text{-}1800\text{ cm}^{-1}$	78
Figure 40. Raman spectra of Gatorade lemon, orange and fruit punch.....	79
Figure 41. Spectrum of neat triethylphosphonate. The shaded area responds to the area used for TEP detection. The peak at 734 cm^{-1} is characteristic of organic phosphates like the CWAs.....	80
Figure 42. Peak area for the region of $675\text{ cm}^{-1}\text{-}855\text{ cm}^{-1}$ in orange, fruit punch and lemon Gatorade juice as a function of TEP concentration.....	81

1 INTRODUCTION

The molecular properties of the components of an explosive formulation are important both from the point of view of explosive power and stability considerations, since these can differ from individual components and from the point of view of threat detection because complex systems can mask the signatures used in current detection technologies. Often, the molecular interactions are said to sensitize or desensitize an explosive, changing its activation energy and decomposition behavior. Moreover, when using vibrational spectroscopy detection techniques, the resulting signatures may blend with non-explosive additives to mask the vibrational markers. The current work considers the scenario where explosives and other toxic chemicals are blended with home products or homemade compositions to modify its sensitivity or just to concealed or hide it for later use.

1.1 Motivation

Worldwide terrorist activity has led to an elevated concern toward national and international security.¹ Special interest has been placed in developing detection technologies for the early identification and response to threats. This threats may include more frequently homemade explosives (HME) assembled into improvised explosive devices (IED) than traditional artifacts. Also recent security restrictions on transporting liquids into an aircraft recognize the possibility of concealing a

hazardous material like a liquid explosive, chemical warfare agent (CWA) or toxic industrial compound (TIC) within commercial products to be used against people or property.

The use of homemade explosives (HME) has recently become more common and accessible. A recent search for “homemade explosives” in an internet search engine showed 198,000 files (“hits”) related to the term. The list included recipes, videos and complete downloadable manuals on the preparation of “recreational explosives”. The most cited HME are based on ammonium nitrate (AN) and acetone peroxide (AP). Ammonium nitrate is a very common material. It is the main component of many fertilizers. When combined with oil or a fuel, the mixture is known as ANFO, a powerful explosive used commercially. Peroxide-based explosives have become of increased interest mainly because they are easily prepared and are not detected by conventional methods of explosives detection since they do not contain nitrogen as constituent element. Peroxide based explosives are widely used all over the Middle East, and have recently been used in attacks like the explosion in the mass transportation system in London (2005). Triacetone triperoxide (AP) is a very unstable and powerful HME. It can be used both as a primary explosive and as a secondary explosive. In 2001 Richard Reid was arrested after attempting to detonate inside an aircraft a mixture of AP and pentaerythrol tetranitrate (PETN) hidden in his shoes. Apparently his plan failed because the sole of his shoes became wet deactivating the mixture. One of our objectives of the contributed work

is to study the interaction of AP with other energetic materials such as PETN to report the spectroscopic signature of the mixture and potential reactivity.

In August 2006 a terrorist plot to destroy aircrafts on transatlantic flights was discovered and timely stopped in London.² The plan involved the use of liquid explosives stored in beverage bottles that would pass check points without being detected. The liquids were going to be mixed in flight, generating an improvised explosive device (IED) and were going to be left in the aircraft and detonated remotely after the aircraft landed. Immediately, airport security agencies at UK and USA established a ban to all liquids except from medicine and infants food beyond checkpoint. The position has been changed several times to allow certain amount of liquid or gel based products. However, when or how terrorists would try to pass hazardous liquids into an aircraft to create a threat, explosive or chemical, is uncertain. For this reason it is important to develop a methodology through which it would be possible to differentiate between common products and compounds that can be combined for terrorisms intends.³

The use of hazardous liquids as tools for terrorist intentions is not a new modality. Terrorists have used hazardous chemicals that are liquids at room temperature in many occasions. Some examples are the bombing to the World Trade Center in 1993, the attempt to a Philippine Air flight in 1994 and the deployment of the CWA Sarin in a Japan subway in 1995. Some of these attempts involved the use of liquid explosives like nitroglycerin and other nitro compounds. Peroxide based explosives are also easily prepared from common liquids such as acetone. Other extremely

hazardous liquids are chemical warfare agents (CWAs) and Toxic Industrial Compounds (TICs). TICs are chemicals toxic to humans that are widely used in manufacturing or primary material processing. They have received more attention in recent years because ease of accessible in large quantities by potential terrorists.⁴ Chemical warfare agents (CWA) differ from TICs in that they are intended to immediately incapacitate as many soldiers as possible when released against an enemy in war. To do this, the CWA must be toxic enough to cause an instant response when it is inhaled or comes into contact with the skin. Table 1 contains examples of some hazardous liquids and their volatility. Highly volatile materials can be easily deployed just by opening the container. Along with the volatility of these chemical is the Immediately Dangerous to Life or Health (IDLH) level and is defined by the US National Institute for Occupational Safety and Health. This value is the concentration in air that would cause immediate or delayed adverse health effects after 30 min of unprotected exposure.

Table 1 Volatility and IDLH levels for hazardous chemicals that are liquid at room temperature.

Chemical	Description	Volatility (mg/m ³)	IDLH (ppm)
GB (C ₄ H ₁₀ FO ₂ P)	CWA. Sarin. Organophosphate nerve agent.	16,091	.03
AC (HCN)	CWA. Hydrogen Cyanide, Blood agent	1,080,000	N.A.
HNO ₃	TIC. Nitric acid	63,000	25
H ₂ SO ₄	TIC. Sulfuric acid. A strong acid	1.3	3.7
GD (C ₇ H ₁₆ FO ₂ P)	CWA. Soman, a Nerve agent	3,900	.008
PCl ₃	Phosphorus Chloride	130,000	25

If these chemical are used in big quantities toward civilians, the amount of casualties will be huge. However even small quantities of a toxic chemical or a small IED can cause chaos specially in closed environments like an aircraft or a train or high transit areas like a building or a transportation terminal.

Various approaches have been taken to detect and identify chemical agents including HPLC/MS,⁵ GC/MS,^{6, 7} Ion Mobility Spectroscopy,^{8, 9} Infrared Spectroscopy and Raman Spectroscopy.¹⁰⁻¹³ Vibrational spectroscopy has the advantage that provides chemical information and provide with the sensitivity and selectivity required for Chemical Point Detection (CPD) systems and has the potential for remote sensing. In specific Raman is able to analyze samples though various transparent glass and plastic containers, such as beverage bottles or food containers.^{12, 14, 15} This allows the contents of a container to be analyzed without opening the container, minimizing exposure to potentially harmful substances and

helping to speed the screening process. In this work concealed liquids scenarios are studied by Raman spectroscopy. Hazardous liquids including CWAs TICs and other prohibited are studied through the walls of commercial drink containers. Fiber optic coupled Raman was used to evaluate the content of plastic and glass containers. Standoff Raman detection was used to obtain information of hazardous liquids and mixtures from 20 feet distance. The objective of this work is to study, in real field conditions, the detection of CWAs and TIC's by point detection or with a as a remote surveillance tool.

1.2 Literature Review

1.2.1 Thermal characterization of energetic materials

Energetic materials have been extensively characterized by thermal analysis (TA). Differential thermal analysis (DTA), differential scanning calorimetry (DSC) and thermal gravimetric analysis (TGA) are probably the most used methods for energetic materials. For example In 1995 Liu reported phase diagrams for binary systems consisting of energetic materials. The eutectic compositions of eleven mixture systems of energetic materials, including Tetryl/PETN, PETN/RDX, HMX/P Explosive and RDX/NQ, were obtained by constructing a special phase diagram for the correlation of the apparent heat of fusion with composition. This method allowed the estimation of the eutectic point for materials that decompose exothermically at melting. In order to construct HX-phase diagrams of binary and ternary systems, it was assumed that the eutectic is a mechanical mixture, that its apparent fusion heat

(ΔH) involves no heat of mixing, and that the temperature dependence of ΔH is negligible. This method does not consider intermolecular forces and assemblies.¹⁶

In 1993 Brill and James presented an extensive review on the thermal decomposition mechanisms of nitroaromatic explosives. The review included thermal and computational data that describe the decomposition of materials such as nitrobenzenes and nitrotoluenes. He also presented discrepancies in literature and voids in related research.¹⁷

The determination of kinetic parameters involves a critical aspect to compare the stability of reactive compounds. In 2002 the thermal decomposition behavior of PETN, RDX, HNS and HMX were studied by differential scanning calorimetry (DSC). The activation energy for the decomposition process and frequency factor was obtained by the Kissinger model for non-isothermal analysis. The comparison of melting point, peak temperature of exothermic peak and the activation energies was used to describe reactivity and compatibility with silicone binders.¹⁸

The use of TA has supported not only the development of new materials but also support manufacturing of commercial formulations. In 2000, the thermal properties of composition-B were reported by Lee and Hsu. Composition B is a military explosive composed of RDX and TNT and wax. The typical manufacturing process of this material is by melting all components and pouring into a shell followed by crystallizing by a controlled cooling rate to room temperature. The motivation for this study was that the DSC curves of materials have changed in recent manufactured lots. Therefore, they wanted to know how the presence of the differences in mixtures

influenced the thermal behaviors and safety characteristics of the explosive formulation. Hazard assessment was performed by evaluating the activation energy of decomposition by DSC (Kissinger method) and by TGA (Ozawa method). They concluded that deviation in the composition induced lower activation energies and increased sensitivity.¹⁹

The potential hazard of unexpected contaminants in explosives was studied by Peng et al. (2004) using DSC. This group reported on the stability and reactivity of HMX when interacting with common contaminants such as solvents, salts and acids. The incompatibility of HMX with contaminant reactions influenced temperature control, heating and cooling systems, and produced a secondary unexpected explosion.²⁰

The mechanism of decomposition of ammonium nitrate (AN) and its role in the sensitization of nitro compound like TNT have been studied in detail. In 1994 Oxley reported the effect of ammonium nitrate on nitroexplosives mixtures. Ammonium nitrate acted as an oxidizing agent in these blends. The decomposition of AN produces HNO_3 and NH_3 . These species can attack the nitro compound destabilizing the mixture and reducing the activation energy.

Various approaches can be taken to characterize the vapor pressure of materials. These involve direct measurements with a monometer, the use of mass spectrometry to monitor the gas phase concentration or the species, the measure of sample volatilization by vacuum diffusion (use of a Knudsen cell) and the boiling point determination under different pressures by differential scanning calorimetry.

Several studies mention thermal gravimetric analysis as a rapid and convenient method to characterize the vapor pressure curves and enthalpies of sublimation and vaporization of volatile materials. Guekel et al measured the volatilization rates of pesticides at ambient pressure by isothermal thermogravimetry.²¹ Other groups have used the techniques to estimate the vapor pressure of pharmaceutical compounds.²²⁻²⁵ The applications include the examination of antioxidants, dyes and explosives of different vapor pressures.^{26, 27}

1.2.2 Characterization of triacetone peroxide (AP) and other peroxides

Organic peroxides tend to be very reactive materials. Their hazards are not only associated to HME. Accidental explosions in industries that work with bulk amounts of peroxides led to many investigations of the thermal hazards associated to mixing peroxide with other chemicals. However, the thermal analysis of peroxides is not as frequent as for other energetic materials.

The use of thermal analysis to study the reactivity and thermal decomposition of specific peroxide based hazardous industrial compounds such as methylethylketone peroxide (MEKPO) was studied by Differential Scanning Calorimetry and kinetic analysis.^{28, 29}

Miyake created a flow diagram to classify organic peroxides hazard on the basis of their mixing reactivity at different levels from test tubes to DSC.³⁰

Regarding AP, in 2002 Oxley characterized by thermal analysis and GC-MS the decomposition of AP. The decomposition products were characterized and a decomposition mechanism was proposed. The activation energy was calculated by isothermal analysis.³¹

In 2005 Oxley studied the vapor density of AP by GC-MS. The vapor pressure and enthalpy of sublimation were calculated and reported.³²

Our objective is to report the comparison of thermal properties of AP with respect to more known energetic materials like TNT and PETN. This will help in the assessment of the reactivity of this material. Also the known instability of AP will be quantitatively described by thermal analysis.

1.2.3 Use of computational analysis to study energetic systems

Computational methods have been used for energetic materials mainly to characterize materials structure and proposed decomposition mechanisms. Saraf used quantitative structure property relationships (QSPR) system to evaluate thermal properties of nitro compounds. He used quantum descriptors like the energy of the HOMO and LUMO dipole moment and others to correlate with the onset temperature and heat of decomposition for a series of nitro compounds. The reported correlation coefficient squared was 0.7.³³

Karelson and Katrisky compiled a variety of topological and quantum descriptors that can be used for QSPR studies of reactive systems.³⁴ One of the interests of this work is to find trends in thermal properties of high-energy systems by correlating temperatures and heat of transitions to topological and quantum properties.

The interaction of the NH_4^+ and H^+ ions with HMX was studied by optimizing complexes with a B3LYP method. The study consisted in monitoring the bond lengths and cleavage energy for the NNO_2 bond at interaction.³⁵

In 2000 Jinshan used an *ab initio* approach to calculate the interaction energy (IE) between systems containing the NO_2 and NH_2 groups. The approach was used to find interaction geometries between ammonia and nitromethane. For larger systems such as trinitrobenzene (TNB) and triaminotrinitrobenzene (TATB) a PM3 MO was used. The results of interaction energies of the amino group are compared to the IE of systems that are known to act as desensitizers.³⁶ For this work the interaction energy of AP interactions will be determined by semi empirical and DFT methods.

1.2.4 Raman based characterization of hazardous liquids

Raman spectroscopy presents various strengths that make it a potential technique for detection of chemical agents in the field. Since Raman scattering brings information on vibrational modes of molecules it can be used as a specific mean of detection. Water does not present a strong spectra making possible to analyze a variety of samples where water can be interference. In 1999 Christensen reported

the use of a portable Raman system to characterize chemical agents sealed on glass containers. Samples were part of a library for military training in chemical agent identification.¹⁵ Fiber optic coupled Raman spectroscopy (FOCRS) was used to characterize liquid explosives and commercial liquids.³⁷ The results suggested that the technique can be used to discriminate if the commercial liquids are the intended or a hazardous liquid. Eliasson and collaborators have reported the detection of drugs and liquid explosives concealed in dense colored plastic containers.¹⁴ The technique consists of a variation of the angle of detection to collect scattered Raman radiation. This approach allowed to reduce container fluorescence and interference.

In 2002 Harvey evaluated a portable Raman system for forensic applications. The evaluation of chemical agents in glass and plastic vials included library matches and variability due to different user and equipment.¹² The third component of the present work is to evaluate Raman as a detection tool for concealed hazardous liquids. Liquid explosives and chemical agents were detected in a variety of consumer product containers either pure or missed with the commercial product.

1.3 Summary of Following Chapters

This work is organized in three reports containing results published and two manuscripts to be submitted. The justification and relevant literature is discussed in Chapter 1. All methodologies will be discussed in Chapters 2. Then the results will

be discussed in separate chapters. First, the thermal characterization of AP will be presented in Chapter 3. The results will be compared to other energetic materials. The relations between structure and thermal properties will also be discussed. On the second report (Chapter 4), AP was combined from melt and from solution with other energetic materials. The phase diagram is being estimated when the thermal stability has allowed it. The spectroscopic signatures of these compositions will be reported. Then the decomposition of such mixtures was studied by DSC. Computational analysis was used to estimate interaction energies for possible conformations.

Chapter 5 contains the third report; the detection of peroxide based mixtures and other hazardous materials were studied when concealed in commercial products. The detection limits in colored liquids and the effect of the container were studied. Final comments and recommendations are presented in Chapter 6.

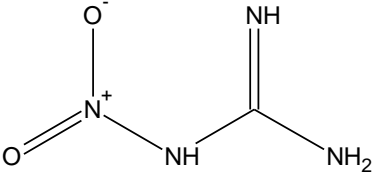
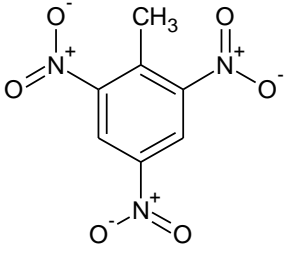
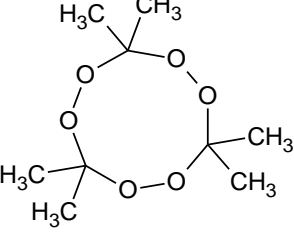
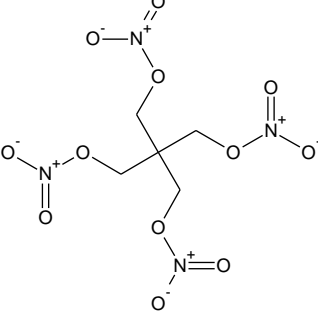
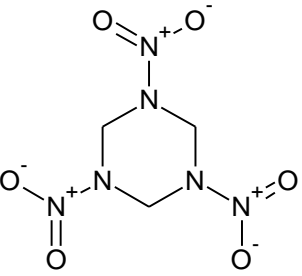
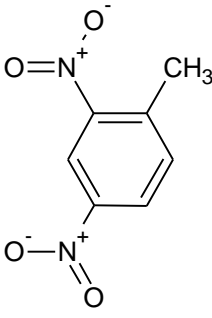
2 MATERIALS AND METHODS

2.1 Materials

2.1.1 AP mixtures

Table 2 contains the structures and properties of the energetic materials used in this work. The synthesis of the AP was done following the general preparation of cyclic peroxides,³⁸ with the specific ketone and hydrogen peroxide in a 1:1 molar ratio in a cold system catalyzed by HCl. Acetone was cooled to between 0°C and -5°C with acid. Addition of hydrogen peroxide was done drop wise to prevent violent reactions. White crystalline products were obtained, filtered and washed with distiller water. Recrystallization of the products was then carried out in dichloromethane. Nitroguanidine, trinitrotoluene and 2,4- dinitrotoluene were acquired from ChemService (USA). RDX and PETN were obtained from synthesis according to current literature.^{39, 40}

Table 2 Properties of the energetic materials used for the study.

 <p>Nitroguanidine Mw= 104.069 g/mol Detonation velocity = NA Secondary explosive Sensitivity= Very low</p>	 <p>TNT MW= 227.13 g/mol Detonation velocity=6930 Secondary explosive Sensitivity= very low</p>
 <p>AP MW= 222.236 g/mol Detonation Velocity=5250 Primary Explosive Sensitivity= High</p>	 <p>PETN MW= 316.135 g/mol Detonation Velocity= 8260 Secondary Explosive Sensitivity=Moderate</p>
 <p>RDX MW=222.117 g/mol Detonation Velocity= 8700 Secondary Explosive Sensitivity = Very low</p>	 <p>2-4 DINITROTOLUENE MW=182.13 g/mol Secondary explosive Sensitivity=Low</p>

2.1.2 Hazardous liquids

The hazardous materials used for the detection experiments were: hydrogen peroxide 50% wt. in water, toluene, benzene and 99.5% ethanol from Aldrich chemicals. Also, acetone, dimethylmethyl phosphonate (DMMP) and triethyl phosphate (TEP) from Fisher Scientific were used. Fisher chemicals were obtained from Fisher Scientific International, Chicago, IL. Aldrich chemicals were obtained from Sigma-Aldrich Chemical Company (St. Louis, MO). DMMP and TEP are structural analogs of chemical warfare agents (CWA) such as TABUN, SARIN, SOMAN, and GF and therefore are commonly used as CWA simulants (CWAs).

2.1.3 Commercial products

The commercial liquid products employed in this study were: Gatorade variety drinks (distributed by The Gatorade company, Chicago, USA), Scope mouthwash (distributed by Procter and Gamble, Cincinnati, USA), Dewar's White Label whiskey (imported by Mendez & Co., PR), Ron Bacardi light rum (Produced by Bacardi Corp, PR), V8 vegetable juice (distributed by Campbell Company, NJ, USA), 7Up (distributed by Coca Cola Company, Puerto Rico).

2.1.4 Containers

The effect of the type of container was studied. Figure 1 presents a variety of the containers used for this study. The effect of thickness and color of commercial glass and plastic containers were evaluated (See Table 3 for details). The Raman spectrum of the original liquid in its container was obtained. Then the liquid was

replaced by a hazardous liquid or mixture. The light absorption of the container at different wavelengths was studied.



Figure 1. Example of the type of consumer products evaluated with Raman Fiber Optic for concealed hazardous liquids detection.

Table 3. Description of containers.

Container	Material	Description
Green glass bottle	Glass	Soda water (Canada Dry®)
Amber glass bottle	Glass	Malt beverage (Malta India®)
Clear glass bottle	Glass	Perfume (Adidas®)
Clear glass bottle	Glass	Juice (Snapple®)
Blue plastic bottle	Plastic (PET)	Water (Aquacal®)
Green Plastic bottle	Plastic (PET)	Refreshment (7up®)
Clear plastic bottle	Plastic (PET)	Baby bottle
Clear plastic bottle	Plastic (PET)	Perfume (Ralph® body spray)

2.2 Differential Scanning Calorimetry (DSC)

A TA Instruments Q10 Differential Scanning Calorimeter (DSC) with a nitrogen gas flow was used. High pressure hermetic pans were used for the DSC experiments.

The samples were sealed under a nitrogen flow to maintain an inert atmosphere. For explosives interactions studies, AP and other solid explosives were measured in a high pressure DSC pan. The total mass was kept at 10 mg. The mixture was melted in the DSC. The sample pan was opened for spectroscopy experiments and DSC to study decomposition products. For these experiments 1-3 mg of the mix were used.

For kinetics experiments, sample sizes were within 0.1 mg. A heating rate of 5°C/min was used for all explosive samples. The DSC was calibrated with respect to temperature and enthalpy with indium (NIST Traceable m.p. 156.89 °C).

The energy of activation of the decomposition process was calculated according to order independent variable heating rate kinetics. This method was applied to differential thermal analysis by Kissinger.⁴¹ Ozawa extended the applicability of this method to DSC and TGA studies.⁴² The Kissinger method estimates the activation energy from the plot of heating rate versus peak transition temperature according to Equation 1:

$$\ln\left(\frac{\beta}{T_p^2}\right) = \ln\left(\frac{AR}{T}\right) - \frac{E_a}{RT_p} \quad 1$$

From this relationship the activation energy is obtained from slope of the plot and the frequency factor (A) can be obtained from the intercept. This method was selected since it is well known, is the basis of an ASTM method to characterize reaction hazards of energetic materials and will allow the comparison of our results to the

literature values of materials such as TNT and PETN.^{18, 43} Dynamic experiments were run at heating rates (β) of 5°C/min, 10°C/min, 15°C/min and 20°C/min.

2.3 Thermal Gravimetric Analysis (TGA)

Standard platinum sample holders were used for all samples. Aluminum pans on top of the platinum holder were used to contain the samples to a specific area. The TGA was calibrated for temperature using the nickel Curie Point (356°C) and for weight according to manufacturer optimized procedures. All samples were first evaluated from room temperature (RT) to 500°C at 10°C/min to preview the mass loss profile. Once the temperature for zero mass loss was attained the method was refined to the appropriate temperature range. All samples were compared at 5°C/min. The study of the sublimation of AP by TGA consisted in the determination of the rate of mass loss at several isothermal points over the temperature range of interest.

The TGA procedures for vapor pressure and enthalpy of sublimation estimation are based in the principle that sublimation as well as evaporation is a zero order process and the mass loss at isothermal conditions must be constant.²³ The mathematical expression that correlates the vapor pressure derives from Langmuir work of 1913:

$$\left(\frac{1}{a}\right) \frac{dm}{dt} = p\alpha \sqrt{\frac{M}{2\pi RT}} \quad 2$$

where $(1/a)dm/dt$ is the rate of mass loss per unit area ($\text{kg s}^{-1} \text{m}^{-2}$), p the vapor pressure (Pa), M the molecular weight of the vapor of the evaporating compound (kg

mol⁻¹), R the gas constant (JK⁻¹ mol⁻¹), T the absolute temperature (K), and α is the vaporization coefficient. In vacuum, α is assumed to be 1, but in a flowing gas atmosphere like in TGA experiments α can have different values. Rearranging the Langmuir equation gives:

$$p = kv \tag{3}$$

where $k = \sqrt{2\pi R/\alpha}$, and $v = (1/a)(dm/dt)\sqrt{(T/M)}$.

If a known, thermally stable, compound of known vapor pressure is used it is possible to correlate the vapor pressure to the mass loss rates obtained by TGA. A plot of ln v against 1/T should give a straight line plot of slope, ΔH/R. In a similar approach the data of dm/dt can be fitted into an Eyring equation by plotting ln (dm/dt /T) vs. 1/T. The graph would have the form;

$$\ln \left(\frac{k}{T} \right) = \left[\ln \left(\frac{k_B}{h} \right) + \frac{\Delta S}{R} \right] - \frac{\Delta H}{RT} \tag{4}$$

The change in enthalpy (ΔH) of sublimation is obtained from the slope of the graph and the intercept can provide the entropy change (ΔS) associated to the process.

2.4 Vibrational Spectroscopy

A Renishaw RM1000 system microscope with a Renishaw NIR 785nm laser was used to obtain the spectra of explosives mixtures. The Raman shift spectra were

obtained from 200 cm^{-1} to 3200 cm^{-1} . The system was calibrated using silicon single crystal sample as an external standard by measuring the vibration at 520.56 cm^{-1} .

Two portable fiber optic Raman spectrometers (Raman Systems R-3000 HR) were used to evaluate the spectral signature of commercial products. The excitation wavelengths used were 532 nm (green) with 25 mw maximum output power and 785 nm (Red) with 250 mw maximum output power. The spectra of the original liquid in its container was collected through the walls. A volume of 30 mL of a hazardous liquid compound was then transferred and analyzed in different commercial containers varying the time and the power. Raman spectra were acquired from 200 cm^{-1} to 1800 cm^{-1} . The systems were calibrated using Fisher Scientific HPLC grade cyclohexane.

Raman measurements at 488 nm excitation line were performed using a MEADE ETX -125, (Maksutov-Cassegrain, D = 127 mm, F = 1900 mm) telescope coupled to a Renishaw Raman microscope RM2000 equipped with a Coherent INNOVA 310-8 Ar+ laser that produced a 488 nm (blue) beam. The liquids in the bottles were placed about 20 feet from telescope. The spectra were recorded in the Raman shift range of 100-3200 cm^{-1} . One acquisition was collected varying the integration time and the laser power.

Attenuated total reflectance spectra were acquired using a Magna FTIR bench (Thermo, USA) and a single bounce ATR accessory with diamond crystal. The

collection parameters were 256 scans at 4 cm⁻¹ resolution. The background is acquired initially. Spectra were background corrected.

2.5 Computational methods

All structures were optimized with Gaussian 03 Package. A B3LYP DFT method with 631G** basis set was applied for the structure optimization. For the structure property relationship study (QSPR) topological descriptor were derived using PCM Software and the Gaussian input file. The quantum descriptors were derived directly from the B3LYP optimization of the molecule, its anion and cation species. All data was analyzed using SSPS software and Statgraphics.

For the interaction studies the structures were optimized in Hyperchem 8.0 software using a MM force field approach to find possible conformations. The structures were optimized using Gaussian and AM1 or PM3 routines.

3 THERMAL CHARACTERIZATION OF ACETONE PEROXIDE

3.1 Introduction

The first step of this work is to characterize by thermal analysis the thermal behavior of triacetone triperoxide (AP). It is well known that peroxides are very unstable compounds there is few information of the thermal properties. AP was characterized by Differential Scanning Calorimetry (DSC) and Thermal Gravimetric Analysis (TGA).

Melting point, decomposition temperature and enthalpies of transitions were determined and compared to other known materials. Statistical analysis was used to find correlations between thermal properties and structural descriptors. The activation energy was calculated to be 50.6 KJ/mol which is well below the secondary explosives evaluated. Dynamic and isothermal methods were used to characterize the sublimation process at a temperature range under exothermic decomposition. The enthalpy of sublimation and kinetic parameters were estimated from direct mass loss rate measurements. The enthalpy of sublimation was estimated in 70 KJ/mol being the lowest between the materials evaluated.

3.2 Results

3.2.1 Differential Scanning Calorimetry

Figure 2 presents the typical thermogram of an energetic material, TNT. Exothermic transitions are upward peaks. The transitions of interest are marked. The melting peak temperature, enthalpy of melting, onset of decomposition, peak decomposition temperature and enthalpy of decomposition were recorded.

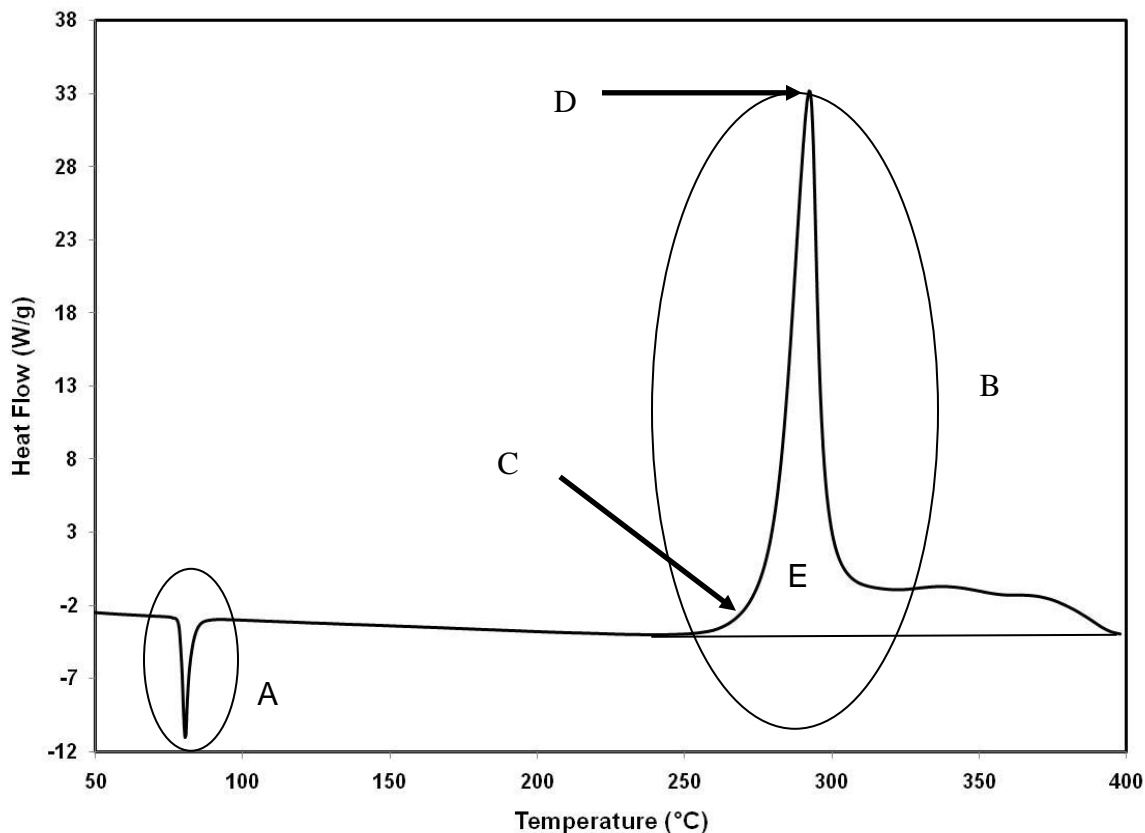


Figure 2. DSC thermogram of 2.5 mg TNT ran at 5 °C/min in a high pressure pan. (A) Melting transition, (B) Exothermic decomposition transition, (C) Onset for decomposition, (D) Peak decomposition temperature, (E) Enthalpy of decomposition

A good explosive must release a high amount of energy and at the same time be thermally stable for processing, handling and storage purposes. TNT presents a low melting temperature (~ 80°C) and its thermal decomposition occurs at relatively high temperature (~ 300°C). These properties have boosted its importance as a commercial and military explosive. The low melting temperature permits to be melt casted with a variety of other explosives such as RDX and HMX into melt casted

compositions. It is commonly used as reference material for assessment of power and stability of new explosives. Figure 3 presents the typical DSC thermogram of AP. The melting temperature of 83 °C is in good agreement with reported values (80°C - 90°C). The enthalpy of the transition was of 95.6 J/g (endothermic transition). This is lower than previous reports (110 J/g), suggesting differences in purity or crystallinity.⁴⁴

The decomposition process of AP has an onset about 170°C (at 5°C/min) and develops to a maximum heat release at 193°C (100° lower than TNT). The exothermic decomposition has an enthalpy of 29537 J/g. The decomposition transition present a shoulder that develops into a small peak at higher heating rates, indicating the decomposition occurs in steps. Note that the released energy of AP at decomposition compares to the exothermic behavior of TNT.

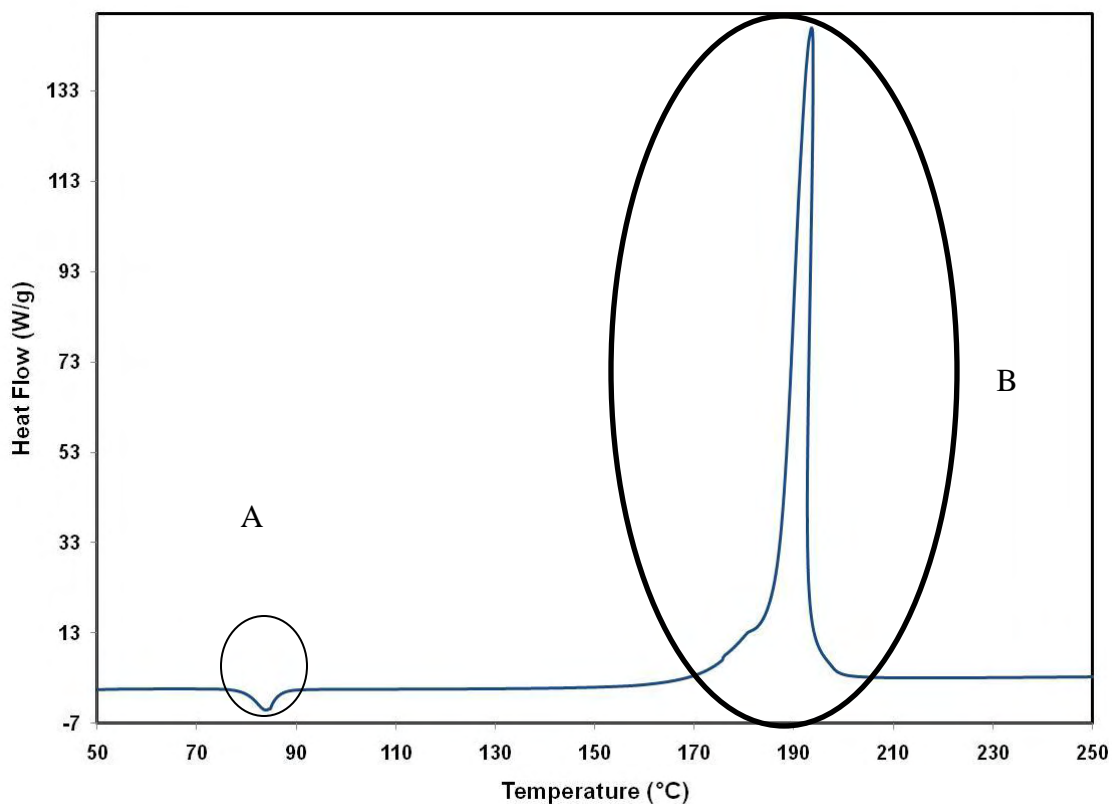


Figure 3. Thermogram of 2.3 mg AP ran at 5°C/min in a high pressure pan. (A) Melting transition; (B) Exothermic decomposition.

Table 4 summarizes the DSC data for TNT, AP, NQ, DNT, RDX and PETN. The thermal data was obtained at 5C for all samples. The order for exothermic released energy at decomposition is TNT > RDX > AP > PETN > 2,4-DNT > NQ. It is noticeable that AP has a decomposition enthalpy comparable to TNT and RDX but has the lower peak decomposition enthalpy.

Table 4. DSC results for energetic materials studied.

Name	T_m (°C)	H_m (J/g)	T_{onset} (°C)	T_{dec} (°C)	H_{dec} (J/g)
TNT	80.8	96.79	306.88	312.71	3486
2,4 DNT	70.17	124.2	290.38	307.55	1695
NQ			226.04	228.73	688
PETN	129.3	85.58	136.92	199.63	2163
RDX	202	105	204	213	3327
AP	83.93	106.3	170	193	2957

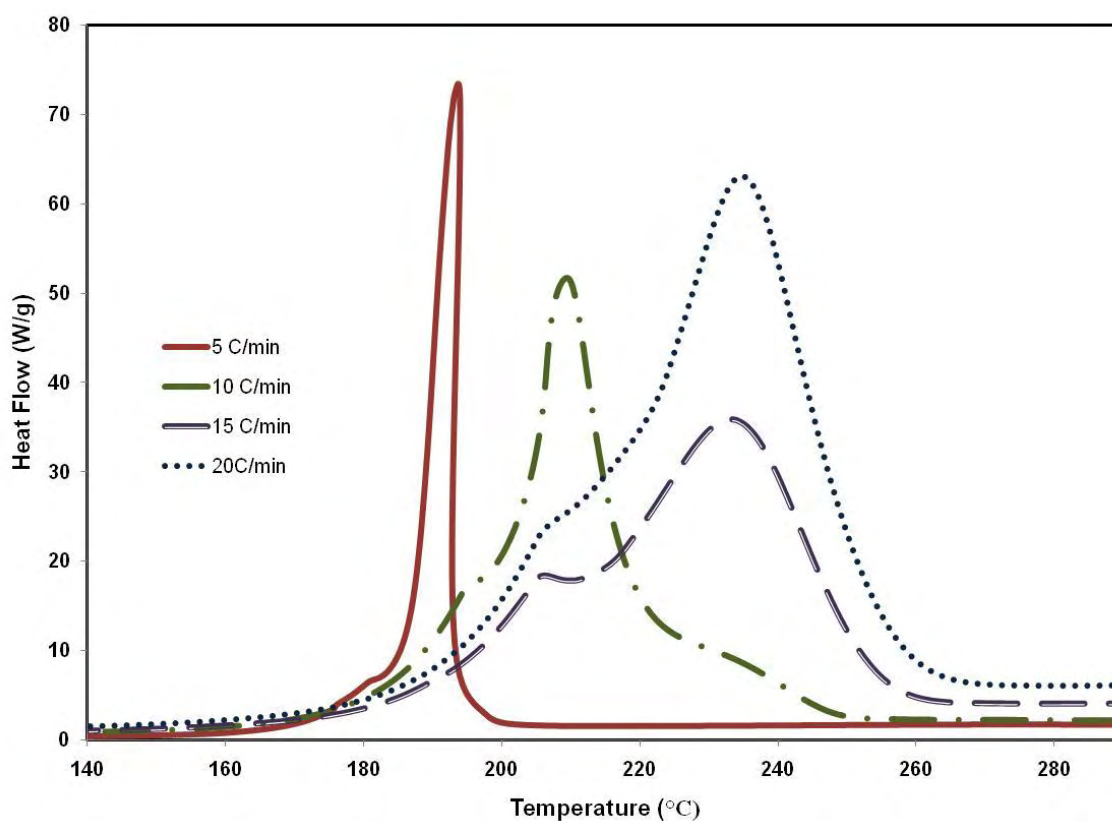


Figure 4. Overlay the decomposition peak of AP at different heating rates.

Figure 4 present the overlay of the decomposition peak of AP at different heating rates (HR, β). At 5 °C/min the decomposition presents a sharp peak. However at

higher heating rates a shoulder develops suggesting that the decomposition occurs on more than one step. The peak temperature is monitored and plotted against heating rate. The plot is fitted into Eq. 1 to obtain the activation energy according to the Kissinger method.

Figure 5 summarizes the data for the determination of activation energy of some energetic materials. The four evaluated materials are grouped into two groups one decomposing near 200 °C (AP and PETN) and the other that decomposes at 300°C (DNT and TNT).

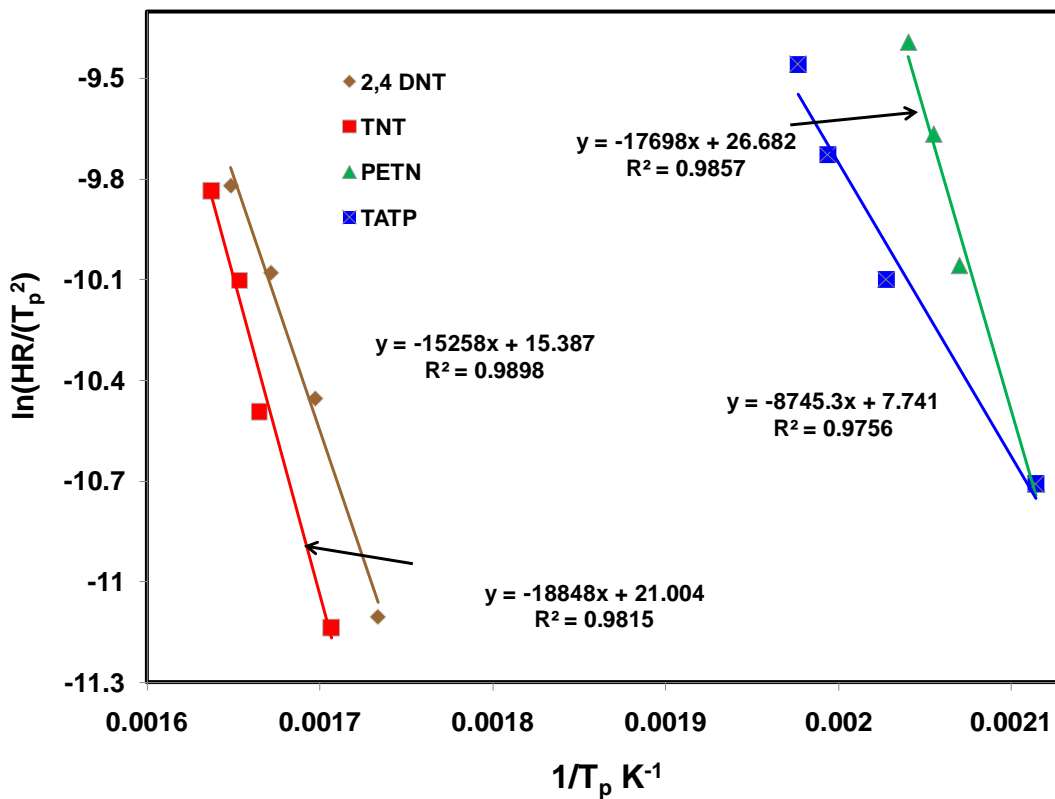


Figure 5. Heating rate vs. peak transition temperature for energetic materials. This representation is used to estimate the activation energy for decomposition. (slope = -E/R)

Table 5. Activation energies for energetic materials.

Material	Activation energy (Peak decomposition) (KJ/mol)	Data Correlation R^2	Literature values (KJ/mol)
TNT	156.7	0.982	144 (1)
Onset	165.5	0.976	
2,4 DNT	126.9	0.989	
Onset	132.4	0.966	
PETN	147.1	0.985	175 (2)
Onset	72.9	0.948	
AP	72.7	0.976	153 (3)
Onset	106.3	0.962	
RDX			144 (2)

(1) Los Alamos Center for Dynamic material properties Explosive properties data Series
(2) Thermochimica Acta 392-393 (2002) 173-176
(3) Propellants, Explosives, Pyrotechnics 27, 209 — 216 (2002)

Table 5 present the activation energies for the materials evaluated. For TNT, DNT and PETN there was good agreement with cited values. However, the activation energy of AP was 50 % lower than the reported value. The value found in the current study is more consistent with a highly reactive material with a high sublimation rate at RT. The value previously reported for AP is very similar to the values of PETN, TNT and RDX, materials known as secondary explosives and with implicit higher activation energy. However the difference suggests numerous possibilities. First it is worth to mention that it is normal to find considerable different values for the cited activation values. Brill and James discussed the origin of these differences in his work.¹⁷ The decomposition process can be divided in three main steps. The induction or bond breaking step tends to be higher but less appreciable by dynamic

methods. The second phase will be lower but comprehend the acceleratory phase of the decomposition to its peak. Most of the reported values are representative of this phase. The values are slightly lower during this phase because of autocatalysis. The third phase is known as the decay phase and is highly dependent of the concentration of decomposition products that will catalyze the process to completion. For the current study the activation energy for AP at peak decomposition temperature is 72.2 KJ/mol. However when the measurement is taken at the onset of decomposition the value is 106.3 KJ/mol. These values indicate that the decomposition is autocatalyzed by the products formed during the first phase.

3.2.2 Thermal Gravimetric Analysis

Figures 6 and 7 include the DSC and TGA data for TNT and AP. Together these data can provide information on the mass changes that can accompany transitions. The heating rate utilized was 5°C/min. TNT does not present a considerable mass loss until passed 150°C. Since this mass loss occurs after the melting, but before decomposition temperature, it can be assumed that it is associated to sublimation. The boiling point is not observed in the DSC because the test is performed in a hermetically sealed pan, keeping the samples mass constant. AP loss of mass before the melting transition suggests a rapid sublimation and high vapor pressure. AP is a good candidate for thermo gravimetric based sublimation studies due to its rapid mass loss at temperatures below decomposition. Figure 8 shows a set of

experimental TGA thermograms which represent isothermal mass loss from 25°C to 50°C. The plots of mass versus time show a reduction that is almost linear, which indicates that the sublimation followed apparent zero-order kinetics. Deviations from a zero order straight line can be due to a change in surface area for powder samples, interaction with the aluminum pans or degradation of the samples.

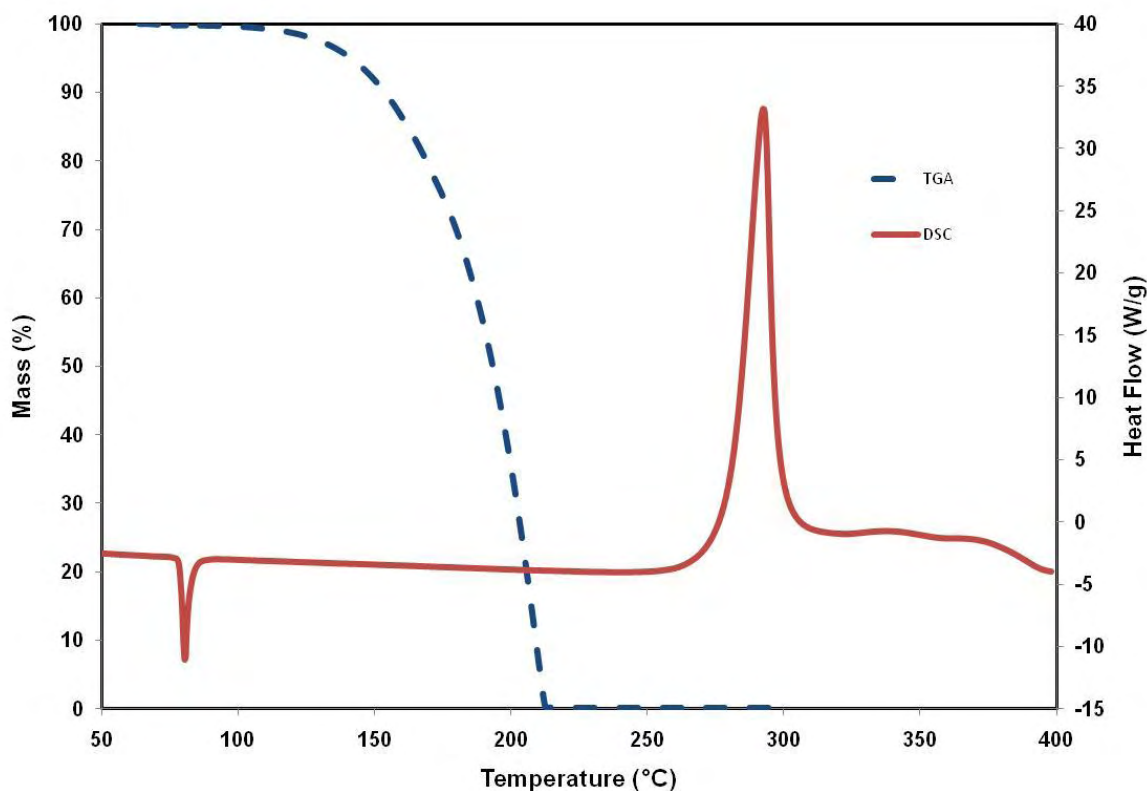


Figure 6. TGA and DSC curves for TNT at 5°C/min. The overlay presents the thermal stability of TNT through heating. The mass loss after 150°C can be associated to vaporization.

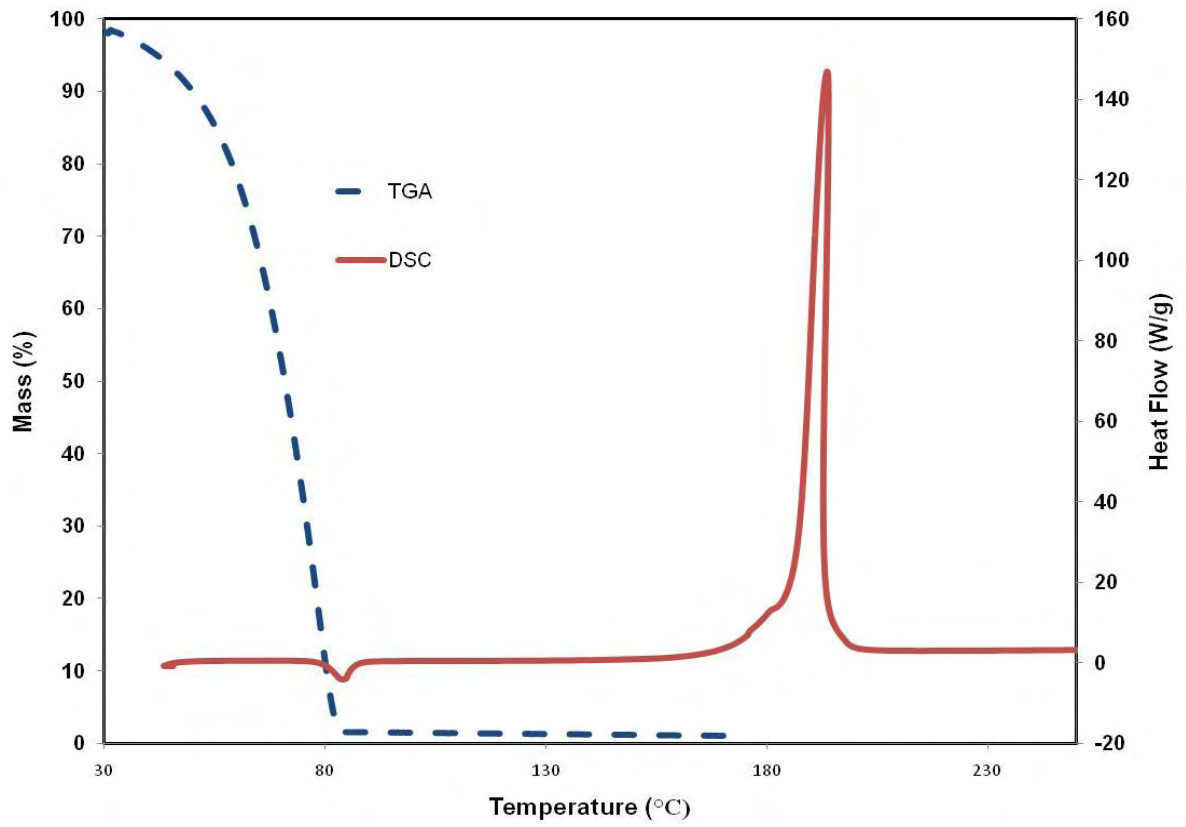


Figure 7. TGA and DSC curves for AP at 5°C/min. The high mass loss before melting is associated to the high sublimation and not to decomposition.

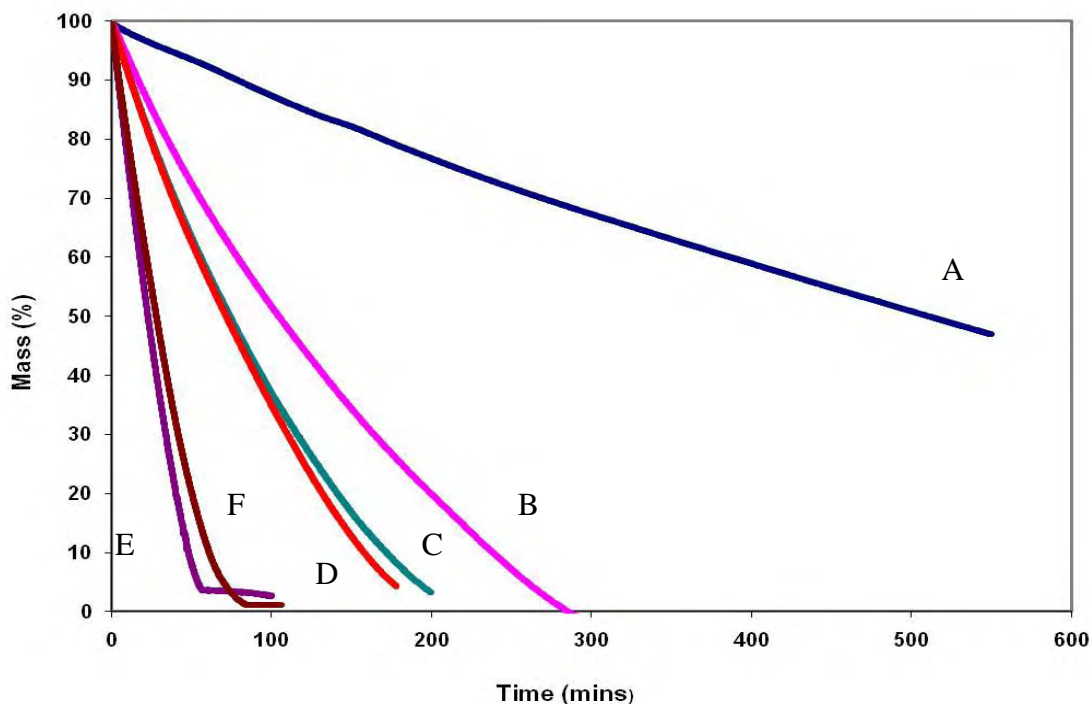


Figure 8. Comparison of the mass loss of AP at different temperatures. (A) 30°C; (B) 35°C; (C) 40°C; (D) 45°C; (E) 50°C; (F) 55°C.

The rate of mass loss (dm/dt) was obtained from TG plot at several temperatures. Figure 9 contains the Eyring plots of AP, RDX, TNT and 2,4 DNT. The enthalpy of sublimation is obtained from the slope of the linear regression. The method is a very appropriate for material that exhibits a high vapor pressure. However for material with low vapor pressure the fit into the model is more difficult due to the noise in the data. This is demonstrated by the lower correlation coefficient (R^2) of RDX. RDX was analyzed at a higher temperature range to induce more mass loss. This approach can induce degradation of the material and loss due to moisture content as well.

Table 5 includes all sublimation enthalpies obtained during this study. Since the enthalpy of sublimation of TNT and DNT has been reported previously, they serve as a standard to confirm how accurate the results by thermogravimetry are. In 2002 Chickos compile the sublimation data of over 1200 references from 1910 to 2001.⁴⁵ In general for TNT the results ranged from 102 KJ/mol to 113 KJ/mol. For 2,4-DNT the values were from 95.8 KJ/mol to 98.8 KJ/mol. The results for DNT and TNT in this work (105.4 KJ/mol for TNT and 95.4 KJ/mol for 2,4-DNT) are comparable to this review. Only one reference was found for sublimation enthalpy of AP. In 2005 Oxley reported the enthalpy of sublimation of AP to be 104 KJ/mol as determined by GC-MS. This result is considerably higher than the found in the current study (70 KJ/mol). In another work from this group in 2006 the enthalpy of sublimation was reported as 85 KJ/mol which is more in agreement with current results. In the same work reported by Oxley the enthalpy of sublimation for TNT was reported as 137 KJ/mol which suggest a tendency to higher values for the method employed. There was not found a recent reference for RDX but a work from 1969 estimated it in 130 KJ/mol for the range of 328-370°K. In the present study the value is reported as 97 KJ/mol for 338-383°K. Figure 10 contains the TGA curves at different heating rates for AP. It was possible to estimate the enthalpy of sublimation of AP in only one test by applying the same mathematical treatment to the instantaneous mass loss rate in the temperature range under melting.

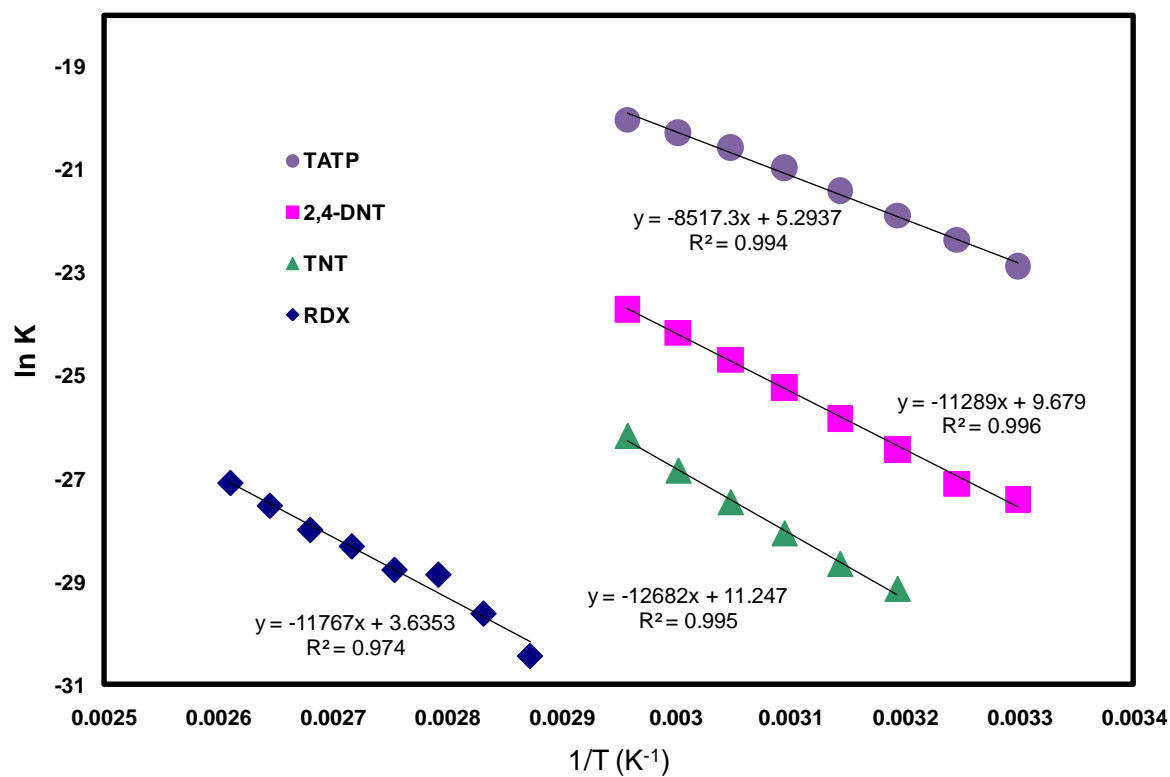


Figure 9. Curves of the rate of mass loss vs. temperature for AP, RDX, TNT and 2,4-DNT. This plot is used to estimate the enthalpy of sublimation. (slope = $-\Delta H/R$)

Table 6. Summary of sublimation results.

Material	Enthalpy of sublimation (KJ/mol)	Temperature Range (°K)	Literature value	Temperature Range (°K)
2,4,6 Trinitrotoluene	105.4 (±3.6)	313-338	¹ 113.2 (±1.5)	297-330
2,4 Dinitrotoluene	93.9 (±2.5)	303-338	¹ 95.8 (±1.25)	277-344
RDX	97.8 (±6.5)	338-383		
AP	70.8 (±2.3)	303-338	² 104 ³ 85	285-331 298-348
	(1) J. Phys. Chem. Ref. Data, Vol. 31, No. 2, 2002 (2) Propellants, Explosives, Pyrotechnics 30 (2005), No. 2 (3) <u>Characterization of peroxide-based explosives by thermal analysis</u> . Sensors, and Command, Control, Communications, and Intelligence (C3I) Technologies for Homeland Security and Homeland Defense V, Orlando (Kissimmee), FL, USA, SPIE. 2006			

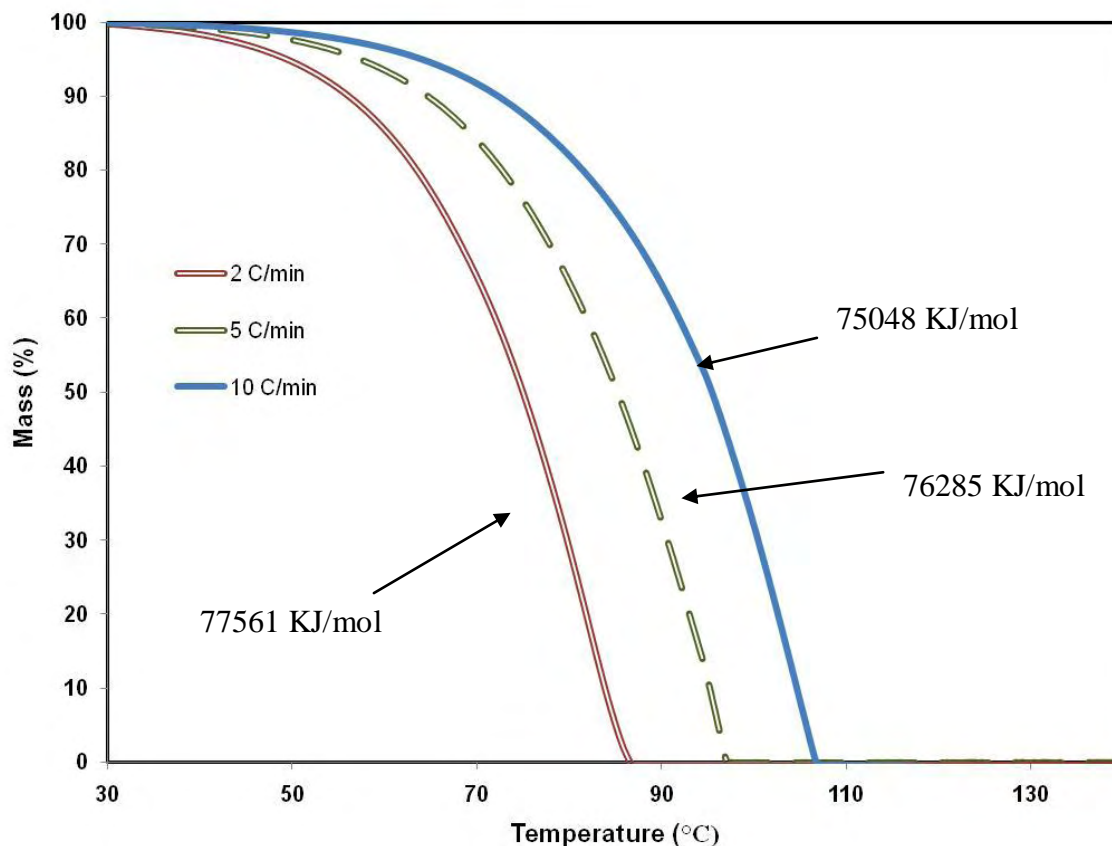


Figure 10. Determination of enthalpy of sublimation by dynamic analysis. An extrapolation to heating rate = 0 gives an enthalpy of sublimation of 78048 KJ/mol.

3.2.3 Structure Property Relationships

The thermal data obtained through all the experiments was analyzed by a statistical program to find relationships between the thermal properties of these compounds and the structural properties. Table 7 summarizes the data utilized. SPSS statistical analysis software program was used to find the descriptors with higher correlation to the properties. These descriptors were then analyzed by Statgraphics to find the

best fit to a two variable model. This model was the more appropriate considering that the data responded to only 6 molecules. Table 8 presents the results of fitting a multiple linear regression model to describe the relationship between the thermal properties and the descriptors. When the P-value of the ANOVA test is less than 0.05, there is a statistically significant relationship between the variables at the 95.0% confidence level. The R-Squared statistic indicates that the model as fitted explains that percent of the variability in the studied property. The standard error of the estimate shows the standard deviation of the residuals. This value can be used to understand prediction limits for new observations. The mean absolute error (MAE) is the average value of the residuals. The combination of topological and quantum descriptors resulted in very linear relationships. For the decomposition temperature (peak and onset) the number of hetero atoms and the information content index correlated with more than 90%. The information content index describes the size and symmetry of the molecule. The melting temperature of the molecules seems to be affected by the number of carbons and the energy of the LUMO (Lowest Occupied Molecular Orbital). For the sublimation enthalpy and enthalpy of decomposition there was no acceptable model. It is possible that with the information of more molecules a better correlation can be attained.

Table 7. Thermal properties and descriptors used for the study.

Thermal properties	Topological descriptors	Quantum descriptors
T_m , $T_{dec\ Onset}$, $T_{dec\ peak}$, H_m , H_{dec} , H_{sub} , Activation energy, $T_{dec\ peak} - T_{dec\ Onset}$	number and type of bonds, number and type of atoms, polarizability, connectivity indexes, information content indexes, partially charged volume	Energy of the molecule, its cation and anion, ionization energy, electron affinity, energy of homo and LUMO, hardness and softness. Dipole moment.

Table 8. Statistical correlation of thermal data and structural descriptors.

Thermal Property	Correlation
T_{dec}	$-46.4351 - 6.15451 \cdot H + 146.647 \cdot IC$ $R^2 = 95.31\%$ ANOVA P value=0.0101 Standard Error of Est. = 16.1334 Mean absolute error = 8.87
T_{onset}	$22.5381 + 131.387 \cdot IC - 11.2243 \cdot H$ $R^2 = 90.29\%$ ANOVA P value=0.0302 Standard Error of Est. = 25.88 Mean absolute error = 15.77
Activation Energy	$134.698 + 26.9679 \cdot A$ $R^2 = 71.52\%$ ANOVA P value=0.0339 Standard Error of Est. = 31.11 Mean absolute error = 22.68
Distance from T_{onset} to T_{dec}	$-18.0443 + 6.05071 \cdot OXIG$ $R^2 = 82.40\%$ ANOVA P value=0.00124 Standard Error of Est. = 10.46 Mean absolute error = 7.98
MP	$305.075 + 374.17 \cdot LU - 26.4913 \cdot NAC$ $R^2 = 98.38\%$ ANOVA P value=0.0021 Standard Error of Est. = 11.91 Mean absolute error = 7.66

3.3 Conclusions

In this work thermal analysis was applied to compare known high explosives such as TNT and RDX to AP, a homemade explosive known for its power, instability and attractiveness to terrorists. The released energy of AP is comparable to the energy release by TNT and RDX. However the activation energy resulted one half the required for TNT and PETN. The discrepancies from the literature were discussed. The sublimation of AP was characterized using thermogravimetry. The kinetics of sublimation follows mostly zero order rate. The enthalpy of sublimation was estimated using an Eyring plot. The value was estimated in 70 KJ/mol for the temperature range.

The collected data was correlated with structural properties obtaining good relationships for melting temperature and temperature of decomposition. However more data is needed for a more robust model. This data should include more energetic compounds. This normally includes nitrocompounds. However the compilation of data from other peroxides is recommended.

4 STUDY OF THE INTERACTION OF AP WITH ENERGETIC MATERIALS USING THERMAL ANALYSIS, SPECTROSCOPY AND COMPUTATIONAL METHODS

4.1 Introduction

In the area of defense and security, explosive compositions are formulated to control properties of explosives such as explosive power, stability and setoff conditions. Many military and commercial explosives are formulated for specific applications: demolition, ammunition, propelling, etc. At the same time, the increase of terrorism is fueled by the development of new explosives and the combination of commercial explosives with domestic fabrication materials into improvised explosive devices (IEDs). For example, the military explosive pentaerythritol tetranitrate (PETN) is combined with hexahydro-1,3,5-triazine (RDX) to form Semtex, and with trinitrotoluene (TNT) to form Pentolyte. In 2002 Richard Reid, known as the shoe bomber, used PETN and AP hidden in his shoe sole during the attempt to blow up a U.S.-bound American Airlines flight⁹. The terrorist passed all security checkpoints without being detected.

It is generally accepted that the activation energy for the decomposition of energetic materials rely on the energy of their weakest bond. A comparison of the activation energy of AP and energetic nitro compounds (Table 4) confirm that the thermal and friction instability of acetone peroxide is originated in the low bond energy of the

peroxide. The low activation energy of AP suggests that it could be used as a primary explosive. However the high vapor pressure and its thermal and friction instability could be extended to compositions based in AP. The objective of this work objective of this work is to study the type of interactions that can be present when AP is mixed with other energetic materials. The materials will be blended as powders and melted. It is expected that when solidified this materials will exhibit properties different to the pure solids.

4.2 Results

4.2.1 The AP/ ammonium nitrate system

Ammonium nitrate is probably the most used material for HME's. AN is widely available as a fertilizer. It's mixing with diesel, kerosene or No. 2 fuel oil is known as ANFO and is considered to be the most used explosive in mining and construction. AN is also known as a sensitizer use to reduce the activation energy of high explosives. This apparently as a result of NO_3H formed during heating of AN.

The spectra of vibrational spectra of AP blended with 35% AN was obtained after melting and cooling (Figure 11). The spectra of the mix is enriched with AP and the presence of AN is only marked by a small peak at 1040 cm^{-1} . The DSC thermogram of AN, AP and the blend is included in figure 12. The thermal profile of AP presents an endothermic transition (melting) at 80°C - 90°C , AP has an onset for exothermic

decomposition at 170°C and the peak exothermic transition occurs at 195 °C. For AN the thermogram presents two endothermic transitions under 150°C. The decomposition process is located at 300°C. The thermogram presents a wide exothermic transition in the temperature range where AP decomposes rapidly. There is an exothermic peak close to 240°C. There is no further transitions that can be attributed to the AN decomposition. The profile suggests that AN will delay AP decomposition and be consumed in the process. At 260°C the remaining AP will decompose violently (sharp exothermic peak).

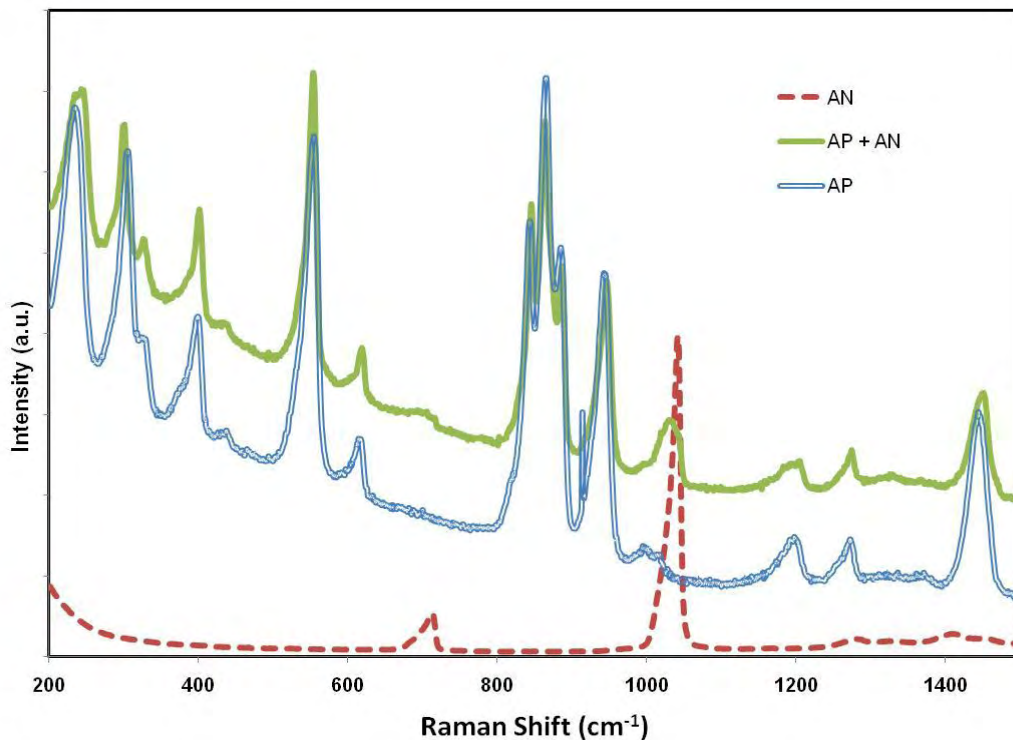


Figure 11. Raman spectra of mixture of AP + AN containing 35% AN. Samples were solidified from a melt. Parameters: 3 scans, 30 s with a 785 nm laser.

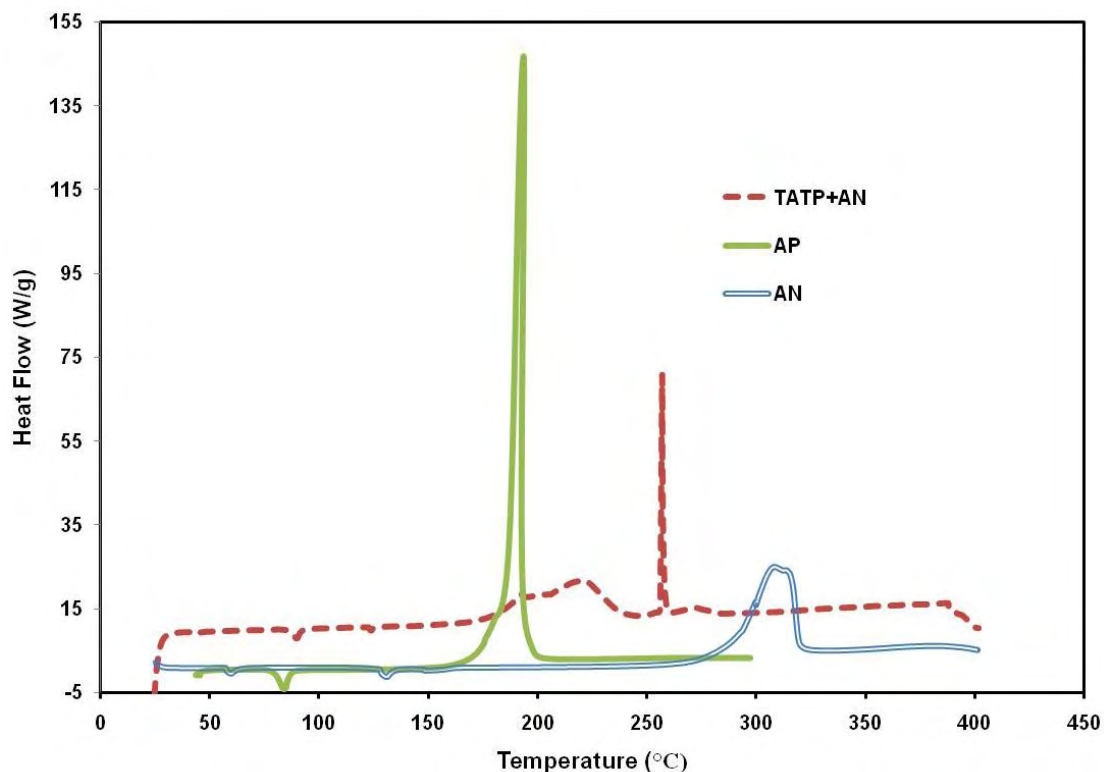


Figure 12. Comparison of the DSC thermograms of AP, AN and a mixture containing 35% AN. Parameters: 2-3 mg sealed in a high pressure pan, 5 °/min.

4.2.2 The AP – Nitroguanidine system

Nitroguanidine (NQ) is considered a nitrimine or primary nitramine. It has applications as an additive for gunpowder and propellants. It is also considered a low performance explosive (low explosive). (Agrawal and Hodgson 2007). The objective of mixing AP with NQ is to study the effect of the amino groups on the peroxide groups of AP. The Raman spectra of a blend of 40% NQ in AP is presented in Figure 13. The spectra have components of both AP and AP suggesting that the sampled area is representative of the mix. Also, the peaks marked as “a” and “b”

have widened, suggesting molecular interparticle interactions. The DSC of the decomposition process of this blend is included in Figure 14. The decomposition of the pure substances are characterized by a sharp exothermic peak at 195°C (AP) and at 235°C (NQ). The thermogram of the blend presents a melting transition close to 90°C. This transition contains two peaks which suggest that NQ is dissolved in AP. Nitroguanidine does not present a melting transition in the DSC and the theoretical peak for this transition is 247°C. The decomposition transition consists of a wide peak from 180°C to 240°C. The region has a maximum at 200°C and at 220°C. There is a secondary exothermic peak at 350°C. This transition was not observed in the thermogram of pure AP or NQ suggesting it is the decomposition of species formed during the exothermic process at lower temperature.

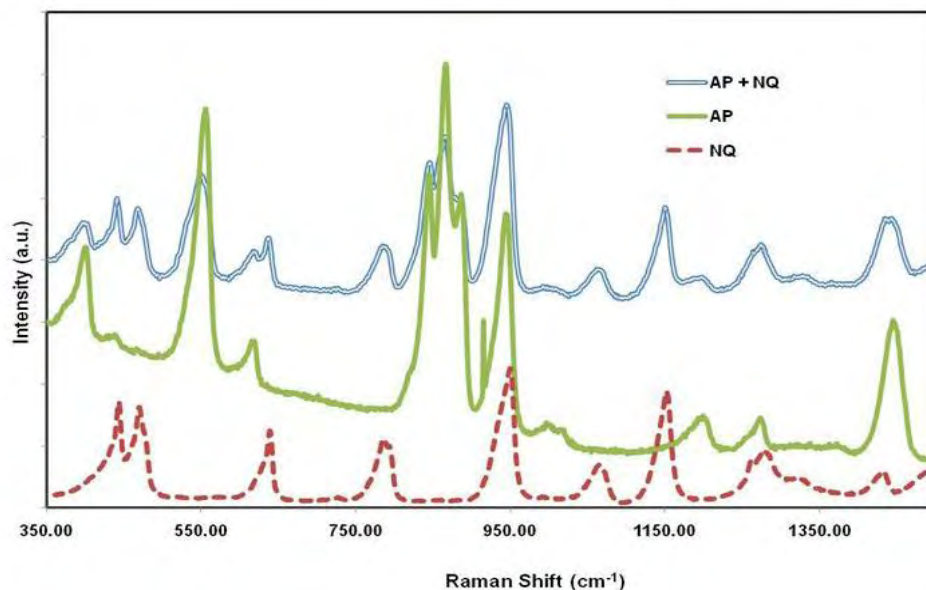


Figure 13. Raman Spectra of AP + 40% NQ. Sample was solidified from a melt. Parameters: 3 scans, 30 s with a 785 nm laser.

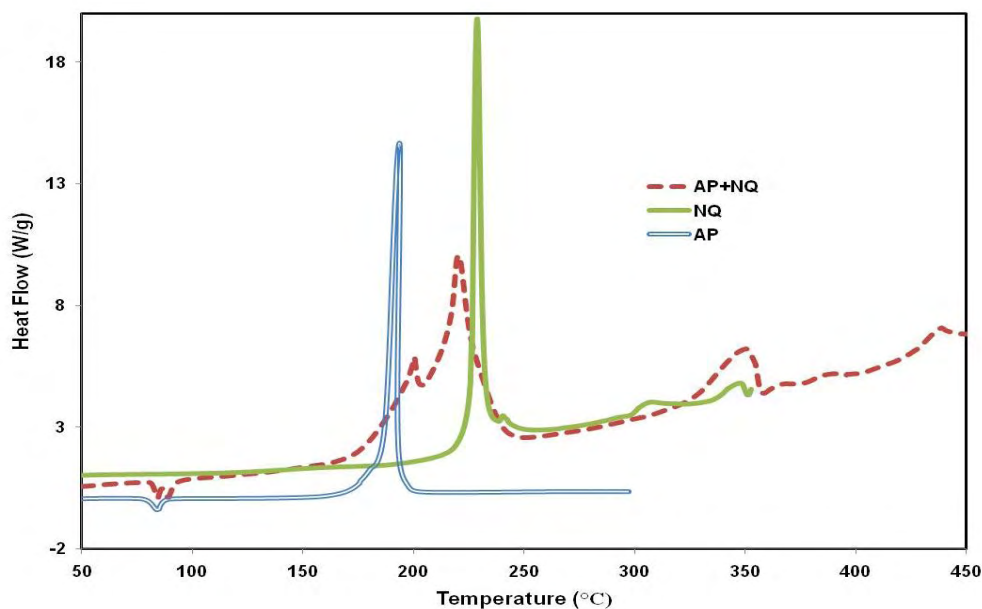


Figure 14. Comparison of the DSC thermogram of AP + 40% NQ with the individual components. Parameters: 2-3 mg sealed in a high pressure pan, heating rate 5°C/min.

4.2.3 The AP – TNT system

The chemistry of TNT is characterized by the strong conjugation derived from having three nitro groups in the benzene ring. The result is the reactivity of the methyl group. The hydrogen atoms of the methyl group have an acidic character making this methyl group to behave as a nucleophile under special circumstances. TNT is very popular as a precursor for polynitroarene synthesis. TNT was blended with AP to study if the methyl group can interact with the peroxide groups of AP.

Figure 15 contains the Raman spectra of (from top to bottom) AP, TNT and a 50% blend of AP and TNT. The resultant spectrum is a composite of the pure material spectra. However the combination of bands from each component result in wide bands in the 768 cm^{-1} to 900 cm^{-1} region and 282 cm^{-1} to 334 cm^{-1} . The DSC thermogram (Figure 16) presents two melting transitions in the 70°C - 80°C region. These peaks are lower than the melting transition of TNT ($\sim 80^{\circ}\text{C}$) therefore an interaction between components can be assumed. The decomposition consists of a wide peak from 180 to 225°C . This transition only presents one maximum at 206°C indicating that the solid behaved as one compound or that the heat released by AP consumed the TNT. There is a small exothermic transition close to 300°C indicating residual TNT material. The transition enthalpy is lower than any of the components indicating that the decomposition occurred by mechanisms different from the dominants in pure materials.

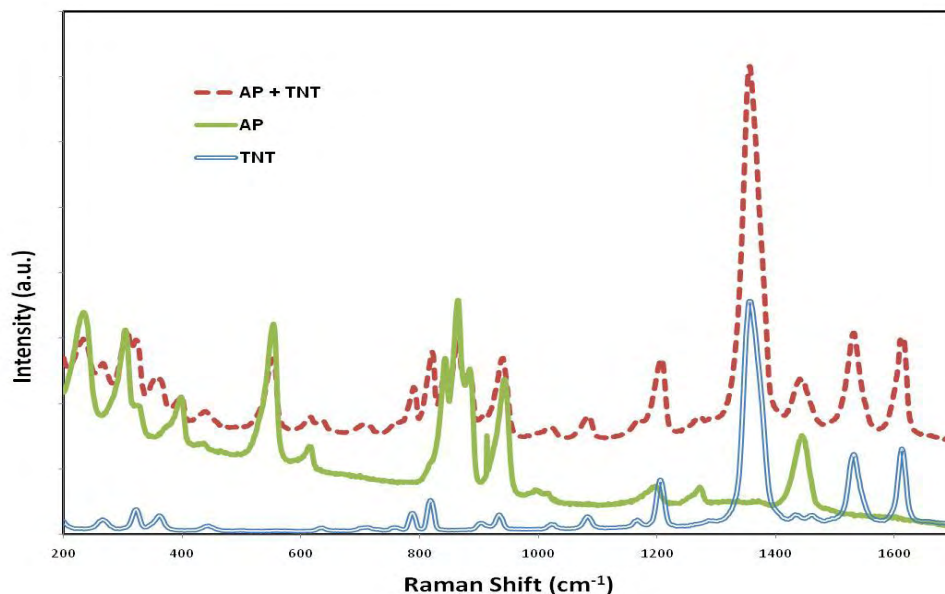


Figure 15. Raman spectra of a mixture 50% TNT and AP. Samples were melted and co-solidified. Parameters: 3 scans, 30 s with a 785 nm laser.

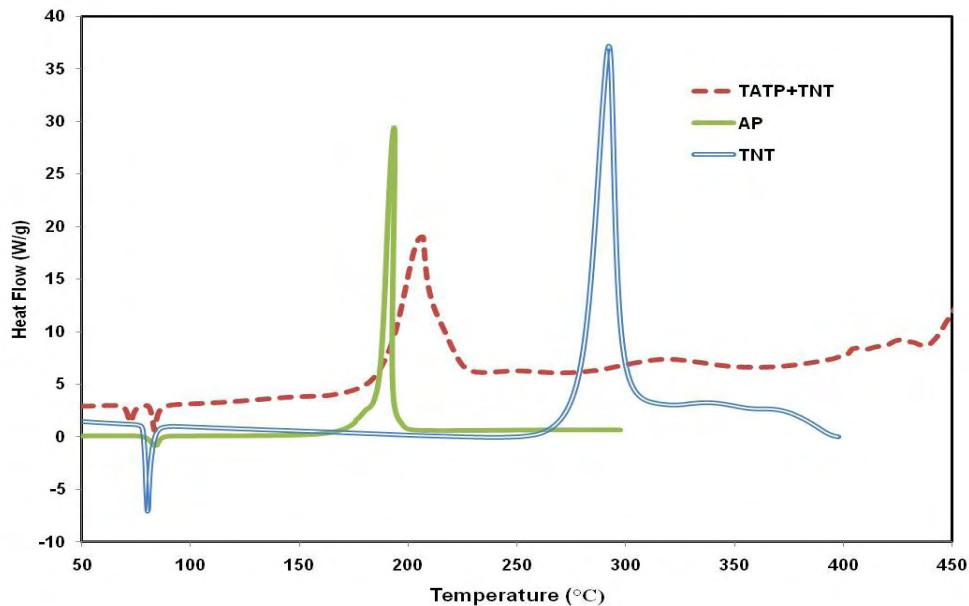


Figure 16. Comparison of the DSC thermogram of 50% TNT and AP. Parameters: 2-3 mg sealed in a high pressure pan, heating rate: 5 °/min.

The AP-TNT system was further studied. Ten milligrams (10 mg) of mixtures of AP (39%-86%) were mixed in a high pressure DSC. The samples were melted to 100 °C at 5°C/min. Then the samples were cooled to 0°C at 5°C/min. Finally the samples were heated at 5°C/min to 100°C. This third cycle was used to study the phase diagram of AP and TNT. The curve for these blends is characterized by two overlapping peaks (Figure 17). The peak temperature of the first peak was used for a plot of melting temperature vs. AP concentration (Figure 18). This can be considered a simple binary phase diagram. Temperature based phase diagrams are graphic representation of the equilibrium conditions between phases. The objective of this experiment is to find to find the eutectic composition of a AP-TNT blend. For the TNT-AP system the first peak is considered the true eutectic transition. This is the transition from a complete solid to a liquid (liquid + solid, in this case). The second transition is more complex since it involves the transition of a liquid + solid blend to complete liquid. The plot of melting temperature vs. concentration presents an inflection close to 45% AP concentration. The change in temperature vs. change in concentration the inflection can be considered to be close to the eutectic composition. It should be noted that our graph seem to be representative of the right side of a phase diagram. This was caused by the range of concentrations (39%-86%). To confirm this behavior it is necessary to include more points under 39 % of AP.

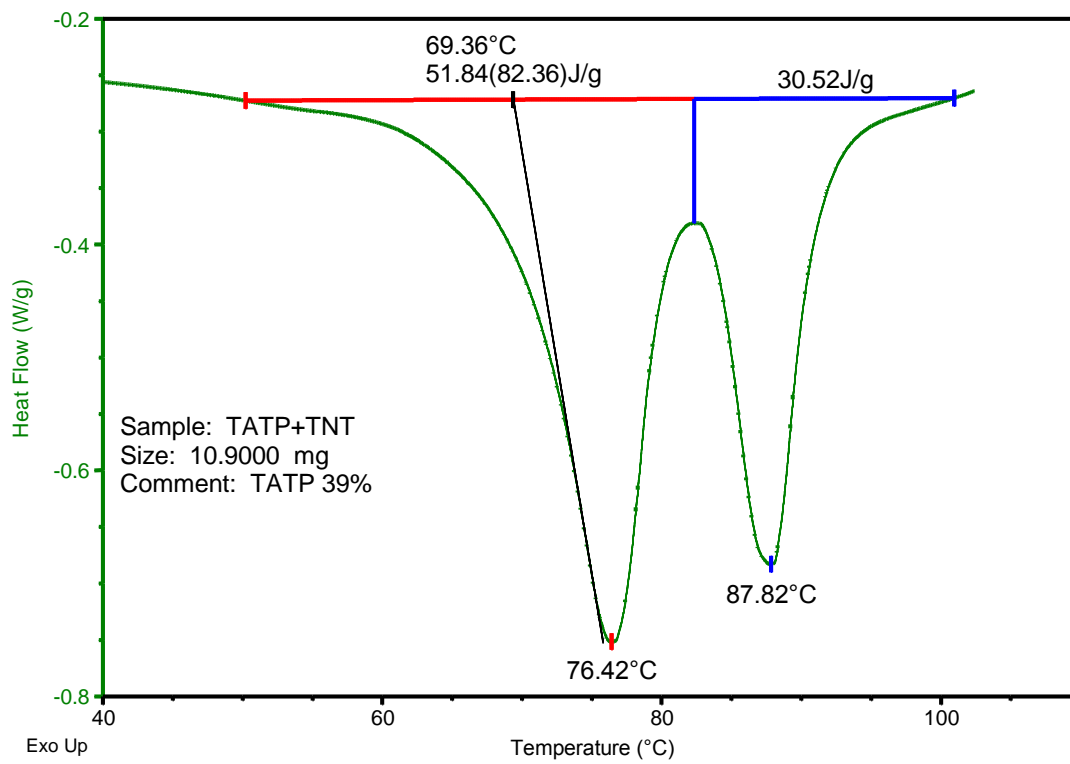


Figure 17. Melting transition of a 39% AP mix with TNT. Sample was first melted and solidified. Parameters: 2-3 mg sealed in a high pressure pan, heating rate: 5 °/min.

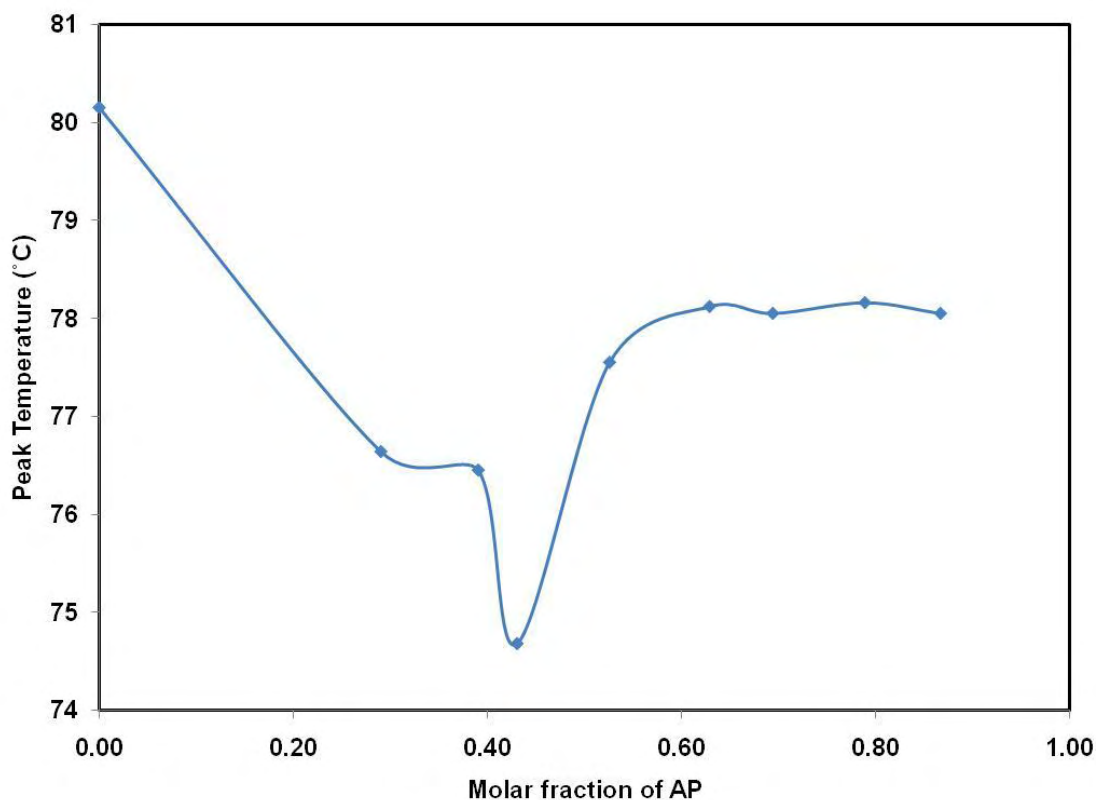


Figure 18. Effect of AP on the melting temperature of TNT.

The solids obtained from the melt were characterized by attenuated total reflectance FTIR (ATR-FTIR). This technique allowed studying changes in the vibrational spectra of the spectra as a function of concentration. Another objective of this study was to report the changes in the spectroscopic signature and the spectroscopic signature of AP blend as this is critical for the development of vibrational spectroscopy based sensors. At the same time it is possible to study interactions between AP and other materials by changes in the spectroscopic signature. Figures

19 to 23 present the ATR-FTIR spectra of AP blends from 100% AP to 29%. Each figure has labels for AP maximum and minimum concentration. The progression in band intensity as AP increase in concentration is noticeable. Many bands are markers of the AP or TNT. In the region from 775 cm^{-1} to 800 cm^{-1} there is a TNT band that overlaps AP bands resulting in a shoulder at low AP concentrations. The band turns into the AP band as concentration increases appearing as a shift in band position. The same happens in Figure 20 at 975 cm^{-1} and 1350 cm^{-1} regions region (Figure 21).

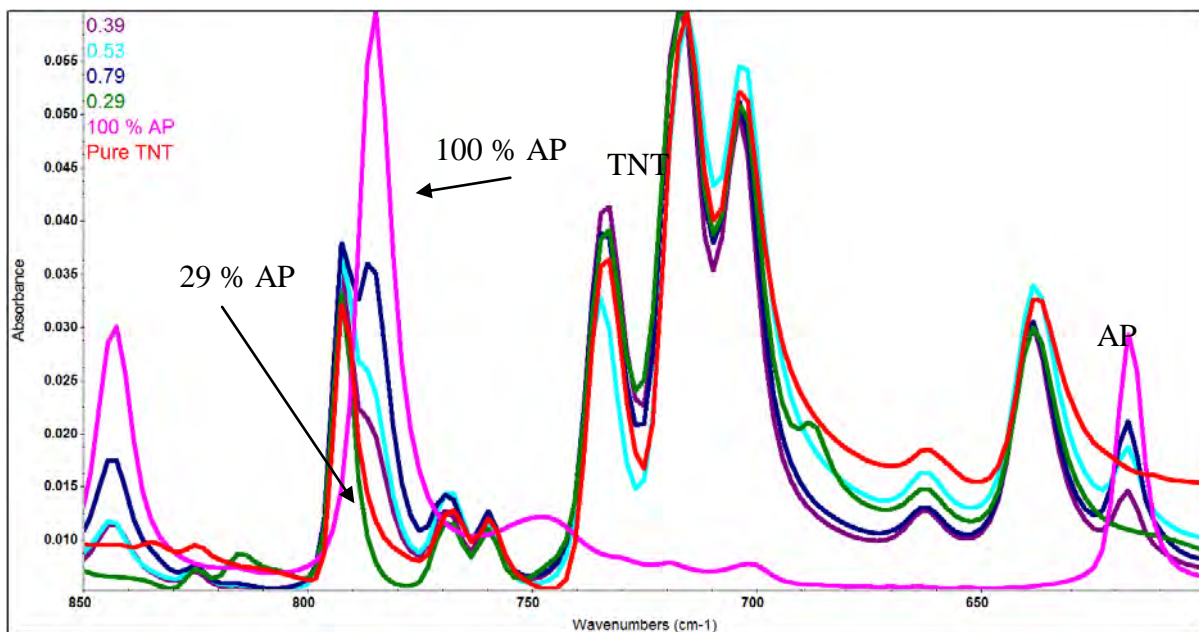


Figure 19. FTIR-ATR spectra of AP-TNT mixtures (600-850 cm^{-1}).

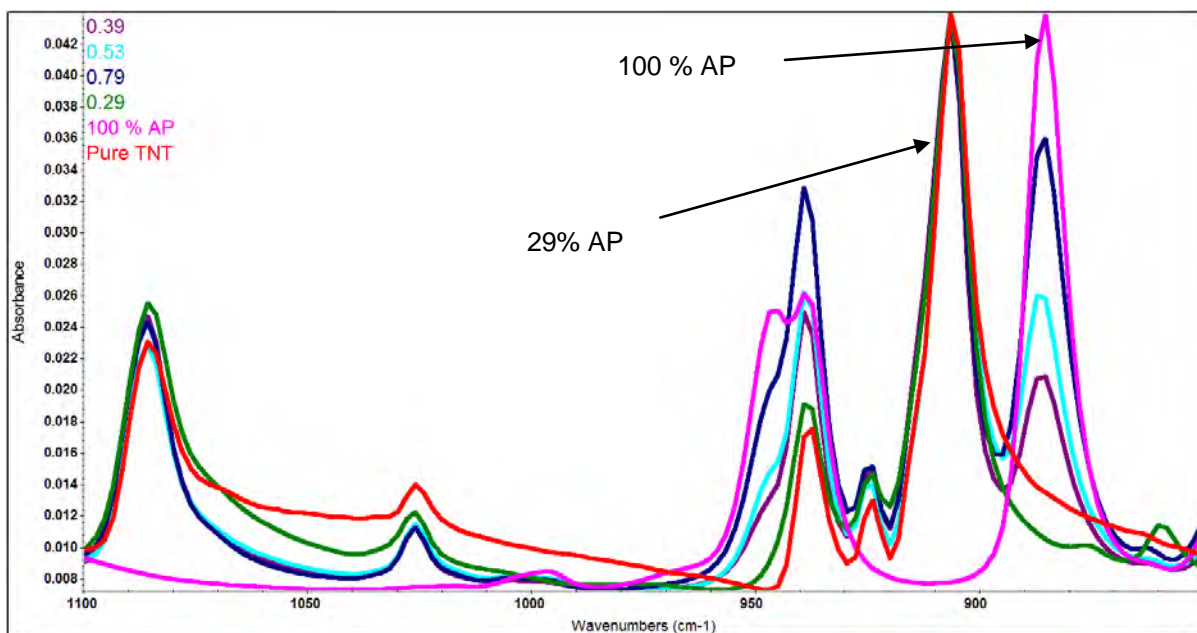


Figure 20. FTIR ATR spectra of AP TNT blends (850-1100 cm⁻¹).

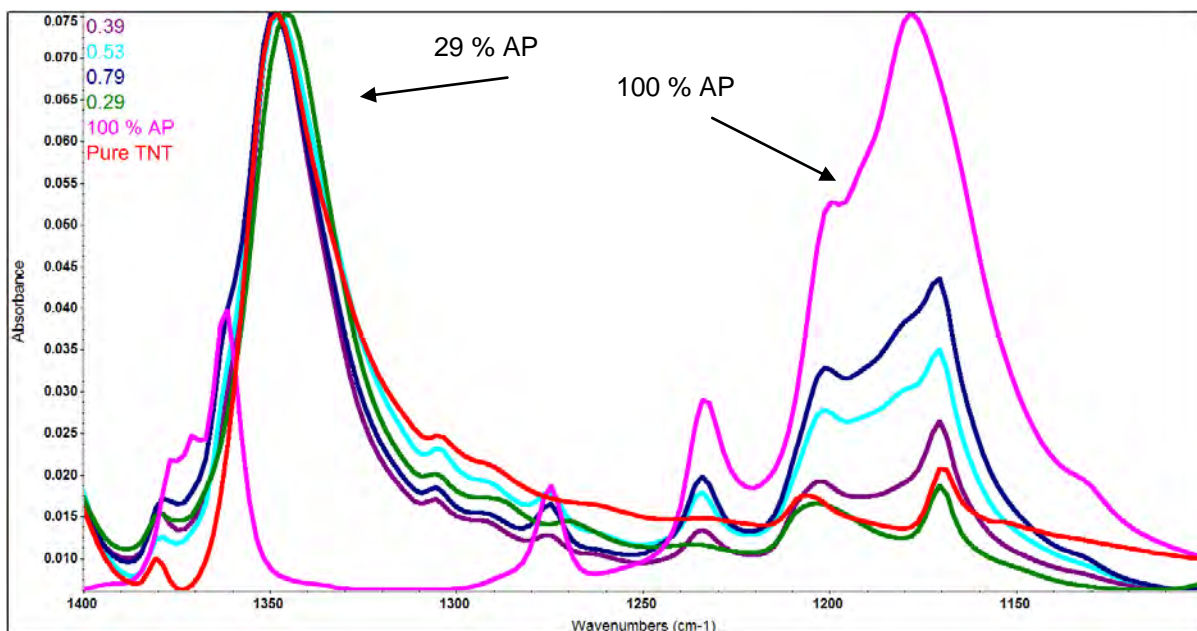


Figure 21. FTIR ATR spectra of AP TNT blends (1100-1400 cm⁻¹).

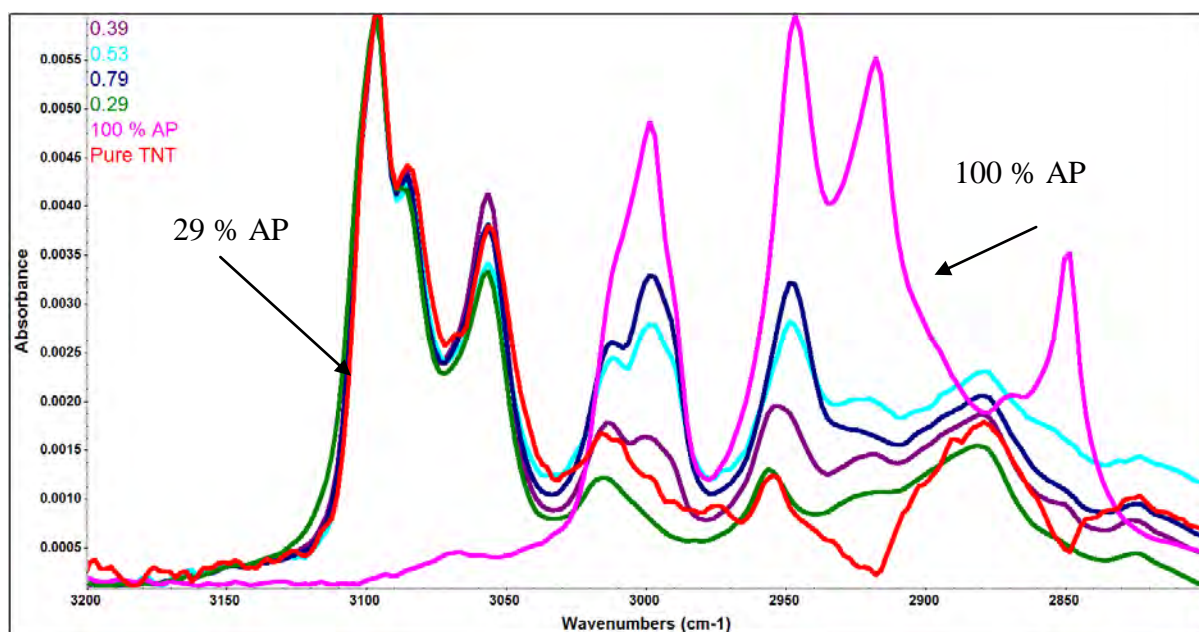


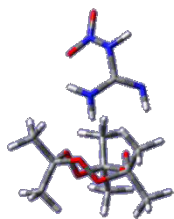
Figure 22. FTIR-ATR spectra of AP-TNT mixtures (2800–3200 cm^{-1}).

4.2.4 The computational analysis

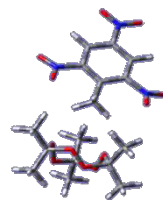
Force field was used as a primary approach to find probable conformations for the interaction of AP with secondary high explosives. The result was optimized by PM3. The interaction energy was defined as the difference between the energy of the system and the energy of its components. In a work of 2000 Jinshan proposed that these calculations were an efficient way to assess intermolecular interactions between amino and nitro compounds.³⁶ It is expected that stronger intermolecular interaction will desensitize AP. Figure 23 presents the conformation of AP systems

after optimization with PM3. An interaction with ammonia is included. The heating of AN produces NH_3 and nitric acid. It has been suggested that cations can stabilize AP. And the thermogram of the system suggests the same since the peak decomposition temperature is shifted. This model considers the interaction with ammonia. The energy of these systems and calculated interaction energy is included in Table 8. The objective of this study was not to find the absolute interaction energy or the most stable conformation but to find how strong can be these interactions and its effect on the decomposition of AP. A plot of interaction energy vs. shift in the peak decomposition temperature of AP confirms the desensitizing effect. Once the AP decomposes the release energy can decompose the rest of the material or its decomposition products may attack the other explosive acting as a sensitizer.

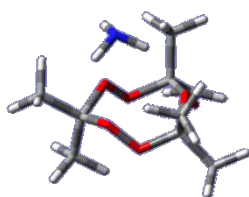
A



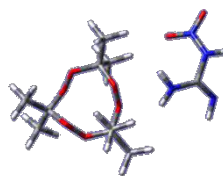
B



C



D



E

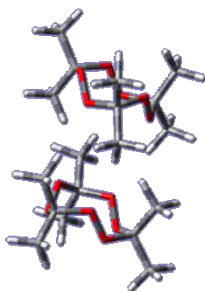


Figure 23. PM3 interaction conformations of: (A) NQ- AP, (B) TNT-AP,(C) NH₃ – AP, (D) NQ-AP, (E) AP-AP

Table 9. Interaction energies of AP based systems.

System	Energies based on PM3 optimization		
	Energy (H)	E (KJ/mol)	Interaction energy (KJ/mol)
AP	-0.15072295	-395.72	N.A.
TNT	0.00493418	12.95	N.A.
NQ	0.03939388	103.43	N.A.
NH3	-0.00490785	-12.89	N.A.
NQ+ AP (A)	-0.11519589	-302.45	-10.15
NH3 + AP (C)	-0.16292078	-427.75	-19.14
NQ+ AP (D)	-0.11532171	-302.78	-10.48
AP + AP (E)	-0.314197	-824.92	-33.48
TNT + AP (B)	-0.15075004	-395.79	-13.03
AP + AP (F)	-0.30915364	-811.68	-20.24
TNT + AP (G)	-0.15027333	-394.54	-11.77
TNT-TNT	0.00009132	0.24	-25.67
NQ-NQ	0.07576128	198.91	-7.95

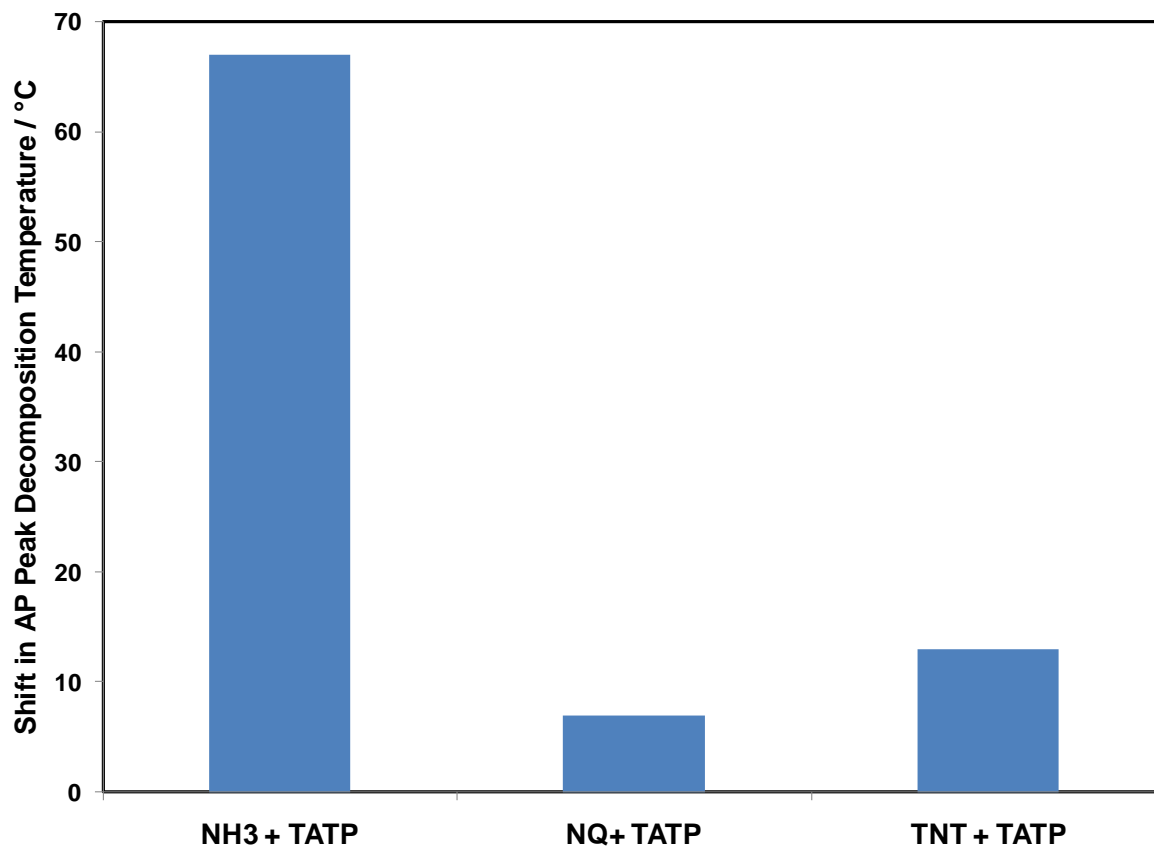


Figure 24. Shift in the decomposition temperature of AP mixed with nitro compounds.

4.3 Conclusions

In this section the effect of mixing AP with other energetic materials was studied by vibrational spectroscopy, thermal analysis and computational methods. As expected AP has a destabilizing effect on other energetic materials. It can be assumed that on decomposition the AP decomposition products can attack the other energetic material.

AN has a stabilizer effect on TATP shifting the decomposition peak to higher temperatures. Computational analysis suggested that an interaction can occur between AP and ammonia formed from heating ammonium nitrate. This agrees with AN decomposition studies mentioning the effect of AN decomposition products on sensitization and desensitization activity.^{17, 46, 47}

5 IDENTIFICATION OF CHEMICAL THREATS IN COMMERCIAL PRODUCTS USING RAMAN SPECTROSCOPY

5.1 Introduction

The London plot consisted in a plan to introduce liquid explosive into an aircraft to build an improvised explosive device (IED) that would detonate and explode various aircrafts on transit. AP is powerful explosive that possesses very low activation energy. This never realized plot brought to the public attention numerous debates. One is that if it was really possible to conceal that much amount of explosive to build an IED in flight. Other was that how far the creativity of men can go for terrorist purposes. But the most important debate is about how vulnerable are our transportation systems and our security for controlled locations. The possibility of using liquid explosives for terrorism purposes is accompanied by the possibility of using chemical warfare agents (CWAs) or toxic industrial compounds (TICs) for the

same purposes. National and international authorities have demanded to pursue research in the characterization, detection and response to chemical threats. Raman spectroscopy is one of the promising tools under consideration. These days, Raman systems are portable, sensitive, flexible tools that are used in the field and the lab. The objective of this chapter is to discuss the applicability of Raman to the detection of concealed chemical threats in commercial products.

5.2 Results

5.2.1 Detection of peroxide in liquors

The spectra of three liquors were obtained in the same clear glass bottle. The results are presented in Figure 25. As expected the rum, gold tequila and whiskey present the same spectra. The yellowish color of the tequila and whiskey presented some fluorescence identified by the shift in the baseline of the spectrum. However it is possible to identify the main peaks associated to the alcohol content. These spectra as well as the spectrum for ethanol, the main component of hard liquors, present peaks at 881(C-C-O stretch), 1048 cm^{-1} (ring vibration), 1186 and 1280 cm^{-1} (ring stretch) and 1456 cm^{-1} (CH_3 deformation).

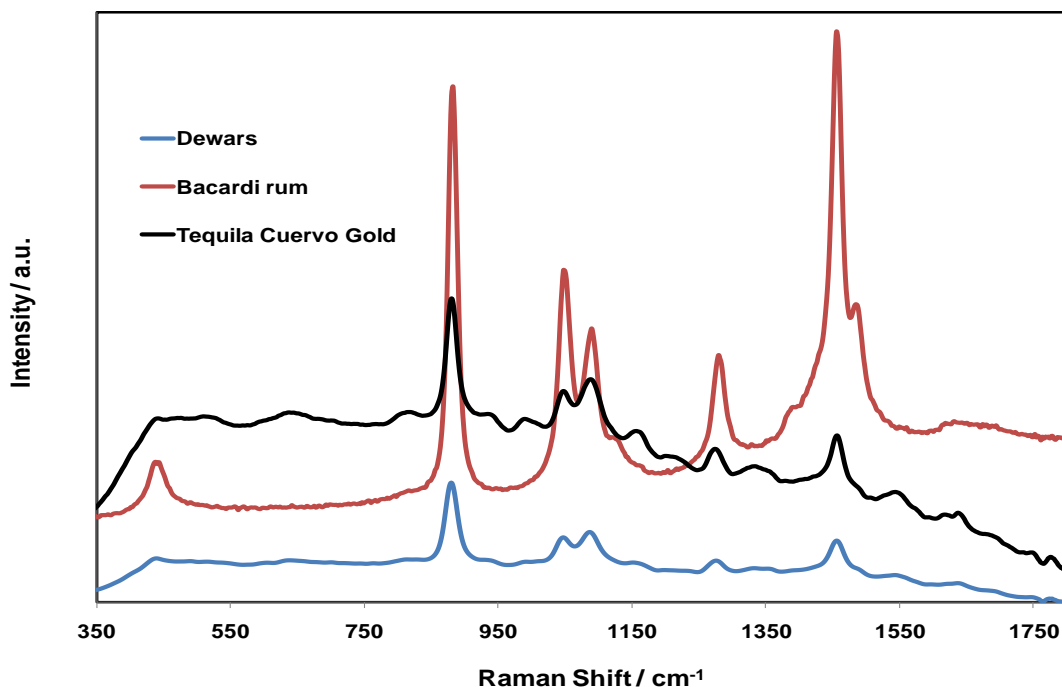


Figure 25. Raman spectrum of liquors in their original containers acquired with fiber optic probe. Parameters were: 785 nm laser, 200mW and 2 sec of integration time.

Then the content of the clear glass bottle was replaced with acetone and hydrogen peroxide so that the content appears to be clear rum. These products can be easily found at beauty supplies and drugstores. These are commonly found in consumer products such as nail polish remover and hair care products. However together they can be mixed to form acetone peroxide, a known homemade explosive. The Raman spectra of acetone, peroxide and the acetone peroxide explosive are presented in Figure 26. Acetone's main peak is located at 789 cm^{-1} . For peroxide the strong Raman line at 878 cm^{-1} , characteristic O–O stretching mode, is stronger than that of the other peaks of the spectra. For the AP the main peaks are located at 588, and

three characteristic peaks at 780 cm^{-1} , 890 cm^{-1} and 936 cm^{-1} . The position and intensity of the major peaks in acetone and peroxide make them easily detected by Raman and can be used as markers for explosive mixtures.

In Figure 27 the acetone and peroxide spectroscopic signatures are compared to the Bacardi rum. The rum's spectrum present clear characteristic bands near 1050 cm^{-1} , 1090 cm^{-1} , 1280 cm^{-1} and 1450 cm^{-1} that together with the band ratios will differentiate the rum from a different pure liquid. It is confirmed that Raman can be used to discriminate between pure liquids. However the strong band at 878 cm^{-1} that all liquors present is located in the same region of the hydrogen peroxide C-O band. This may represent a challenge for detection of peroxide mixed with liquors.

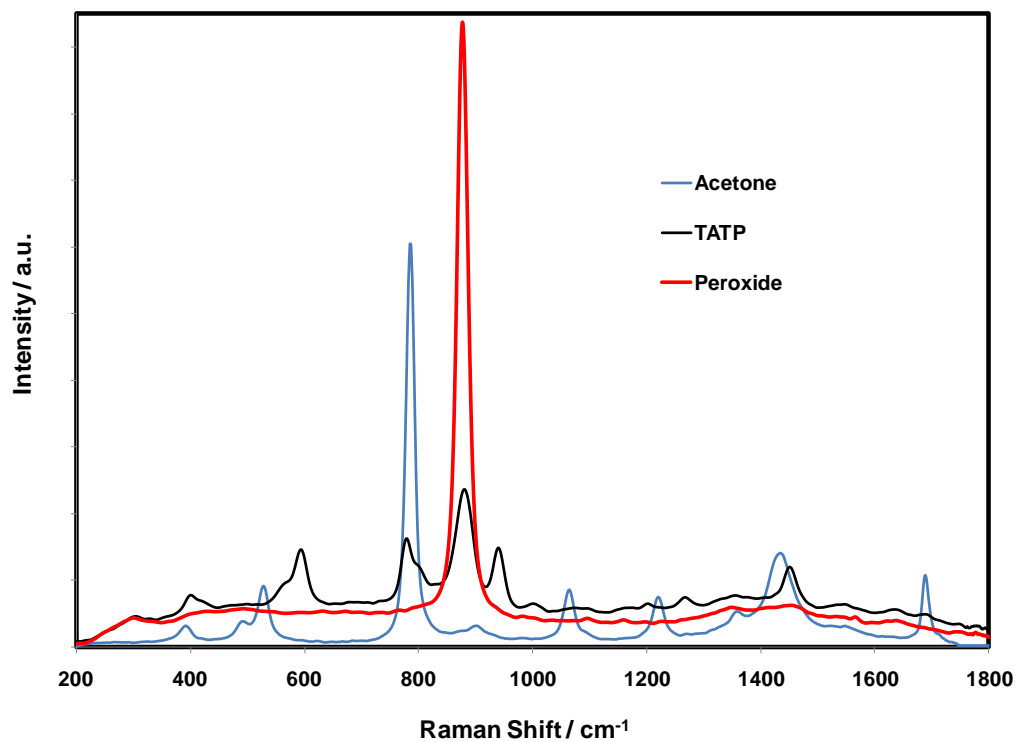


Figure 26. Raman spectra of acetone, peroxide and acetone peroxide explosive within a clear glass bottle at 785 nm, 10 second and a laser power of 200 mW.

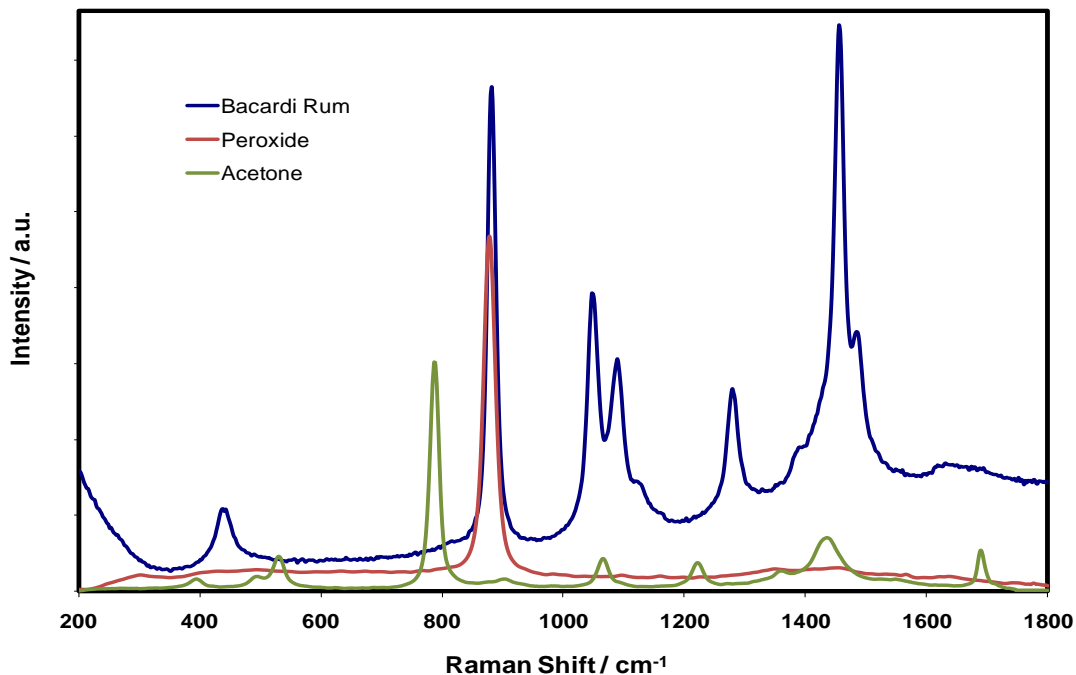


Figure 27. Spectroscopic signatures of rum vs. acetone and peroxide at 785 nm, 10 second and a laser power of 200 mW.

Figure 28 presents the Raman spectra of 20% and 60 % peroxide in whiskey. As previously mentioned, the spectroscopic signature of peroxide is hidden or masked by the whiskey. Samples from 0% to 90% peroxide in whiskey were prepared without changing the location of peaks. Since the presence of peroxide increased the intensity at 874 cm^{-1} the peaks ratio can be used to discriminate between the original liquid and adulterated liquor. OPUS PLS Package was used to build a model to determine the concentration of peroxide in whiskey. The result of the cross validation is included in figure 29. The data from these same samples was correlated

just for presence of peroxide. The graph at figure 30 confirms that peak ratios can be used to discriminate between an original liquid or a concealed hazardous material.

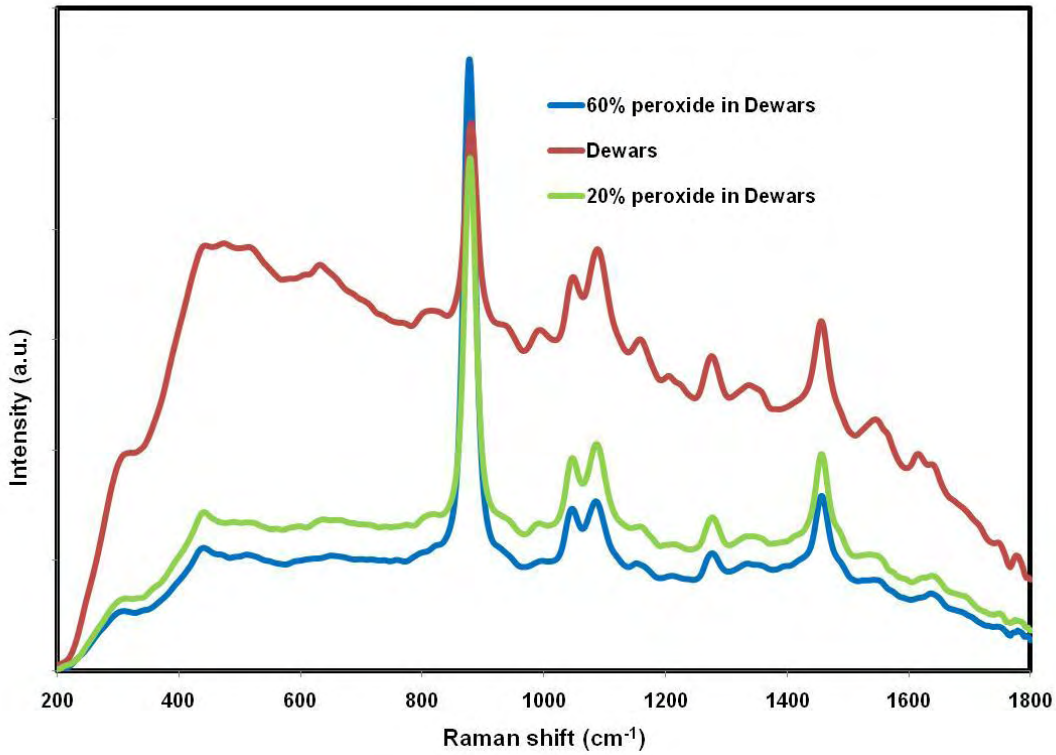


Figure 28. Raman spectra of a mixture of hydrogen peroxide and Dewar's whiskey, using a 785 nm laser 3 scans at 10 s with 200 mW laser power.

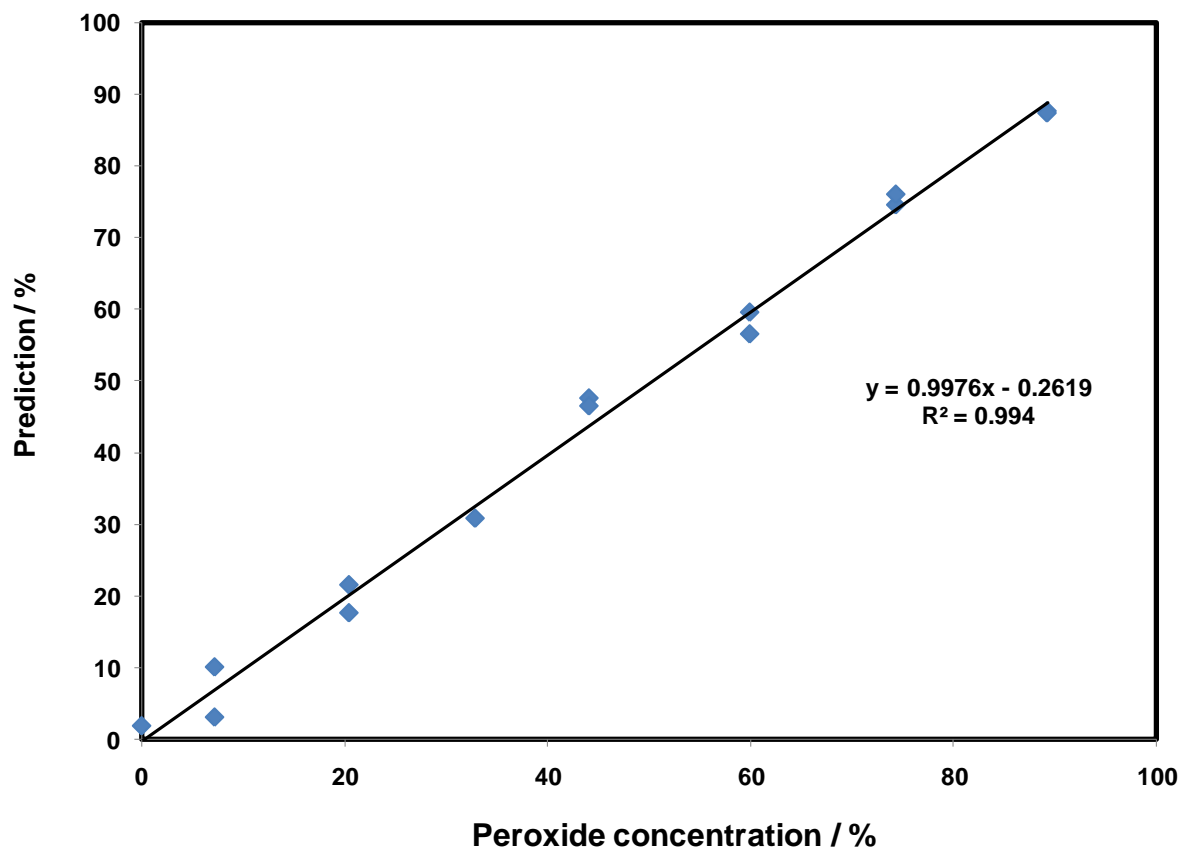


Figure 29. Prediction of the concentration of peroxide in whiskey. Preprocess: None, Rank: 4, RMSECV: 2.41, Region: 539-1080 cm^{-1} .

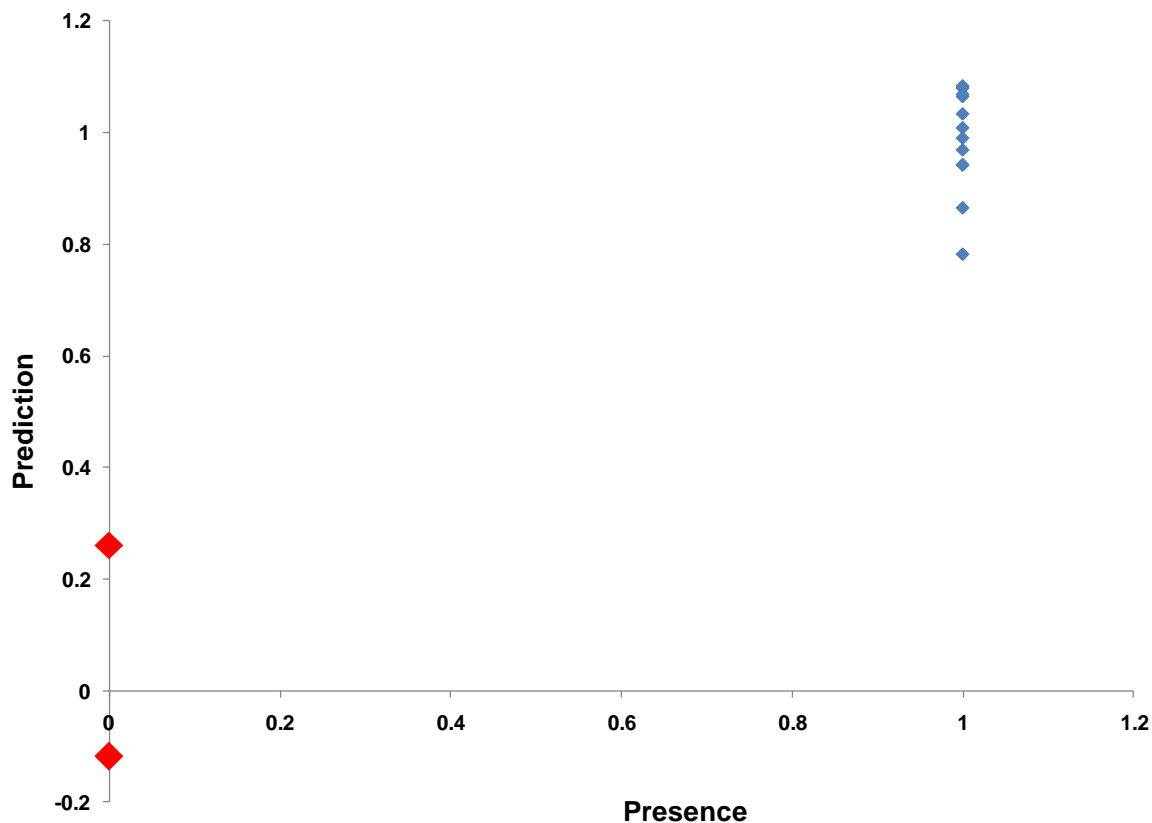


Figure 30. Prediction of presence of peroxide in whiskey using PLS. In this model, 1 = present and 0 =not present.

5.2.2 Detection of toxic industrial compounds in personal care products

The spectra of a perfume and Plax mouthwash are shown in Figure 31. Intensity of the peaks is reduced by the fluorescence of the liquid. Most noticeable peaks for the mouthwash appear at 875 cm^{-1} , 1000 cm^{-1} , 1080 cm^{-1} , and 1450 cm^{-1} . For the perfume the sharper peaks are: 798 cm^{-1} , 878 cm^{-1} , 1260 cm^{-1} , 1090 cm^{-1} , 1450 cm^{-1} and 1610 cm^{-1} . Consumer products such as personal care and cosmetics present a

challenge. Commonly these products contain ingredients such as alcohols, peroxides and others with chemical composition related to hazardous chemicals. Also these liquids are usually colored and present fluorescence.

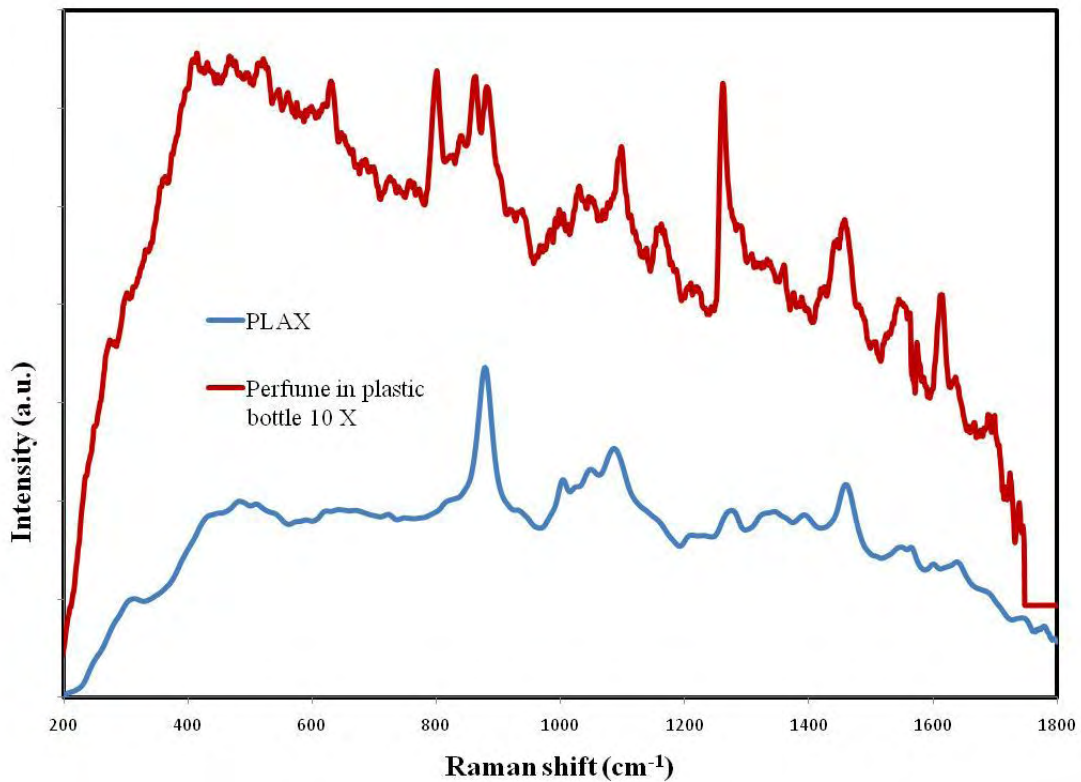


Figure 31. Raman spectrum of a perfume and mouthwash acquired with fiber optic probe. Parameters were: 785 nm laser, 100 mW and 1 s of integration time.

The perfume bottle was emptied and replaced by several toxic industrial compounds.

Figure 32 shows the detection of toxic industrial compounds using a 532 nm laser.

These liquids will exhibit strong peaks that will differentiate the material from the original liquid (perfume).

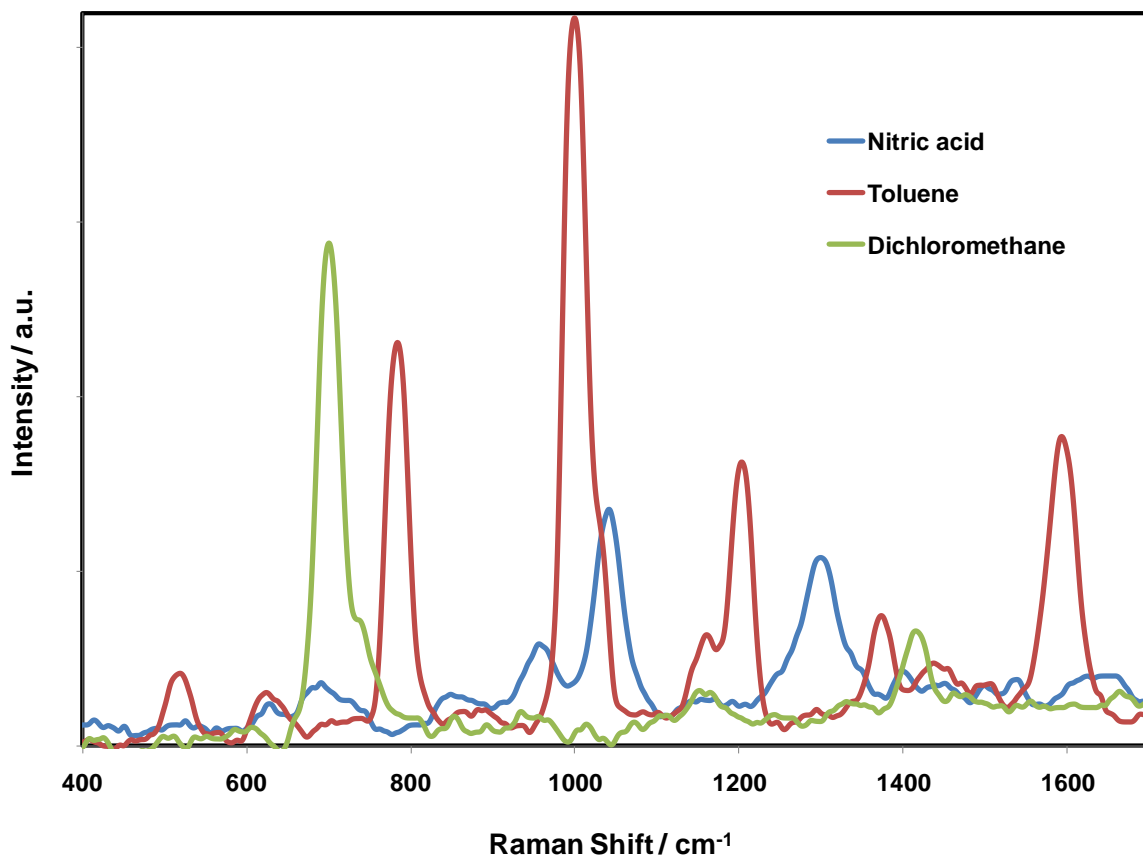


Figure 32. Raman spectra of toxic compounds within a perfume clear glass bottle at 532 nm, 1 s and a laser power of 12 mW.

Figure 33 shows a mixture of Plax mouthwash with 30 % hydrogen peroxide and a mixture with 40% acetone, another potential TIC. The peroxide is used as an example for peroxide based explosives. As mentioned before when the spectrum shows peaks in the same region, peak ratios will provide the discrimination for a

concealed hazardous liquid. For acetone the spectrum is completely different from the original liquid, even when the color is maintained.

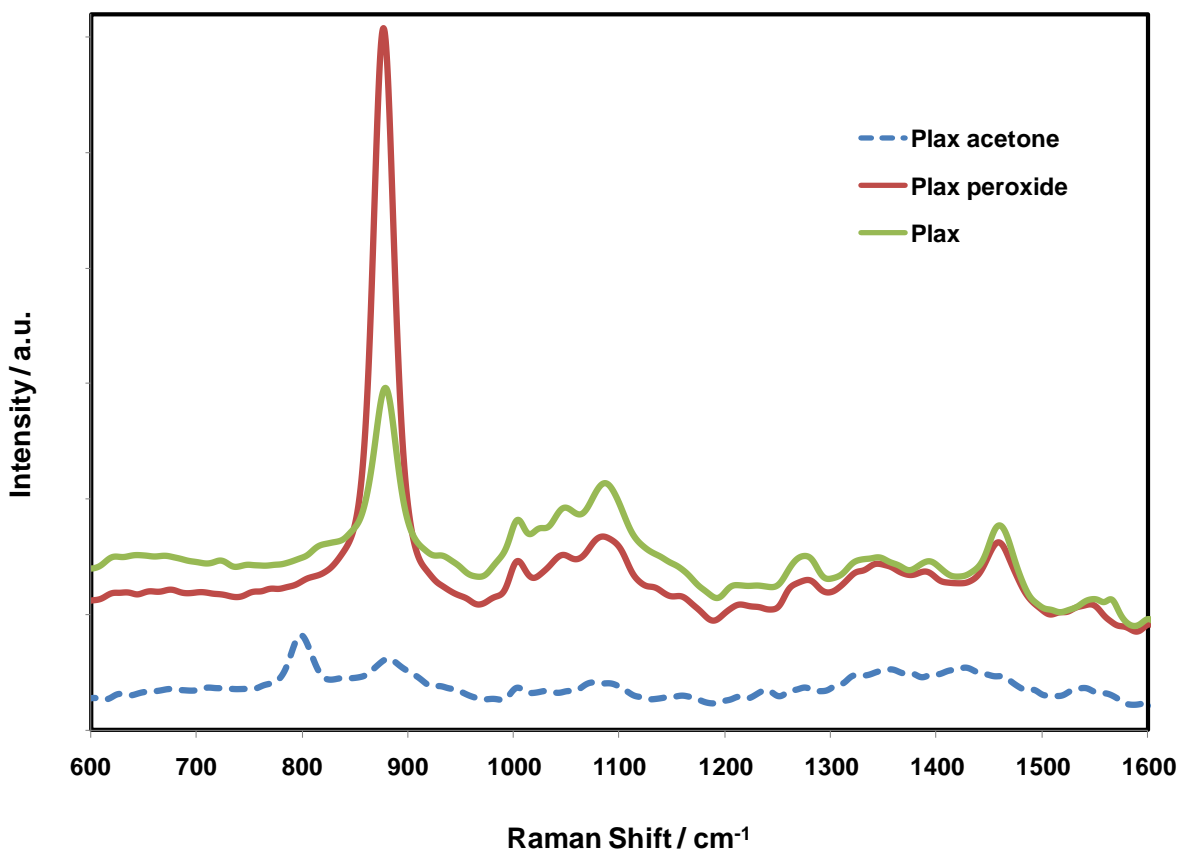


Figure 33. Raman spectra of mouthwash-peroxide and mouthwash acetone mixtures.

5.2.3 Detection of CWAs in soft beverages

The spectra of dimethyl methyl phosphonate (DMMP), a chemical warfare agent simulant is shown in figure 34. This spectrum was collected through the walls of a clear glass juice bottle (Snapple) and was detected using 532 nm laser beam with

10mW and the acquisition time was 1 seconds for recording the spectrum, The peaks at around 715 cm⁻¹ for DMMP correspond to a stretching mode involving the phosphorus atom. Figure 35 shows the remote detection of DMMP. A bottle with Snapple mixed with DMMP was placed at 20 feet of distance from the operator. Detection was achieved by coupling a telescope to a Raman spectrograph.

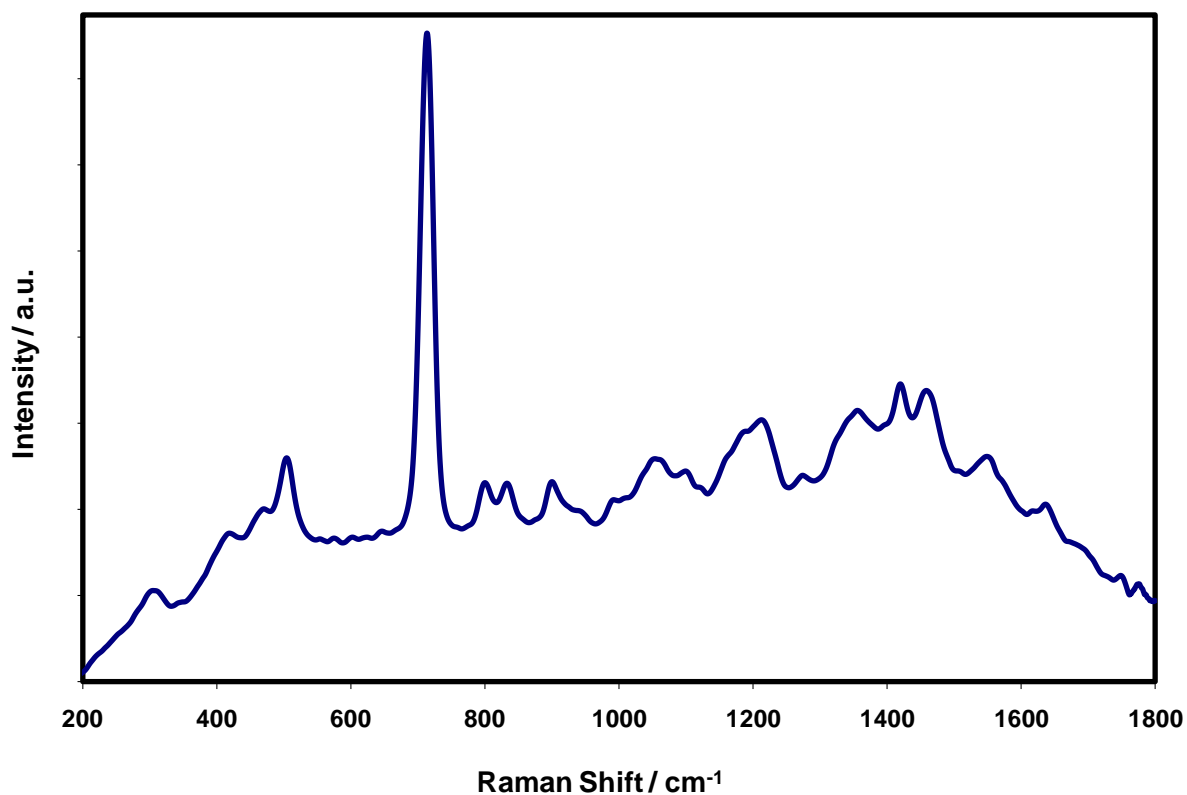


Figure 34. Raman based detection of DMMP (a): Within Snapple clear glass bottle (532 nm laser, 1 acquisition, 1 s, 10 mW) .

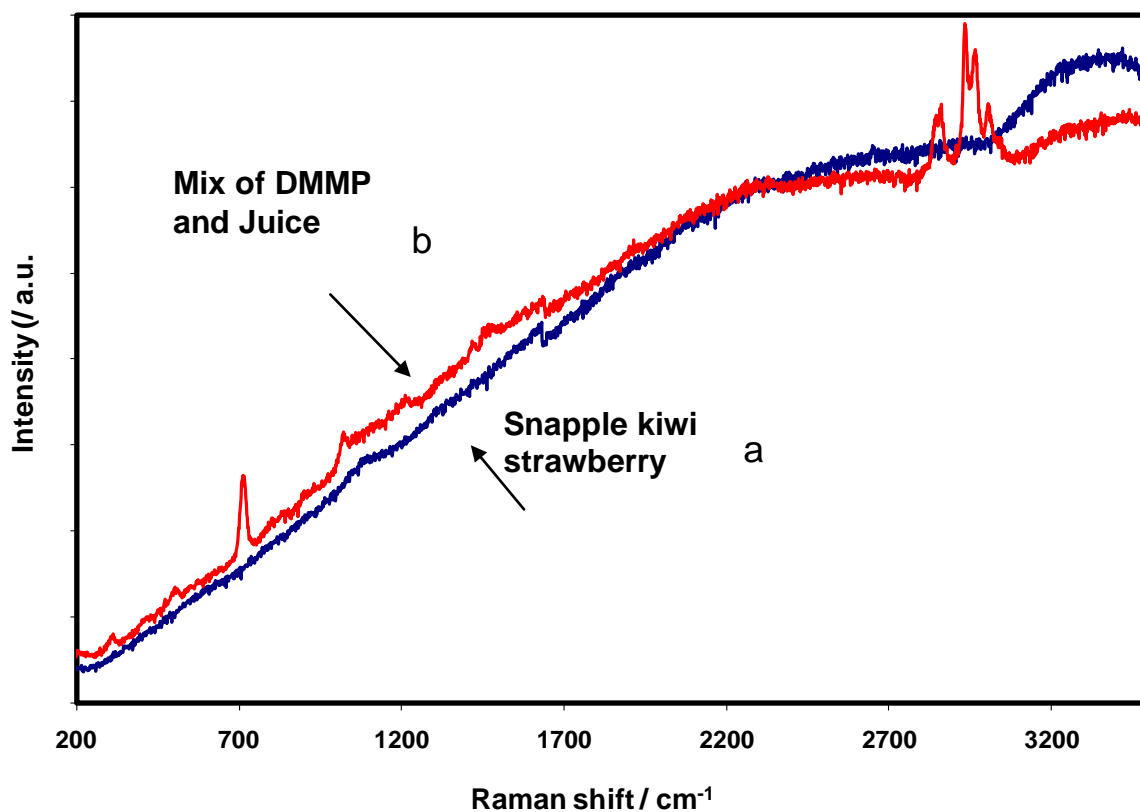


Figure 35. Raman based detection of DMMP. (a) Kiwi flavores Snapple; (b) DMMP in a mixture with Snapple juice in a clear glass bottle. (488 laser source, 1 acquisition, 30 s, 63 mW).

5.2.4 Effect of the type of container

The Raman spectrum of acetone was collected in different bottles using the same acquisition parameters at 532 nm (Figure 36) and 785 nm (Figure 37) laser source. The characteristic peaks of acetone at 780 cm^{-1} , 1400 cm^{-1} and 1700 cm^{-1} were observable for all samples. However for 532 nm data the intensity of the peaks decreased in the following order: clear glass > clear plastic > green glass > amber

glass. When the 785 nm laser was used the order was: clear glass > clear plastic > amber glass > green glass. It was not possible to collect a spectrum of the chemical in the green glass bottle using 30s of 200 mw of 785 nm laser power.

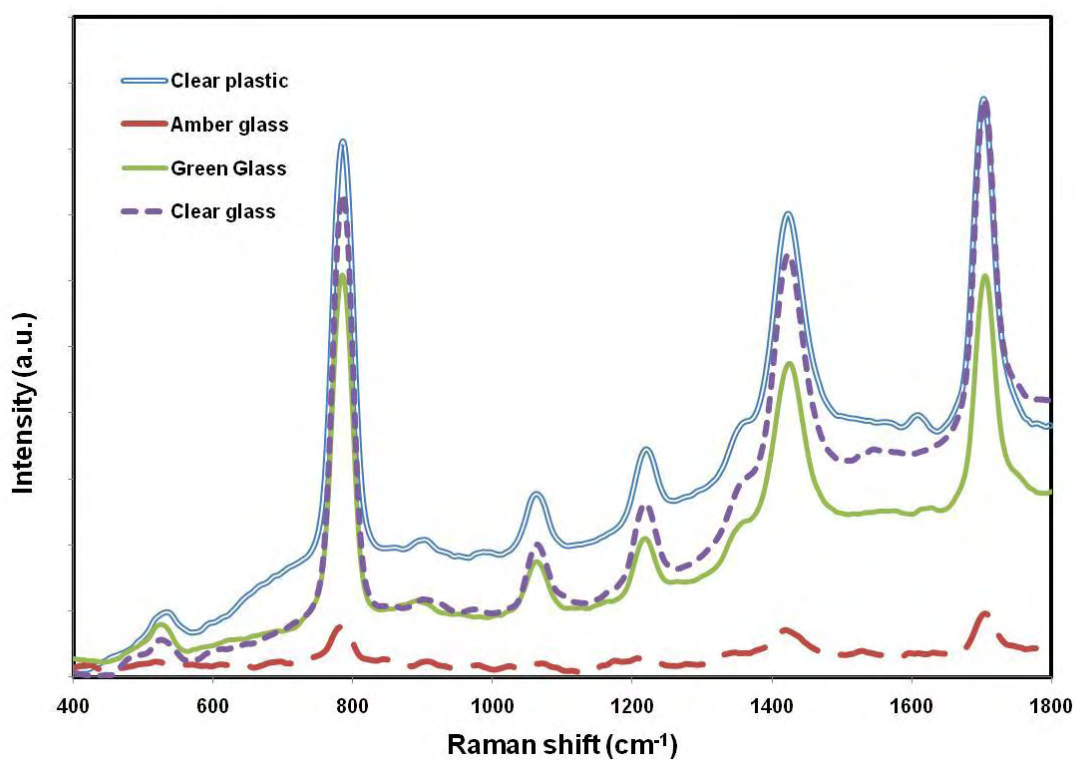


Figure 36. Raman spectra of acetone obtained from different bottles. Parameters: 532 nm laser, 1 scan, 20 s, 33 mW.

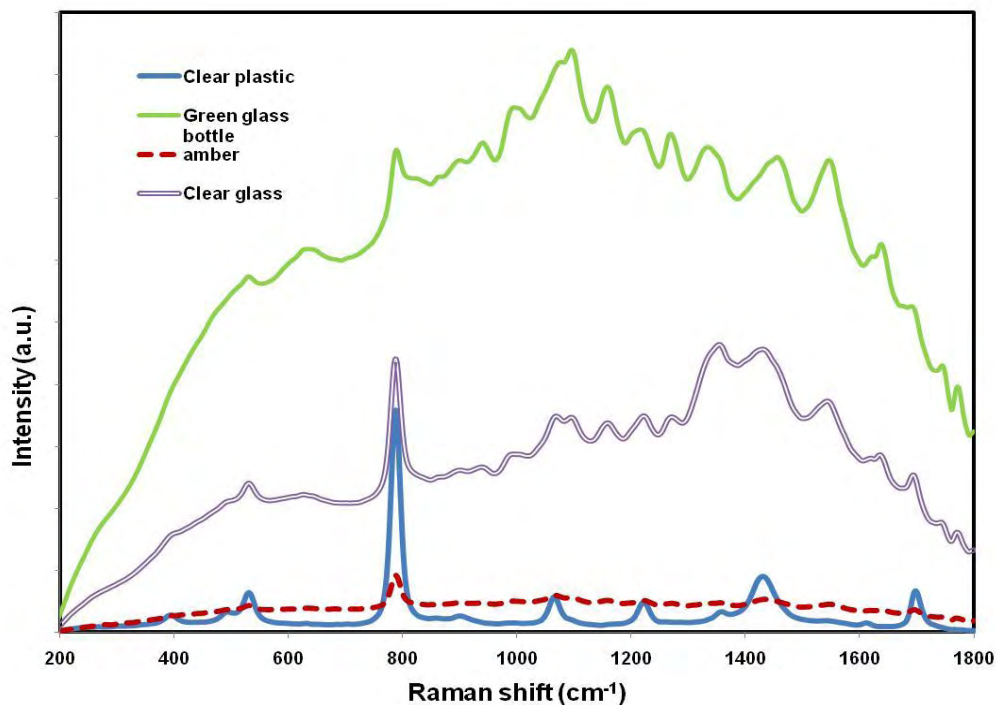


Figure 37. Raman spectra of acetone obtained from different bottles. Parameters: 785 nm 30 s at 200 mW.

Table 10. Thickness of common containers evaluated with FOC Raman.

Product	Material	Color	Thickness (mm)
Water	Plastic (PET)	Clear	0.22 ± 0.02
Fruit juice	Glass	Clear	1.92 ± 0.42
Malt beverage	Glass	Amber	2.28 ± 0.44
Beer	Glass	Green	2.02 ± 0.47

Since it was possible to collect a spectrum from the green plastic bottle, the behavior could be associated to thickness of the walls. The thickness of glass and plastic

bottles was measured. Table 9 present the results that are similar among glass bottles and differing considerably from a water plastic bottle.

Then the region between 700 cm^{-1} and 900 cm^{-1} of acetone was used to study the effect of different collection parameters on the spectra inside different bottles. The acquisition time was changed from 1 to 30 s. The laser power was varied from 11 to 32 mW. The power intensity of the instrument modulating and the output power was measured at the probe with a digital power meter. At fixed laser power of 18 mW the response was linear with increasing acquisition time (Figure 38). For the amber glass bottle the increase in peak area was significantly lower. This suggests that the bottle color is responsible for the fluorescence.

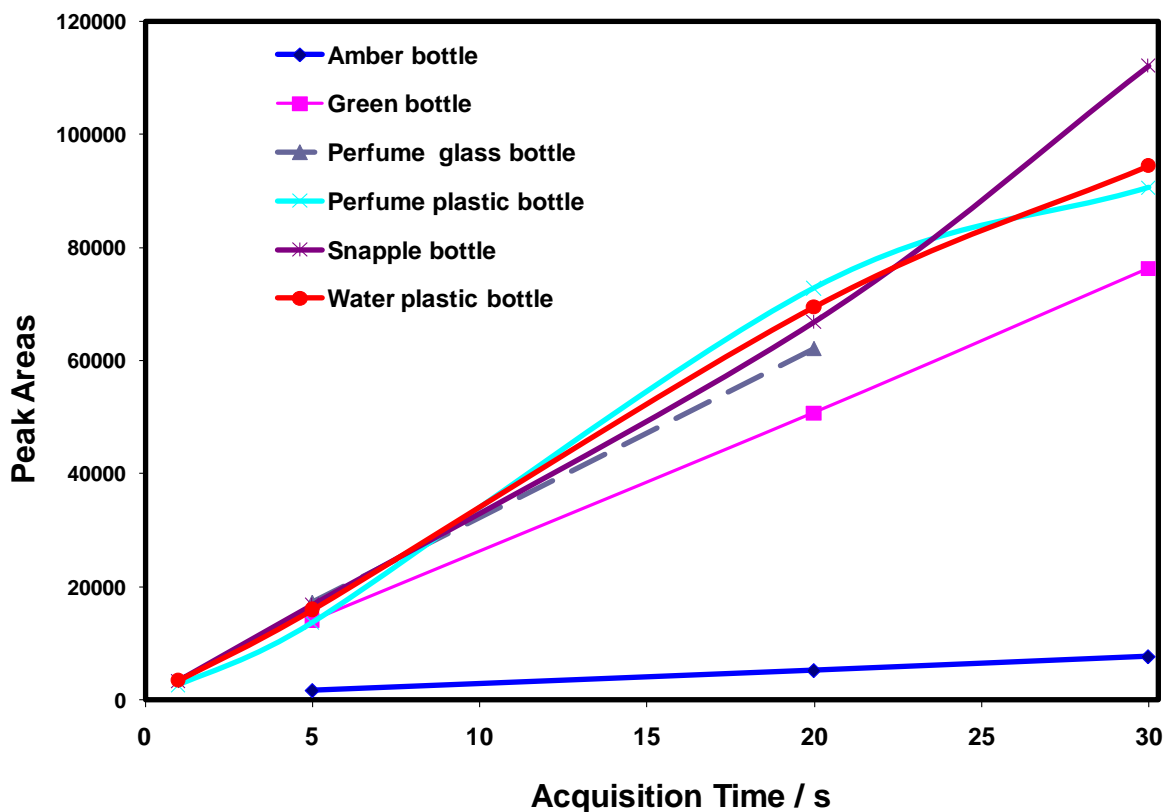


Figure 38. Area of the 800 cm^{-1} peak of acetone at different collection times inside different bottles at 532 nm and 18 mW (1 scan).

The transmission spectra of different bottles are shown in Figure 39. These spectra were acquired in the 220 nm to 1200 nm range. The objective of this experiment was to measure how much light is allowed transmitted in a specific bottle at different wavelengths. Solid vertical lines represent the laser wavelengths evaluated in the present work and dashed vertical lines mark the wavelength range for Raman spectra with shifts from 200 to 1800 cm^{-1} . According to this figure all clear containers (glass and plastic) will allow light of all wavelengths to reach the container as well as allow detecting scattered radiation. However for amber containers the optimum

range for interrogation will be 600 to 750 nm. The comparison with green containers suggests that the container material absorbs most of the light but a spectrum of the content would be possible to acquire with the appropriate laser power.

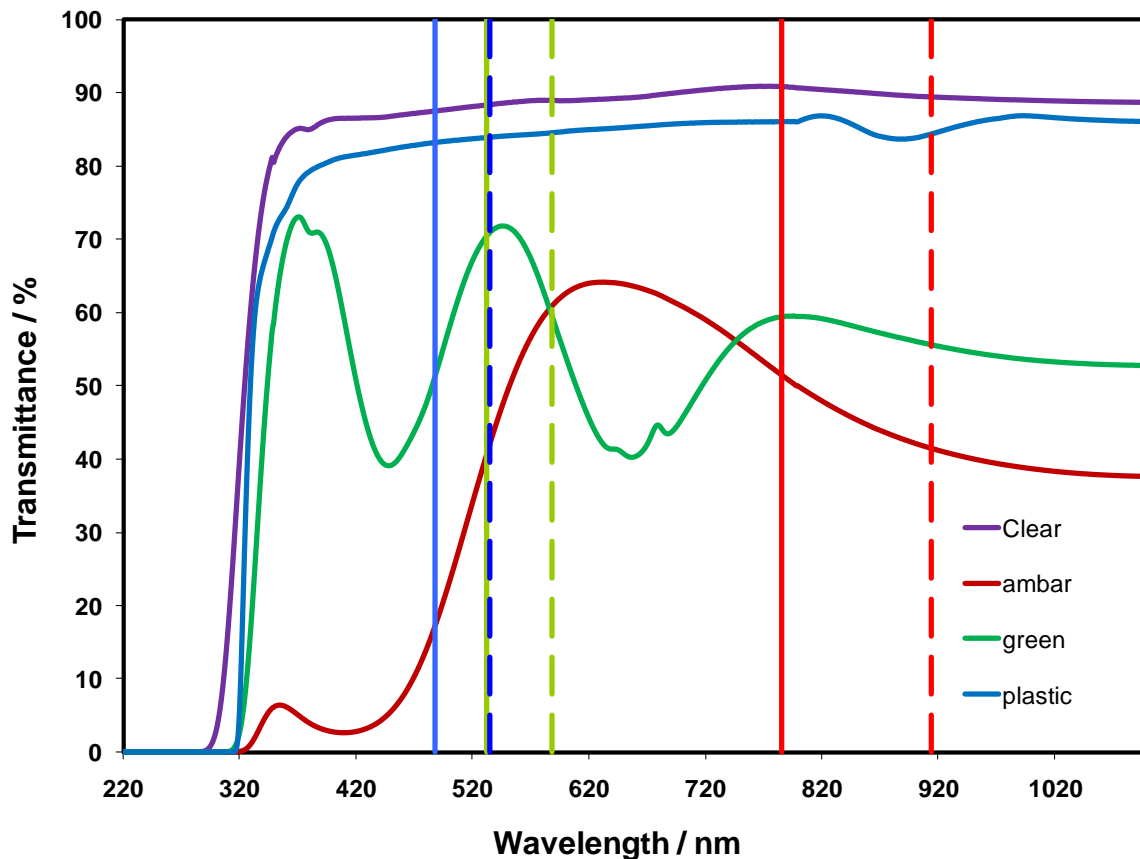


Figure 39. Transmission spectra of different bottles materials. Solid vertical lines indicate excitation lines in Raman experiments. Dashed lines indicate range for detected scattered radiation in the 200- 1800 cm^{-1} .

5.2.5 Detection in colored liquids

The limits of detection of a CWA simulant in heavily colored liquids were studied by FOC Raman. Triethyl phosphate (TEP) is commonly used as a simulant of Soman (GD), a nerve agent. Figure 40 presents the spectra of different flavors of Gatorade. The spectra were obtained at the same parameters. Fruit punch presents a higher baseline associated to fluorescence. TEP was prepared in random concentration from 0 to 100 %. Then the region from 675 cm^{-1} -855 cm^{-1} was integrated (Figure 41). This region was selected because of the presence of the characteristic peaks for phosphates. This region will be the same for the real CWA and related simulants.

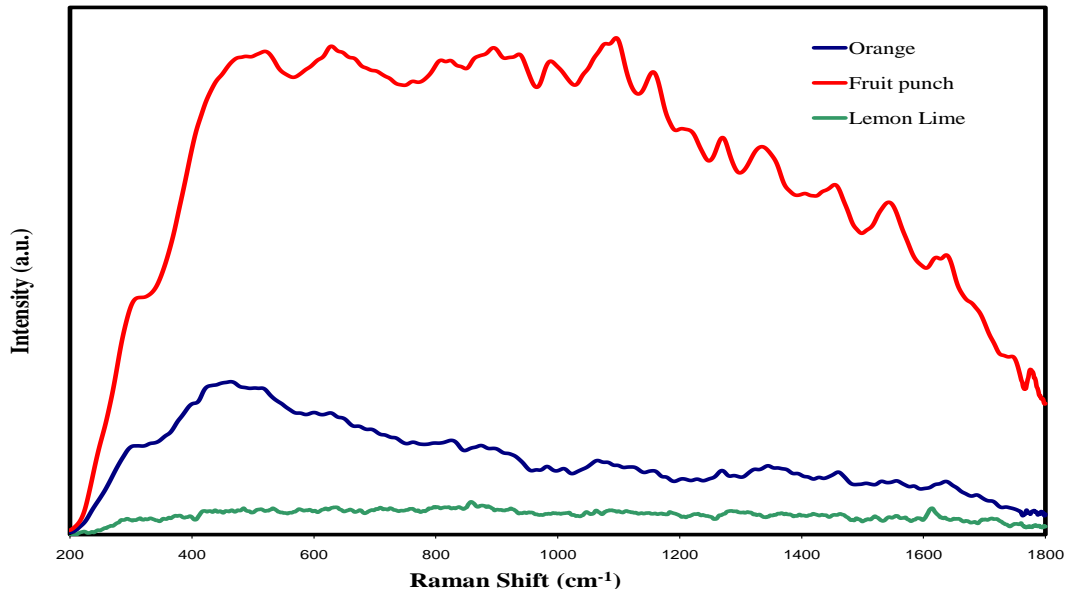


Figure 40. Raman spectra of Gatorade lemon, orange and fruit punch.

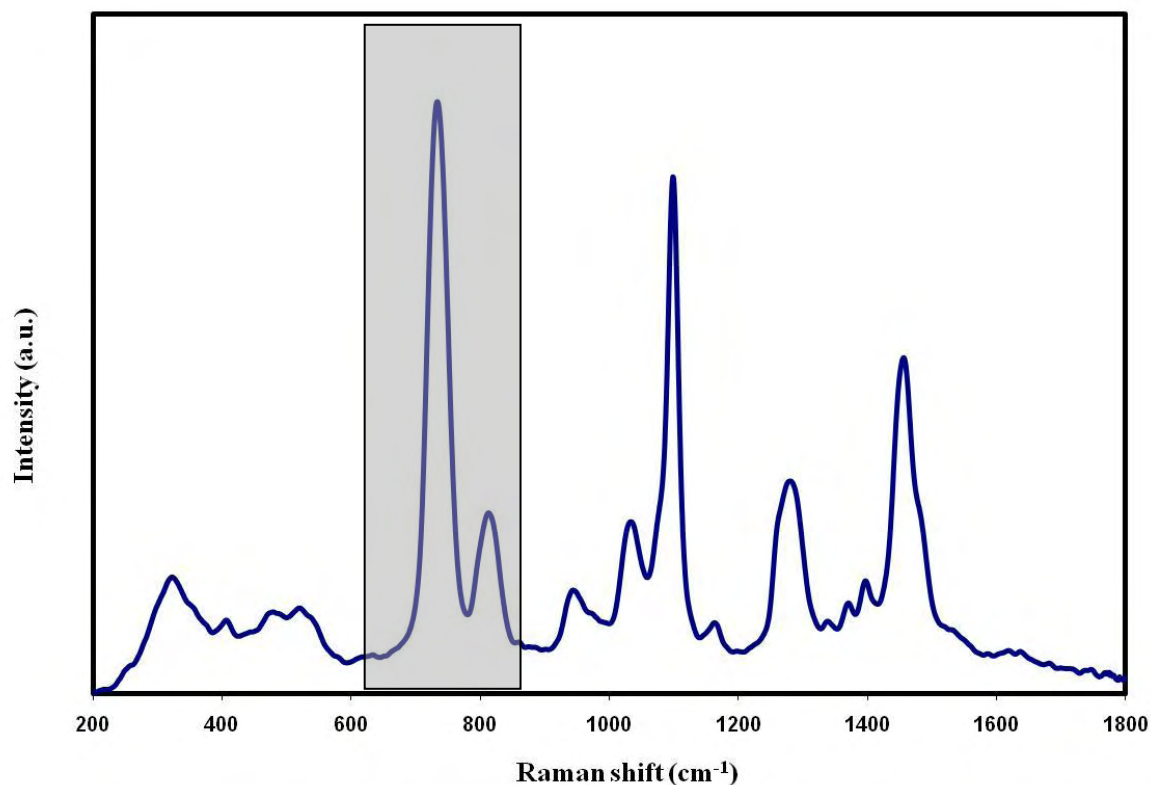


Figure 41. Spectrum of neat triethylphosphonate. The shaded area responds to the area used for TEP detection. The peak at 734 cm⁻¹ is characteristic of organic phosphates like the CWAs.

Measurements were taken in triplicates from 0% to 100 %. Figure 42 presents the areas at different concentration. The objective of these graphs is to compare the limit of detection (LOD) and the limit of quantification (LOQ) between colored liquids. Error bars for each data point represent the calculated standard deviation derived from all repetitive measurements each.

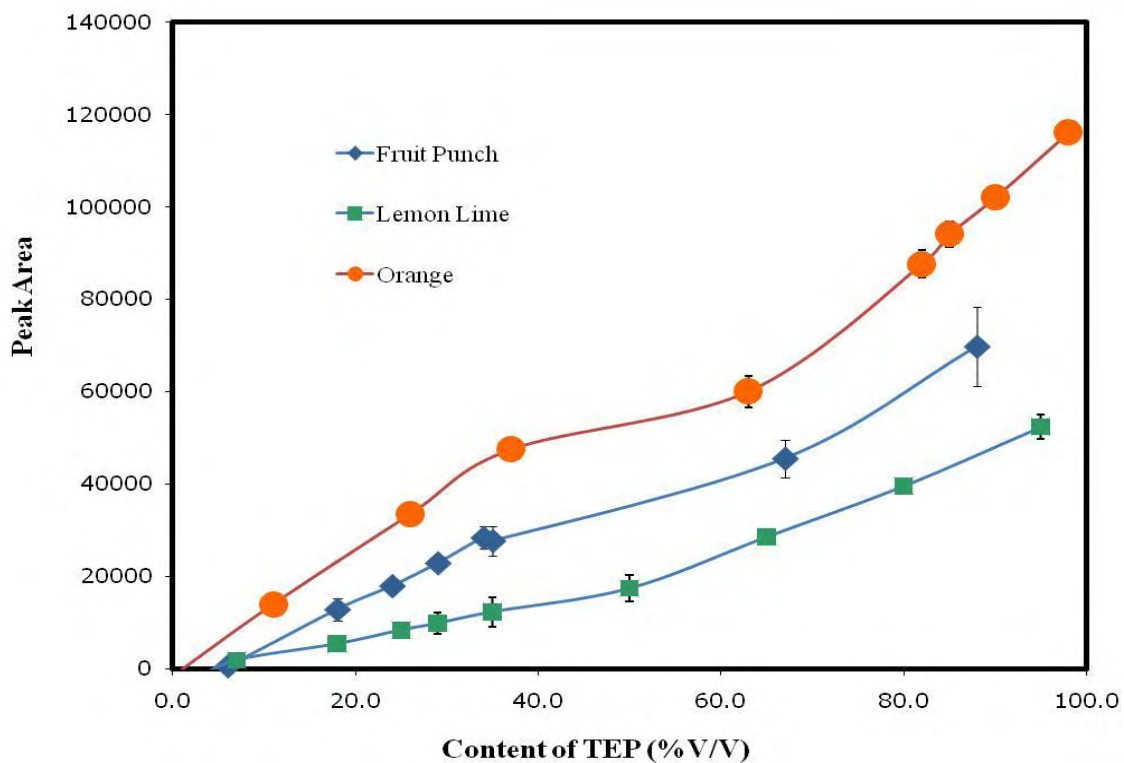


Figure 42. Peak area for the region of 675 cm^{-1} -855 cm^{-1} in orange, fruit punch and lemon Gatorade juice as a function of TEP concentration.

Table 11. LOD and LOQ for TEP in colored liquids.

<i>Gatorade Flavor</i>	<i>LOD (%)</i>	<i>LOQ (%)</i>
Fruit Punch	6	21
Lemon	9	30
Orange	9	32

Limits of detection for this analyte have been calculated according to IUPAC by the 3σ criteria (3 times standard deviation of the peak-to-peak noise related to the slope of the linear regression function). When the signal is 3 times as great as the noise, it is ready detectable but still too small for accurate measurement. A signal that is 10 times as great as the noise is defined as the lower limit of quantification (LOQ), or the smallest amount that can be measured with reasonable accuracy. Table 11 presents the results of LOD and LOQ for TEP in Gatorade Lemon, Orange and Fruit Punch.

5.3 Conclusions

In this work, concealed liquids scenarios are studied by Raman spectroscopy. The Raman spectra of hazardous liquids were differentiated from common drinks and consumer products. A fiber optic coupled Raman probe was applied to the detection of hazardous liquids inside bottles of common drinks. The study included glass and plastic bottles of different colors. The results demonstrated that Raman can be used as tool to quickly characterize if the content of a bottle is the intended commercial product or a hazardous liquid that could be used as a threat to property or human beings. The effect of the absorption of the container was studied. The fluorescence of a red liquid did not affect the detection of a CWA simulant in a clear glass container. The limits of detection for a hazardous liquid in a series of colored liquids were estimated in 6-9 % using standard conditions and no data manipulation. This

suggests that trace level detection can be achieved with enhanced experimental setups and statistical analysis of the data (chemometrics).

6 Final comments and path forward

The low enthalpy of sublimation of AP implies a high sublimation rate and high vapor pressure. This behavior has implications on the residence time and presents challenges for residue detection but open doors for vapor phase detection.

The low activation energy of AP makes it a potential primary explosive however its low thermal stability (primarily due to high vapor pressure and low activation energy) will be extended to mixtures.

The Raman based detection of concealed hazardous liquids does not pretend to establish the limits of the technique. It is intended to bring to the light the potential and challenges for a Raman based bottle screener.

Future experiments should extend the study of sublimation to other materials of interest in order to create a data base and improve the QSPR models.

Also the characterization of HEM mixtures should be continued and study the interactions at trace level and the implications to detection approaches.

Finally the detection of concealed hazardous liquids will be enhanced by the application of modern statistical data analysis. Current challenges include the study of more complex liquids like milk and carbonated drinks.

7 Rerferences

1. National, The 9/11 Commission Report: Final Report of the National Commission on Terrorist Attacks Upon the United States (Indexed Hardcover, Authorized Edition). {W. W. Norton & Company}: 2004.
2. Police: Plot to blow up aircraft foiled. In www.cnn.com, August 10, 2006 ed.; 2006.
3. National Research Council . Committee on the Review of, E.; Potential Standoff Explosives Detection, T., Existing and potential standoff explosives detection techniques. National Academies Press: Washington, D.C., 2004.
4. Sun, Y.; Ong, K. Y., Detection technologies for chemical warfare agents and toxic vapors / Yin Sun and Kwok Y. Ong. Boca Raton, Fla. :, 2004; p 272 p. ;.
5. D'Agostino, P. A.; Hancock, J. R.; Chenier, C. L.; Lepage, C. R., Liquid chromatography electrospray tandem mass spectrometric and desorption electrospray ionization tandem mass spectrometric analysis of chemical warfare agents in office media typically collected during a forensic investigation. *J Chromatogr A* **2006**, 1110 (1-2), 86-94.
6. Pardasani, D.; Palit, M.; Gupta, A. K.; Kanaujia, P. K.; Dubey, D. K., Gas chromatography-mass spectrometry analysis of trifluoroacetyl derivatives of precursors of nitrogen and sulfur mustards for verification of chemical weapons convention. *J Chromatogr A* **2004**, 1059 (1-2), 157-64.
7. Smith, P. A.; Koch, D.; Hook, G. L.; Erickson, R. P.; Jackson, C. R.; Haley, L.; Wyatt, D. M.; Betsinger, G.; Eckenrode, B. A., Detection of gas-phase chemical warfare agents using field-portable gas chromatography/mass spectrometry systems: Instrument and sampling strategy considerations. *Trends in analytical chemistry* **2004**, 23 (4), 296-306.
8. Steiner, W. E.; Harden, C. S.; Hong, F.; Klopsch, S. J.; Hill, H. H., Jr.; McHugh, V. M., Detection of aqueous phase chemical warfare agent degradation products by negative mode ion mobility time-of-flight mass spectrometry [IM(tof)MS]. *J Am Soc Mass Spectrom* **2006**, 17 (2), 241-5.
9. Kanu, A.; Haigh, P.; Hill, H., Surface detection of chemical warfare agent simulants and degradation products. *Analytica Chimica Acta* **2005**, 553 (1-2), 148-159.
10. Farquharson, S.; Gift, A.; Maksymiuk, P.; Inscore, F., Surface-enhanced Raman spectra of VX and its hydrolysis products. *Appl Spectrosc* **2005**, 59 (5), 654-60.
11. Pearman, W. F.; Fountain, A. W., 3rd, Classification of chemical and biological warfare agent simulants by surface-enhanced Raman spectroscopy and multivariate statistical techniques. *Appl Spectrosc* **2006**, 60 (4), 356-65.

12. Harvey, S. D.; Vucelick, M. E.; Lee, R. N.; Wright, B. W., Blind field test evaluation of Raman spectroscopy as a forensic tool. *Forensic Science International* **2002**.
13. Christesen, S. D.; Pendell Jones, J.; Lochner, J. M.; Hyre, A. M., Ultraviolet Raman spectra and cross-sections of the G-series nerve agents. *Appl Spectrosc* **2008**, 62 (10), 1078-83.
14. Eliasson, C.; Macleod, N.; Matousek, P., Noninvasive Detection of Concealed Liquid Explosives Using Raman Spectroscopy. *Analytical Chemistry* **2007**, 79 (21), 8185-8189.
15. Christesen, S.; Maciver, B.; Procell, L.; Sorrick, D.; Carrabba, M.; Bello, J., Nonintrusive Analysis of Chemical Agent Identification Sets Using a Portable Fiber-Optic Raman Spectrometer. *Applied Spectroscopy* **1999**, 53, 850-855.
16. Liu, Z.; Shao, Y.; Yin, C.; Kong, Y., Measurement of the eutectic composition and temperature of energetic materials. Part 1. The phase diagram of binary systems. *Thermochimica Acta* **1995**, 250 (1), 65-76.
17. Brill, T. B.; James, K. J., Kinetics and mechanisms of thermal decomposition of nitroaromatic explosives. *Chemical Reviews* **1993**.
18. Lee, J.-S.; Hsu, C.-K.; Chang, C.-L., A study on the thermal decomposition behaviors of PETN, RDX, HNS and HMX. *Thermochimica Acta* **2002**, 392-393, 173-176.
19. Lee, J.; Hsu, C., The thermal behaviors and safety characteristics of composition B explosive. *Thermochimica Acta* **2001**, 367, 371-374.
20. Peng, D.; Chang, C.; Chiu, M., Thermal reactive hazards of HMX with contaminants. *Journal of Hazardous Materials* **2004**, 114 (1-3), 1-13.
21. W. Gueckel, F. R. R., G. Synnatschke, Method for determining the volatility of active ingredients used in plant protection. *Pestic. Sci.* **1974**, 5, 393-400.
22. Elder, J. P., Sublimation measurements of pharmaceutical compounds by isothermal thermogravimetry. *Journal of Thermal Analysis and calorimetry* **1997**, 49, 897-905.
23. Chatterjee, K.; Hazra, A.; Dollimore, D.; Alexander, K., Estimating vapor pressure curves by thermogravimetry: a rapid and convenient method for characterization of pharmaceuticals. *European Journal of Pharmaceutics and Biopharmaceutics* **2002**, 54 (2), 171-180.
24. Xie, M.; Ziemba, T. M.; Maurin, M. B., Enthalpy of sublimation and vapor pressure estimation of an HIV nonnucleoside reverse transcriptase inhibitor using thermogravimetric *AAPS PharmSciTech* **2003**, 4 (2), 1-10.
25. Wright, S., Determination of the vapor pressure curves of adipic acid and triethanolamine using thermogravimetric analysis. *Thermochimica Acta* **2004**, 421 (1-2), 25-30.
26. Price, D. M., Volatilisation, Evaporation and Vapour Pressure Studies Using a Thermobalance. *Journal of Thermal Analysis and calorimetry* **2001**, 64, 315-322.

27. Jones, D. E. G.; Lightfoot, P. D.; Fouchard, R. C.; Kwok, Q. S. M., Thermal properties of DMNB, a detection agent for explosives. *Thermochimica Acta* **2002**.
28. Chang, R.; Shu, C.; Duh, Y.; Jehng, J., Calorimetric studies on the thermal hazard of methyl ethyl ketone peroxide with incompatible substances. *Journal of Hazardous Materials* **2007**, 141 (3), 762-768.
29. Yuan, M.; Shu, C.; Kossoy, A., Kinetics and hazards of thermal decomposition of methyl ethyl ketone peroxide by DSC. *Thermochimica Acta* **2005**, 430 (1-2), 67-71.
30. Miyake, A.; Yamada, N.; Ogawa, T., Mixing hazard evaluation of organic peroxides with other chemicals. *Journal of Loss Prevention in the Process Industries* **2005**, 18 (4-6), 380-383.
31. Oxley, J.; Smith, J.; Chen, H., Decomposition of a multi-peroxidic compound: Triacetone triperoxide (TATP). *Propellants, Explosives, Pyrotechnics* **2002**, 27 (4), 209-216.
32. Oxley, J.; Smith, J.; Shinde, K.; Moran, J., Determination of the Vapor Density of Triacetone Triperoxide (TATP) Using a Gas Chromatography Headspace Technique. *Propellants, Explosives, Pyrotechnics* **2005**, 30 (2), 127-130.
33. Saraf, S., Prediction of reactive hazards based on molecular structure. *Journal of Hazardous Materials* **2003**, 98 (1-3), 15-29.
34. Karelson, M.; Lobanov, V.; Katritzky, A., Quantum-chemical descriptors in QSAR/QSPR studies. *Chemical Reviews* **1996**, 96 (3), 1027-1044.
35. Wang, L.; Tuo, X.; Yi, C.; Wang, X., Ab initio calculations of the effects of H⁺ and NH₄⁺ on the initial decomposition of HMX. *Journal of Molecular Graphics and Modelling* **2008**, 27 (3), 388-393.
36. Jinshan, L.; Heming, X.; Haishan, D., A Study on the Intermolecular Interaction of Energetic System-Mixtures Containing-CNO₂ and-NH₂ Groups. *Propellants, Explosives, Pyrotechnics* **2000**, 25 (1).
37. Alvarez-Rivera, M. Fiber optic Coupled Raman Spectroscopy of liquid explosives mixtures. University of Puerto Rico, Mayaguez, 2002.
38. Pacheco-Londono, L. C.; Pena, A. J.; Primera-Pedrozo, O. M.; Hernandez-Rivera, S. P.; Mina, N.; Garcia, R.; Chamberlain, R. T.; Lareau, R. T. In An experimental and theoretical study of the synthesis and vibrational spectroscopy of triacetone triperoxide (TATP), Sensors, and Command, Control, Communications, and Intelligence (C3I) Technologies for Homeland Security and Homeland Defense III, Orlando, FL, USA, SPIE: Orlando, FL, USA, 2004; pp 279-287.
39. Ballesteros, L. M.; Herrera, G. M.; Castro, M. E.; Briano, J.; Mina, N.; Hernandez-Rivera, S. P. In Spectroscopic signatures of PETN in contact with sand particles, Detection and Remediation Technologies for Mines and Minelike Targets X, Orlando, FL, USA, SPIE: Orlando, FL, USA, 2005; pp 1254-1262.
40. Infante-Castillo, R.; Hernandez-Rivera, S. P. In Theoretical and experimental vibrational and NMR studies of RDX, Sensors, and Command, Control, Communications, and Intelligence (C3I) Technologies for Homeland Security and

Homeland Defense V, Orlando (Kissimmee), FL, USA, SPIE: Orlando (Kissimmee), FL, USA, 2006; pp 62012F-8.

41. Kissinger, H. E., Reaction Kinetics in Differential Thermal Analysis. *Analytical Chemistry* **1957**, 29 (11), 1702-1706.

42. Ozawa, T., Critical investigation of methods for kinetic analysis of thermoanalytical data. *Journal of Thermal Analysis and calorimetry* **1975**, 7 (3), 601-617.

43. ASTM, Standard test method for Arrhenius kinetic constants for thermally unstable materials. **1982**, Part 41 (E 698-79), 1012-19.

44. Ramirez, M. L.; Pacheco-Londono, L. C.; Pena, A. J.; Hernandez-Rivera, S. P. Characterization of peroxide-based explosives by thermal analysis, Sensors, and Command, Control, Communications, and Intelligence (C3I) Technologies for Homeland Security and Homeland Defense V, Orlando (Kissimmee), FL, USA, SPIE: Orlando (Kissimmee), FL, USA, 2006; pp 62012B-10.

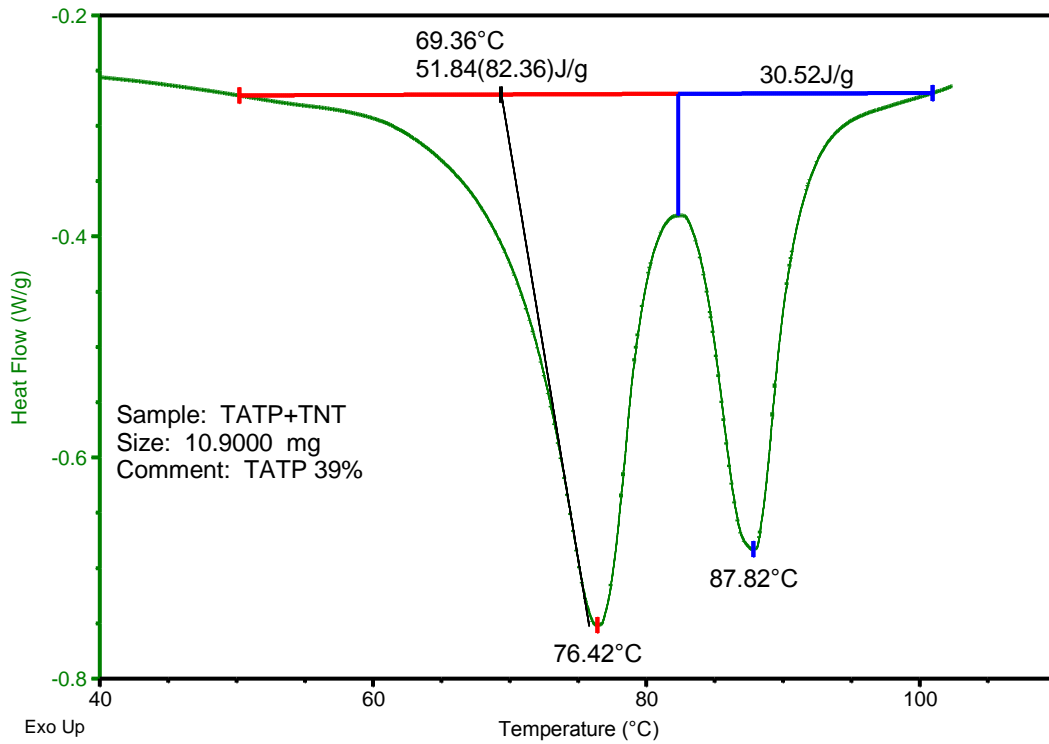
45. Chickos, J.; Acree Jr, W., Enthalpies of Sublimation of Organic and Organometallic Compounds. 1910–2001. *Journal of Physical and Chemical Reference Data* **2002**, 31, 537.

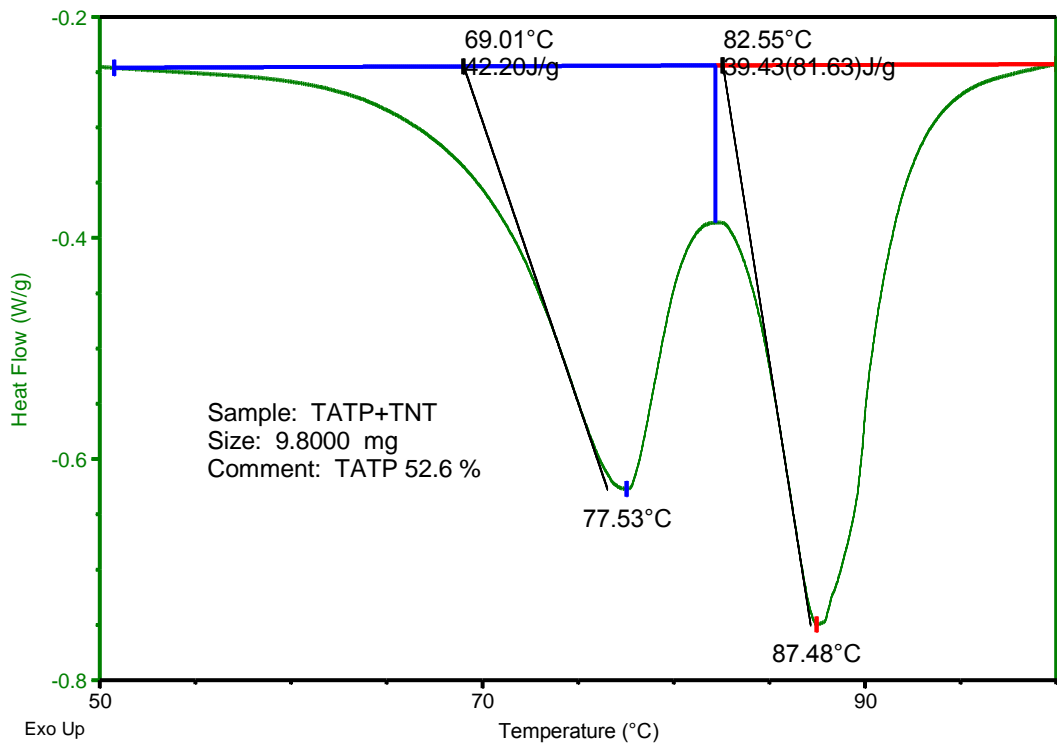
46. Oxley, J. C.; Smith, J. L.; Wang, W., Compatibility of Ammonium Nitrate with Monomolecular Explosives. 1. *The Journal of Physical Chemistry* **1994**, 98 (14), 3893-3900.

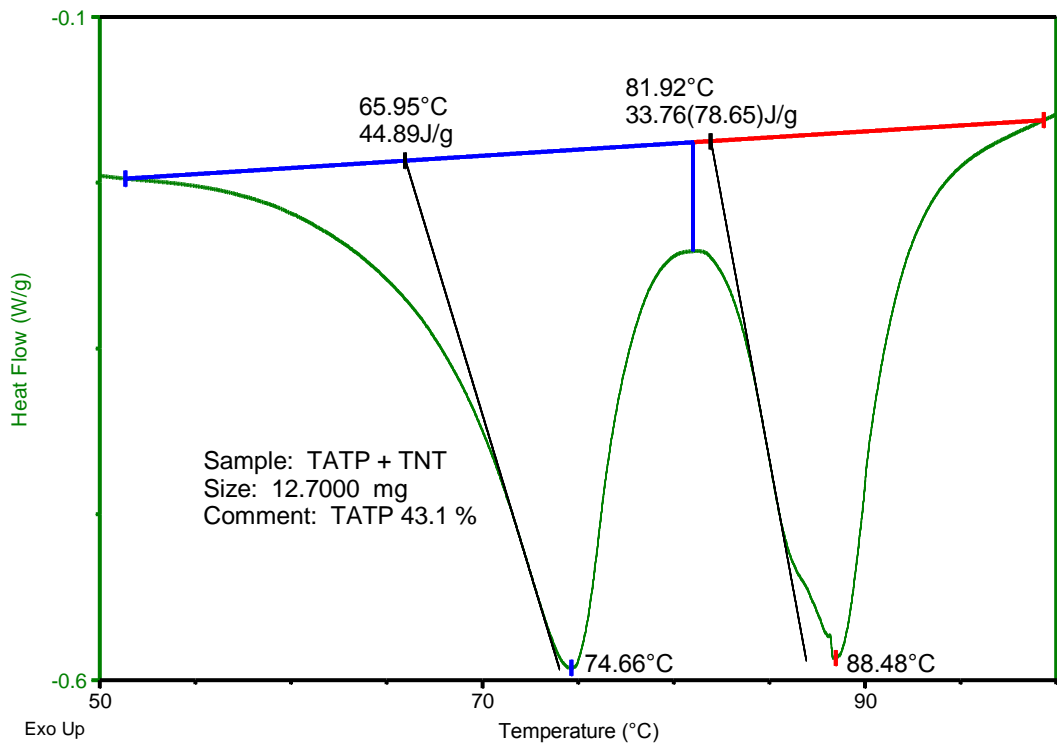
47. Oxley, J. C.; Smith, J. L.; Wang, W., Compatibility of Ammonium Nitrate with Monomolecular Explosives. 2. Nitroarenes. *The Journal of Physical Chemistry* **1994**, 98 (14), 3901-3907.

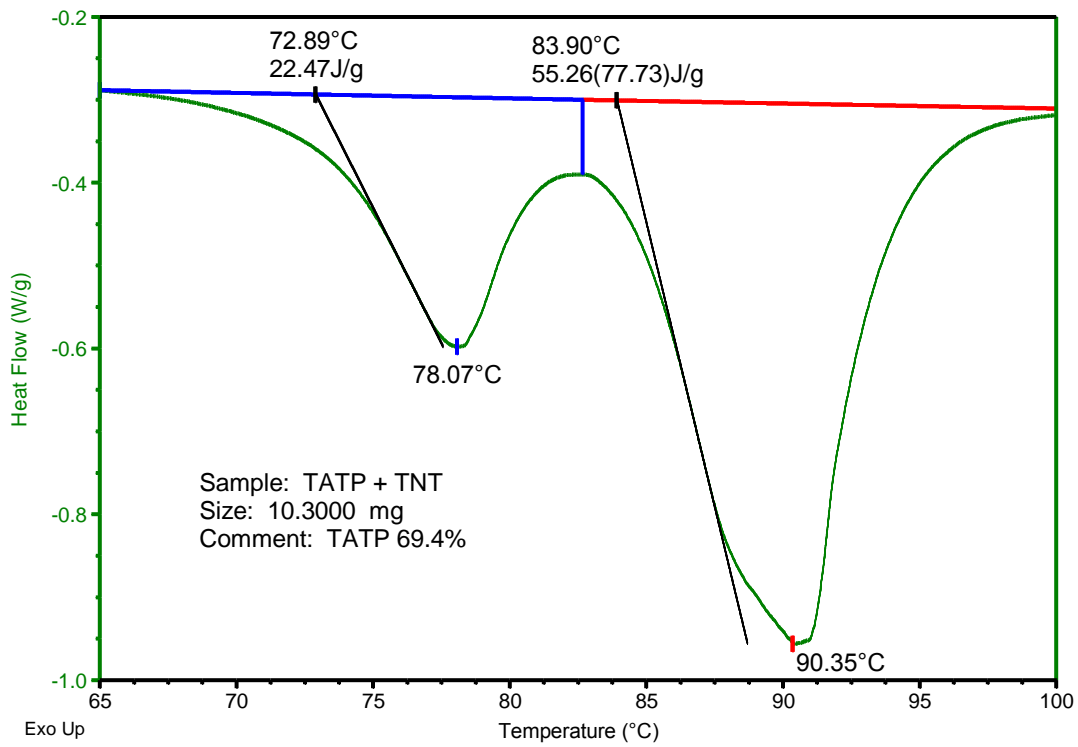
Appendix A. Thermograms of energetic materials

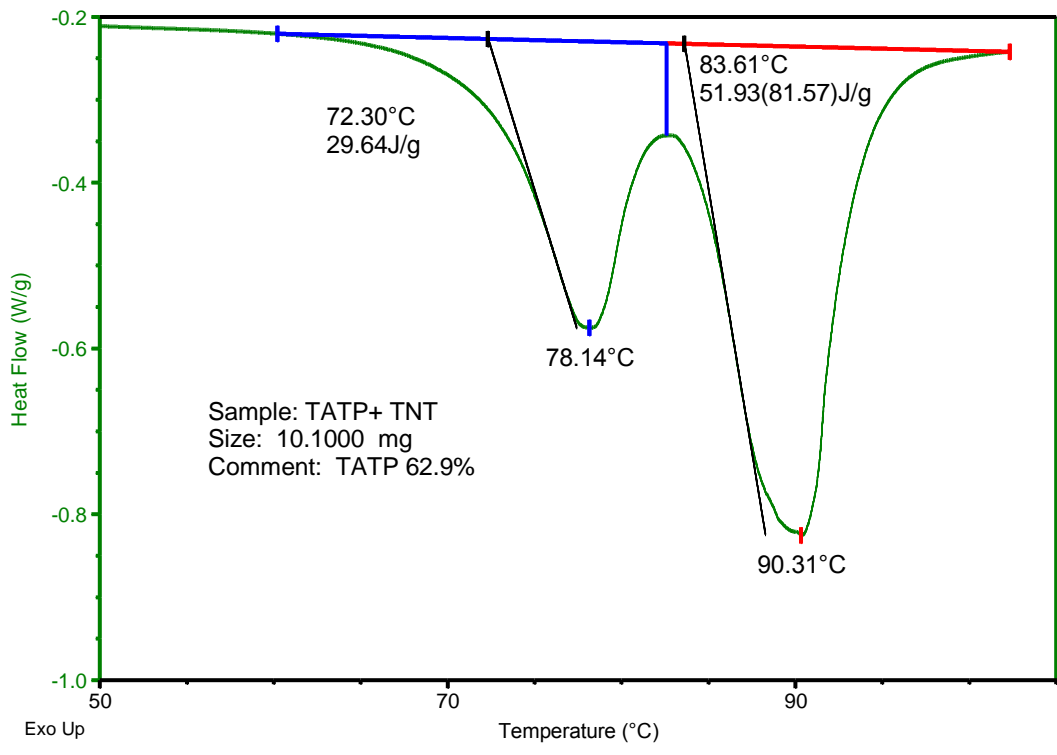
A.1 Curves for the AP-TNT blend melting. Data used for the phase diagrams

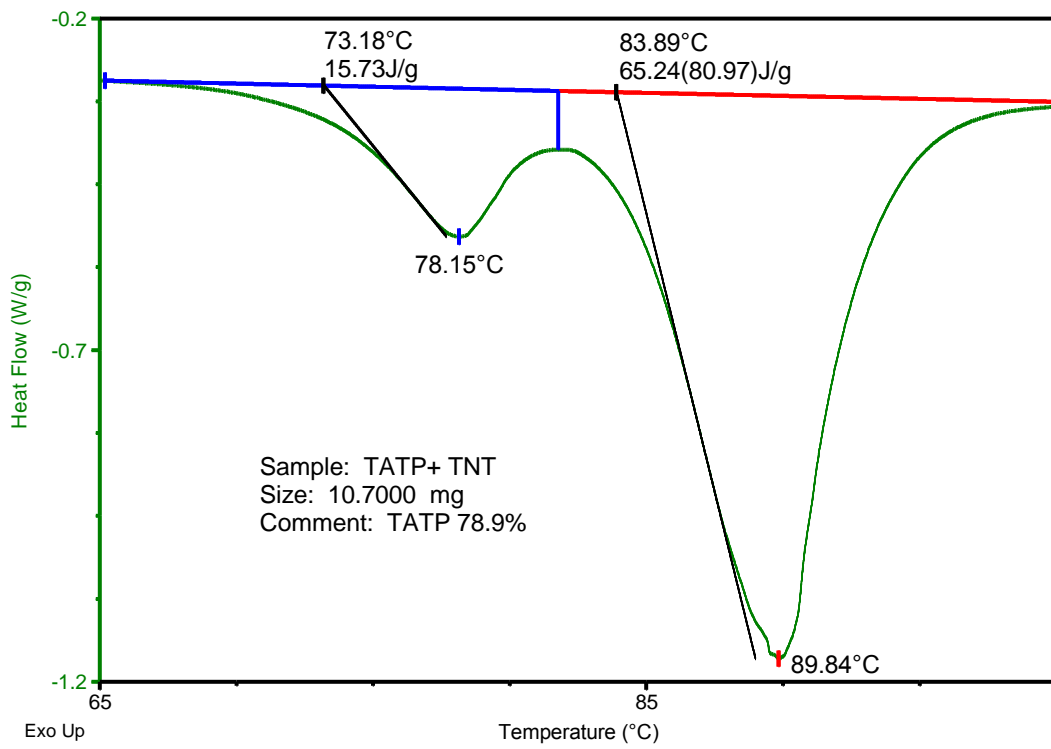


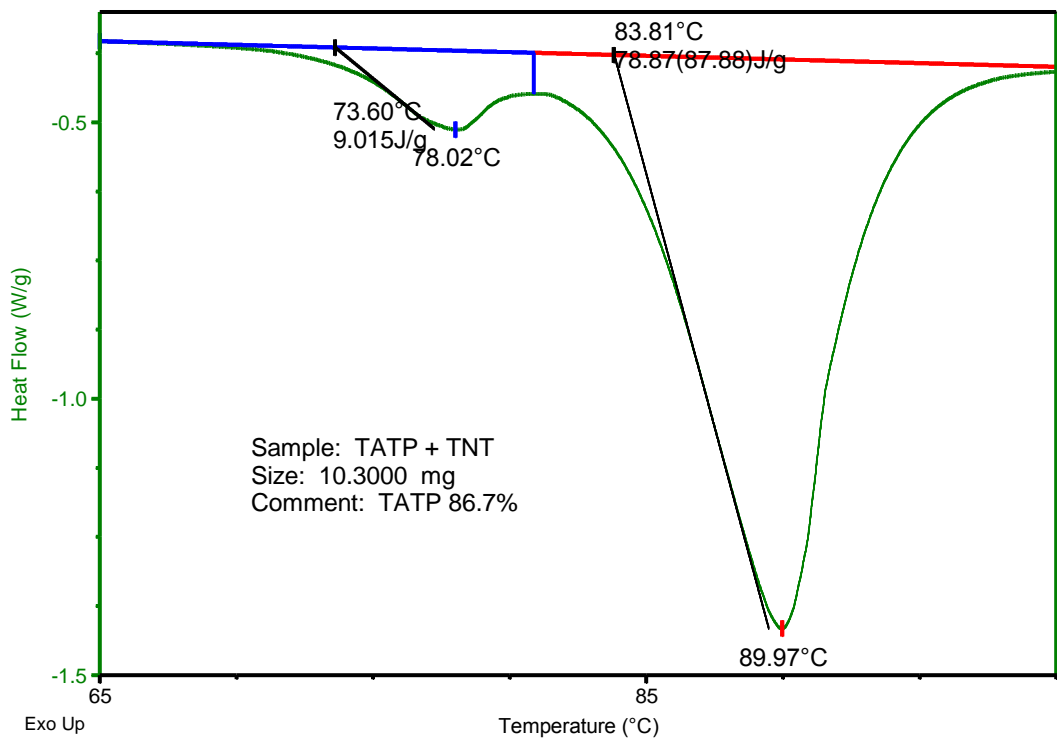












A.2 Solidification data for the blends.

